Lepton Flavor Violation Phenomenology Beyond the Standard Model

Dissertation
zur
Erlangung des Doktorgrades (Dr. rer. nat.)
der
Mathematisch-Naturwissenschaftlichen Fakultät
der
Rheinischen Friedrich-Wilhelms-Universität Bonn

von
María Paulina Rocha Morán
aus
León, Guanajuato, México

Bonn, 15.04.2019

Angefertigt mit Genehmigung der Mathematisch-Naturwissenschaftlichen Fakultät der Rheinischen Friedrich-Wilhelms-Universität Bonn

1. Gutachter:	Prof. Dr. Manuel Drees
2. Gutachter:	Dr. Avelino Vicente
Tag der Promotion:	30.08.2019
Erscheinungsjahr:	2020

Dedicated to my loving parents
Baltazar and Amelia.

Abstract

Historically, experimental searches for flavor violating processes have been essential for the theoretical developments in Particle Physics. After the detection of neutrino oscillations, the most clear experimental evidence for new physics at present comes from lepton flavor violation (LFV) in the neutrino sector. Whereas a new window to physics beyond the Standard Model (SM) and even beyond neutrino masses can be opened if a positive signal from LFV processes in the charge sector is observed by ongoing or future facilities. The upper limits on these kind of processes serve as a very powerful probe to test new models of neutrino masses. In this thesis we analyze the LFV phenomenology generated by two models that induce neutrino masses through different mechanisms. In the first case, we investigate LFV in the the singlet-triplet scotogenic model in which neutrinos acquire non-zero masses at the 1-loop level. In contrast to the most popular variant of this setup, the singlet scotogenic model, this version includes a triplet fermion as well as a triplet scalar, leading to a scenario with a richer dark matter phenomenology. Taking into account results from neutrino oscillation experiments, we explore some aspects of the LFV phenomenology of the model. In particular, we study the relative weight of the dipole operators with respect to other contributions to the LFV amplitudes and determine the most constraining observables. We show that in large portions of the parameter space, the most promising experimental perspectives are found for LFV 3-body decays and for coherent $\mu - e$ conversion in nuclei.
Given that in recent years several observables associated to semileptonic $b \to s$ processes have been found to depart from their predicted values in the SM, including a few tantalizing hints of lepton flavor universality violation. In the second work we consider an existing model with a massive Z' boson that addresses the anomalies in $b \to s$ transitions and extend it with a non-trivial embedding of neutrino masses. We analyze LFV effects induced by the non-universal interaction associated to the $b \to s$ anomalies and by the new physics associated to the neutrino mass generation, and determine the expected ranges for the most relevant observables.

Acknowledgements

I want to begin by expressing my gratitude to Prof. Manuel Drees for giving me the opportunity of carrying out my PhD as part of his group in the BCTP, for his constant support on my research, and for allowing me to join in collaboration with the AHEP group.
I am really greatful to Prof. Jose Valle for welcoming me in the AHEP group to undertake part of my research. To the many members of AHEP that I had the pleasure to meet throughout my visits along these years. In particular I would like to thank Avelino Vicente for taking me under his wing and guiding me throughout my PhD studies. Without his motivation and support I would not be here today.
Over the course of these four years I have split my life between two cities. Bonn became my second home outside Mexico, and I could not have imagined living somewhere else. I am thankful to my friends Roberto, César, Andrés, Ripunjay, Dilege, Charlotte and Lucie, together we enjoyed many moments that I will forever treasure. Even though most of us have parted ways, I am grateful that we continue finding ways to gather and that we are still part of each others lives. Some honorable mentions go to my favorite Greek Elena, thanks for all the good times. To Thaisa for constantly uplifting me. And to Rocio, thank you for always listening to me and helping me whenever you can.
I did not know what to expect the first time I moved to Valencia and I never imagined that I would find so many amazing people. Thank you Ana, Nuria, Tania, Tanya, Valentina, Giulia, Rebecca, Roger, Félix, Carlos, Nico and Roberto. It was a pleasure to spend time with you inside and outside the IFIC and I appreciate all the life lessons that you have given me.
Quiero expresar mi gratitud hacia mis amigas incondicionales Alejandra Galindo y Pilar Rodriguez (PJM) quienes han estado conmigo siempre a distancia en las buenas y en las malas, animándome y haciéndome saber que alguien espera por mí en mi ciudad para seguir compartiendo éxitos y memorias.
I am deeply thankful to the BCTP staff, Christa Boersch, Petra Weiss and Patricia Zuendorf and our IT expert Andreas Wisskirchen, for the efforts they put in helping me through all kinds of personal and legal matters. They saved me from a lot of trouble.
I would be nothing without music, I dedicate these lines as appreciation for the work of a few artist that kept me going when writting this manuscript: Kate Bush, Trent Reznor, Brian Wilson, Nick Cave, Michael Gira, Solange, Maurice Ravel, Robert Smith, Dev Hynes, Johnny Cash, Elton John, Death Grips, Glenn Gould, Kendrick, Marko Haavisto, Atticus Ross, Daniel Caesar, Yaeji and Mina.
I am also indebted to Daniel for always being there. For his love and support through out this time, I am forever grateful.
Quiero agradecer a mi familia: A mis padres, hermanos y sobrinos por apoyarme y echarme porras en cada una de mis decisiones, por brindarme su confianza y sobretodo gracias por creer en mí y por demostrarme día a día que no hay nada más importante que el amor de una familia.
Finally, I thank Mexico and CONACYT for supporting my studies.

Contents

CHAPTER 1

Introduction

From predicting the existence of the massive gauge bosons W and Z, and CP-violation in mesons, to the existence of the Higgs particle, the Standard Model (SM) has successfully explained countless experimental facts [1], some of them at a very precise level [2]. The SM is built as a renormalizable gauge theory [3–5] based on the symmetry group $\mathrm{SU}(3)_C \times \mathrm{SU}(2)_L \times \mathrm{U}(1)_Y$. This structure provides accidental global U(1) symmetries that are not fundamental to the theory. Such is the case of the lepton flavor rotations $\mathrm{U}(1)_e \times \mathrm{U}(1)_\mu \times \mathrm{U}(1)_\tau$, which implies that electron number, muon number and tau number are expected to be conserved. Naturally, the total lepton number associated to $U(1)_L$, the "diagonal" subgroup of $U(1)_e \times U(1)_\mu \times U(1)_\tau$, is a strictly conserved quantity [6]. Acording to numerous experiments, nature seems to obey lepton flavor symmetries in the charged sector. However, in the neutrino sector, the evidence for flavor violation is now established beyond any doubt due to the detection of neutrino oscillations [7–12]. Neutrino flavor transitions can only occur if there is a non-diagonal leptonic mixing matrix and neutrinos have non-zero masses, which is a feature for which the SM does not account in its construction. The incapability of the SM to explain neutrino oscillations is evidence of the existence of new physics (NP). The presence of dark matter (DM) in the universe [13] constitutes another experimental observation that the SM fails to address, as well as the right amount of baryon asymmetry observed in the universe [14].

The established existence of neutrino flavor violation in neutrino oscillations does not necessarily imply that total lepton number is violated. If neutrinos behave like Dirac fermions, the global symmetry $U(1)_L$ may still remain as a good symmetry of the NP Lagrangian. On the other hand, if neutrinos are of Majorana nature, total lepton number must be broken. One expects to distinguish between Dirac and Majorana neutrinos through the detection of processes such as neutrinoless double beta decay [15, 16]. Although an impressive number of experiments have searched for this decay using different isotopes, none of them have provided conclusive results on the nature of neutrinos. The validity of lepton number conservation can help us discriminate between NP models that consider Dirac fermions from those that use Majorana particles for the generation of neutrino masses.

Concerning lepton flavor violation (LFV) in the charged sector, searches for LFV in μ and τ decays at low energy experiments have been analyzed for decades [17], resulting in ever more stringent limits on various LFV observables of the aforementioned particles. The rates of LFV processes cannot be estimated model-independently, however, precision high-intensity experiments are sensitive to the existence of NP at very high energies, which makes flavor physics a powerful discovery tool, as demonstrated by its central role in the making of the SM. Very promising experimental projects in the search for LFV will begin their operation in the near future. In addition to the planned upgrade for the MEG experiment, which will improve its sensitivity to $\mu \to e\gamma$ branching ratios as low as $6 \cdot 10^{-14}$ [18], other new experiments

will also join the effort. Among them, one can highlight the Mu3e experiment [19], which will look for the 3-body decay $\mu \to 3\,e$, as well as a plethora of experiments looking for $\mu - e$ conversion in nuclei, like Mu2e [20–24], DeeMe[25, 26], COMET [27–29] and PRISM/PRIME [30], in all cases with spectacular sensitivity improvements compared to previous experiments. This remarkable multi-channel experimental effort in the search for LFV encourages detailed LFV studies in specific neutrino mass models.
Rare decays are another powerful test of the SM. In recent years, several observables associated to semileptonic $b \to s$ processes have been found to depart from their predicted values in the SM, including a few tantalizing hints of lepton flavor universality violation. It has been pointed out that the violation of lepton flavor universality generically implies the violation of lepton flavor [31]. Although there are several explicit counterexamples to this rule [32, 33], this connection does indeed exist in most of the models introduced to explain the $b \to s$ anomalies. In fact, this connection may be used to learn about neutrino oscillation parameters [34]. However, since many of these models do not account for the observed neutrino masses and mixings, one may question whether the most relevant LFV effects are generally induced by the non-universal interactions associated to the $b \to s$ anomalies or by the NP associated to the generation of neutrino masses. Furthermore, even if the explanation to the $b \to s$ anomalies also involves LFV, the resulting rates could perhaps be too low to be observed by the experiments taking place in the near future.

In this thesis we present the LFV phenomenological analysis of two SM extensions that generate neutrino masses through different mechanisms. In the first model neutrino masses are induced at 1-loop level, whereas, in the second, neutrinos acquire masses at the tree-level in a non-trivial way. Apart from explaining neutrino masses, both models possess a DM candidate. The first scenario that we studied is the singlet-triplet scotogenic model [35]. What stands this model out from the simple singlet and triplet versions is the interplay between the two singlet and triplet fermions that provides a richer phenomenology. The second model under consideration was presented in [36]. This scenario considers a U(1) gauge extension of the SM that leads to the existence of a new massive gauge boson. The resulting Z' boson induces a new neutral current contribution in $b \to s$ transitions and can also mediate the DM production in the early universe. In both cases we determine the expected ranges for the most relevant LFV observables.

The content of this manuscript is organized as follows. Chapter 2 gives an overview of the composition of the electroweak Lagrangian of the SM, as well as a description of the relevant SM parameters. A review of neutrino physics is presented in Chapter 3, which contains theoretical considerations, and the determination of neutrino parameters in current experiments. In Chapter 4 we introduce the most relevant searches of LFV in the charged sector. This chapter also contains important elements for a model-independent treatment of LFV phenomena using an effective approach to the SM. Computational tools that facilitate the analysis of the phenomenological consequences of NP scenarios are reviewed at the end of the chapter. Chapters 5 and 6 contain the research we developed. Chapter 5 focuses on the LFV phenomenology of the singlet-triplet scotogenic model, while Chapter 6 deals with the LFV phenomenology of a Z' model for the $b \to s$ anomalies. Finally, general conclusions about the work carried out along this thesis are stressed in Chapter 7.

1.1 List of publications

Parts of this thesis have been published in the following articles:

i. [37] P. Rocha-Moran, A. Vicente, *Lepton Flavor Violation in the singlet-triplet scotogenic model*,

JHEP **07** (2016) 078, [1605.01915].

ii. [38] P. Rocha-Moran, A. Vicente, *Lepton Flavor Violation in a Z' model for the $b \to s$ anomalies*, *Phys. Rev.* **D99** (2019) 035016, [1810.02135].

CHAPTER 2

The Electroweak Theory

The SM is a gauge theory of the strong, weak and electromagnetic interactions described by the local symmetry group $SU(3)_C \times SU(2)_L \times U(1)_Y$, where the subscripts C, L and Y denote color, left-handed chirality and weak hypercharge, respectively. Each of these gauge groups have their corresponding coupling constant, bosons and generators as listed in Table 2.1. The electromagnetic and weak interactions unify at energies above 100 GeV into the *electroweak (EW) theory* [3–5].
Strong interactions can be studied independently from the EW interactions since the symmetry under $SU(3)_C$ is unbroken and does not mix with the $SU(2)_L \times U(1)_Y$ sector. The color group $SU(3)_C$ constitutes the theory of the strong interactions between quarks and gluons, which is referred to Quantum Chromodynamics (QCD). [1] In the EW theory, left-handed (LH) chiral components of the quarks and leptons are grouped into weak isospin doublets, and those of right-handed (RH) chirality as singlets. Table 2.2 summarizes the gauge charge assignment and the fermion representation, which comes in three copies as we will see later.

In order to have local gauge invariance, one must introduce three SU(2) vector gauge bosons W^i_μ, $i = 1, 2, 3$ and one U(1) vector gauge boson B_μ. These vector bosons are massless, however, they can acquire mass after the spontaneous symmetry breaking (SSB) of the EW theory. The SSB is caused by the Higgs mechanism [39–41], in which a new scalar field is required. The Higgs scalar is a doublet field H with hypercharge $1/2$ and a Higgs potential given by

$$V(H) = \mu^2 H^\dagger H + \lambda (H^\dagger H)^2. \tag{2.1}$$

For μ^2 negative, H develops a vacuum expectation value (VEV) of $v = 246$ GeV, known as the Higgs VEV. The non-zero VEV induces a SSB with the following pattern

$$SU(2)_L \times U(1)_Y \quad \rightarrow \quad U(1)_{Q=T_3+Y}, \tag{2.2}$$

where Q is the electric charge and T_3 is the third component of the weak isospin. After the EW symmetry is broken, the theory remains invariant under gauge transformations that belong to the group $U(1)_Q$. This invariance guarantees the existence of a massless gauge boson associated with the electromagnetic interaction identified as the photon. The fermion masses are also generated by the Higgs mechanism through the presence of Yukawa couplings of the fermion fields with the scalar Higgs doublet. These interactions are incorporated in the EW Lagrangian $\mathcal{L}_{EW}$ described in the following section.

[1] Quarks are color charged fields represented as triplets of $SU(3)_C$, while gluons are octets in the adjoint representation. Given that this work focuses in EW effects, we restrain from providing any information about QCD.

Group	Gauge coupling	Gauge bosons	Generators
$SU(3)_C$	g_s	G^a_μ	$a = 1, ...8$, gluons
$SU(2)_L$	g	W^a_μ	$a = 1, 2, 3$, W bosons
$U(1)_Y$	g'	B_μ	B boson

Table 2.1: SM gauge groups, couplings, bosons and generators

Fermionic field	SU(2) representation	I_3	Y	Q
LH lepton doublet	$l_L = \begin{pmatrix} \nu_e \\ e \end{pmatrix}_L$	$1/2$ $-1/2$	$-1/2$	0 -1
LH quark doublet	$q_L = \begin{pmatrix} u \\ d \end{pmatrix}_L$	$1/2$ $-1/2$	$1/6$	$2/3$ $-1/3$
RH lepton singlet	e_R	0	-1	-1
RH quark singlets	u_R d_R	0	$2/3$ $-1/3$	$2/3$ $-1/3$

Table 2.2: Assignment of third component of the weak isospin I_3, hypercharge Y and charge Q for the first fermion family.

2.1 Electroweak interactions

$\mathcal{L}_{EW}$ is the most general renormalizable Lagrangian invariant under the local symmetry group $SU(2)_L \times U(1)_Y$. It can be divided into four parts,

$$\mathcal{L}_{EW} = \mathcal{L}_{gauge} + \mathcal{L}_H + \mathcal{L}_{kinetic} + \mathcal{L}_{Yukawa}. \tag{2.3}$$

The $\mathcal{L}_{gauge}$ term is the pure gauge Lagrangian

$$\mathcal{L}_{gauge} = -\frac{1}{4} W^i_{\mu\nu} W^{\mu\nu i} - \frac{1}{4} B_{\mu\nu} B^{\mu\nu}. \tag{2.4}$$

With the field strength tensors $W^i_{\mu\nu}$ and $B^{\mu\nu}$ defined as

$$\begin{aligned} W^i_{\mu\nu} &= \partial_\mu W^i_\nu - \partial_\nu W^i_\mu + g\epsilon^{ijk} W^j_\mu W^k_\nu, \\ B_{\mu\nu} &= \partial_\mu B_\nu - \partial_\nu B_\mu, \end{aligned} \tag{2.5}$$

where ϵ^{ijk} is the structure constant. [2] $\mathcal{L}_H$ includes the kinetic term for the scalar H as well as the Higgs scalar potential introduced in Eq. (2.1),

$$\mathcal{L}_H = (D^\mu H)^\dagger D_\mu H - V(H). \tag{2.6}$$

The expanded covariant derivative contains the vector bosons and their corresponding coupling constant

$$D_\mu H = \left(\partial_\mu - ig\vec{\sigma}\vec{W}_\mu - i\frac{g'}{2} B_\mu \right) H, \tag{2.7}$$

[2] In the SU(2) special unitary group, the generators satisfy the algebra $[\sigma_i, \sigma_j] = i\epsilon^{ijk}\sigma_k$, with ϵ^{ijk} corresponding to the Levi-Civita tensor.

where the elements of $\vec{\sigma} = (\sigma_1, \sigma_2, \sigma_3)$ are the Pauli matrices. From the trilinear and quadratic terms in $(D^\mu H)^\dagger D_\mu H$, one gets all the different interactions between the gauge bosons and the Higgs field. The potential $V(H)$ defines the scalar self interactions and the Higgs mass which depends on its VEV v, and the value of the coupling λ. One can obtain the masses of the physical gauge bosons from the product of the covariant derivatives, by omitting the kinetic scalar term and defining the charged and neutral bosons as linear combinations of the fields $W\mu^1$-W_μ^2 and W_μ^3-B_μ respectively

$$\begin{aligned} W_\mu^\pm &= \frac{1}{\sqrt{2}}\left(W_\mu^1 \pm iW_\mu^2\right), \\ Z_\mu &= -\sin\theta_W B_\mu + \cos\theta_W W_\mu^3, \\ A_\mu &= \cos\theta_W B_\mu + \sin\theta_W W_\mu^3, \end{aligned} \tag{2.8}$$

where θ_W is the weak mixing angle. This angle relates the SU(2) and U(1) couplings as $\tan\theta_W = g'/g$. After EW symmetry breaking, the gauge boson A_μ remains massless, thus it can be identified as the photon. On the other hand, the Z and W bosons get the following masses[3]

$$m_W^2 = \frac{v^2 g^2}{4}, \quad m_Z^2 = \frac{v^2}{4}\left(g^2 + g'^2\right). \tag{2.9}$$

The following term in $\mathcal{L}_{EW}$ is the kinetic Lagrangian, which describes the interactions between the gauge bosons and the fermions. For the first generation of leptons and quarks we have

$$\mathcal{L}_{kinetic} = i\overline{l_L}\gamma^\mu D_\mu l_L + i\overline{q_L}\gamma^\mu D_\mu q_L + \sum_{f=e,u,d} i\overline{f_R}\gamma^\mu D_\mu f_R. \tag{2.10}$$

Ignoring the dynamic terms when the covariant derivative is expanded, the relevant terms are

$$\begin{aligned} \mathcal{L}_{kinetic} \supset\ & \bar{l}_L\left(g\vec{\sigma}\vec{W}_\mu - \frac{g'}{2}B_\mu\right)\gamma^\mu l_L + \bar{q}_L\left(g\vec{\sigma}\vec{W}_\mu + \frac{g'}{6}B_\mu\right)\gamma^\mu q_L \\ & -\bar{e}_R g' B_\mu \gamma^\mu e_R + \bar{u}_R \frac{2}{3} g' B_\mu \gamma^\mu u_R - \bar{d}_R \frac{1}{3} g' B_\mu \gamma^\mu d_R. \end{aligned} \tag{2.11}$$

Substituting the gauge bosons for the definitions in Eq. (2.8), one obtains the expressions for the charged currents mediated by the massive W boson, and the neutral currents mediated by the photon and the Z boson.

$$\mathcal{L}_{CC} = \frac{g}{\sqrt{2}}\left(J_\mu^+ W_\mu^+ + \text{H.c.}\right), \tag{2.12}$$

$$\mathcal{L}_{NC} = g\sin\theta_W J_\mu^{em} A^\mu + \frac{g}{\cos\theta_W}\left(J_\mu^3 - \sin^2\theta_W J_\mu^{em}\right) Z^\mu. \tag{2.13}$$

[3] With experimental values: $m_W = 80.379 \pm 0.012$ GeV, $m_Z = 91.1876 \pm 0.0021$ GeV [43].

From the neutral vector current J_μ^{em} interacting with the photon, the fundamental electric charge e is identified as $e = g \sin\theta_W$. The vector currentes J_μ^+, J_μ^3 and J_μ^{em} are defined to be

$$J_\mu^+ = \frac{1}{2}\left[\bar{\nu}\gamma_\mu(1-\gamma_5)e + \bar{u}\gamma_\mu(1-\gamma_5)d\right], \tag{2.14}$$

$$J_\mu^3 = \frac{1}{2}\left[\bar{\nu}_L\gamma_\mu\nu_L - \bar{e}_L\gamma_\mu e_L + \bar{u}_L\gamma_\mu u_L - \bar{d}_L\gamma_\mu d_L\right], \tag{2.15}$$

$$J_\mu^{em} = \sum_{f=e,u,d} q_f \bar{f}\gamma_\mu f, \quad \text{with } q_f = \text{fermion charge}. \tag{2.16}$$

So far, none of these Lagrangian terms make mention of the fermion mass generation. And given that Dirac mass terms are forbidden due to gauge symmetry, the only interactions allowed by the EW theory that achieve massive fermions are those involving couplings between the Higgs scalar and the fermions. These interacions are present in the Yukawa Lagrangian. For the first generation of fermions the Yukawa interactions are

$$\mathcal{L}_{Yukawa} = -y_e\left(\overline{l_L}He_R + \overline{e_R}H^\dagger l_L\right) - y_d\left(\overline{q_L}Hd_R + \overline{d_R}H^\dagger q_L\right) - y_u\left(\overline{q_L}\tilde{H}u_R + \overline{d_R}\tilde{H}^\dagger q_L\right) + \text{H.c.}. \tag{2.17}$$

After the neutral Higgs field acquires a VEV, the fermionic mass terms arise

$$\mathcal{L}_{mass}^f = \frac{v}{\sqrt{2}}y_e\overline{e}_L e_R + \frac{v}{\sqrt{2}}y_d\overline{d}_L d_R + \frac{v}{\sqrt{2}}y_u\overline{u}_L u_R + \text{H.c.}. \tag{2.18}$$

The assigned Dirac mass for each fermion $f = e, d, u$ is proportional to the product of the VEV v and the corresponding Yukawa coupling y_f.

$$m_D^f = \frac{v}{\sqrt{2}}y_f. \tag{2.19}$$

It is important to note that neutrinos remain massless after EW symmetry breaking. However, this is due to the absence of RH neutrinos in the construction of the theory. A more in-depth discussion of neutrinos is presented in Chapter 3. In the following section we focus on the mass and flavor of the three generations of quarks and charged leptons.

2.2 Mass and flavor mixing of fermions

Experimentally, we have observed three different charged leptons e, μ, τ and their corresponding neutrinos ν_e, ν_μ, ν_τ, and six different quark flavors u, d, s, c, b, t. All of these elementary particles can be organized into three families[4] (or generations), as indicated in Table 2.3. Thus, we have three nearly identical copies of the same $SU(2)_L \times U(1)_Y$ structure. As previously pointed out, the masses of the fermions are generated after SSB due to the Yukawa interactions (Eq. (2.17)). The complete fermion mass Lagrangian is then

$$\mathcal{L}_{mass}^f = \overline{\ell}_{Li}\, M_{ij}^\ell\, \ell_{Rj} + \overline{d}_{Li}\, M_{ij}^d\, d_{Rj} + \overline{u}_{Li}\, M_{ij}^u\, u_{Rj} + \text{H.c.}, \tag{2.20}$$

[4] The exact number of families of fermions remains a mystery. Theoretically, the EW theory could accomodate any number of families of the same type. However, EW precision measurements disfavor the possibility of a fourth family [42].

	1st generation	2nd generation	3ed generation
LH lepton doublets	$\begin{pmatrix} \nu_e \\ e^- \end{pmatrix}_L$	$\begin{pmatrix} \nu_\mu \\ \mu^- \end{pmatrix}_L$	$\begin{pmatrix} \nu_\tau \\ \tau^- \end{pmatrix}_L$
RH lepton singlets	e_R	μ_R	τ_R
LH quark doublets	$\begin{pmatrix} u \\ d \end{pmatrix}_L$	$\begin{pmatrix} c \\ s \end{pmatrix}_L$	$\begin{pmatrix} t \\ b \end{pmatrix}_L$
RH quark singlets	d_R, u_R	s_R, c_R	b_R, t_R

Table 2.3: Fermion generations in the SM.

where the subindices $i, j = 1, 2, 3$, denote the family elements: $\ell_i = (e, \mu, \tau)$, $d_i = (d, s, b)$ and $u_i = (u, c, t)$. $M_{ij}^{\ell,d,u}$ is a 3×3 mass matrix defined by the Yukawa matrices $y_{ij}^{\ell,d,u}$ as

$$M_{ij}^{\ell} = \frac{v}{\sqrt{2}} y_{ij}^{\ell}, \quad M_{ij}^{d} = \frac{v}{\sqrt{2}} y_{ij}^{d}, \quad M_{ij}^{u} = \frac{v}{\sqrt{2}} y_{ij}^{u}. \tag{2.21}$$

Given that the EW theory is unable to predict the fermion masses, the three charged lepton masses and the six quark masses are free parameters of the SM, which are determined through experiments [43]. In the case of charged leptons, their physical mass is just the pole of its propagator and can be measured directly

$$\begin{aligned} m_e &= 0.5109989461 \pm 0.0000000031 \text{ MeV}, \\ m_\mu &= 105.6583745 \pm 0.0000024 \text{ MeV}, \\ m_\tau &= 1776.86 \pm 0.12 \text{ MeV}. \end{aligned} \tag{2.22}$$

Since quarks are confined inside hadrons, the extraction of their mass value from experiments is not straightforward. For light quarks u, d, s, masses are estimates of so called "current-quark masses", in a mass independent substraction scheme such as $\overline{MS}$ [5] at a scale $\mu \approx 2$ GeV.

$$\begin{aligned} m_u &= 2.2^{+0.5}_{-0.4} \text{ MeV}, \\ m_d &= 4.7^{+0.5}_{-0.3} \text{ MeV}, \\ m_s &= 95^{+9}_{-3} \text{ MeV}. \end{aligned} \tag{2.23}$$

(2.24)

On the other hand, the identification of heavy quark masses is not particularly hard. One evaluates it at the location of some of its bound states. Their masses are the "running" masses in the $\overline{MS}$ scheme.

$$\begin{aligned} m_c &= 1.275^{+0.025}_{-0.035} \text{ GeV}, \\ m_b &= 4.18^{+0.04}_{-0.03} \text{ GeV}, \\ m_t &= 173.0 \pm 0.4 \text{ GeV}. \end{aligned} \tag{2.25}$$

It is noteworthy that the fermionic mass spectrum follows a hierarchical pattern along families: masses increase as one goes from the first to third generation. The mass spectrum of the charged leptons is dominated almost entirely by the tau-lepton mass. Likewise, quarks of the first family are exceedingly

[5] Modified minimal substraction or MS-bar renormalization scheme [44].

Figure 2.1: Mass spectrum of leptons (blue), quarks (red) and gauge bosons (green).

light in comparison to the third generation quarks. Furthermore, if one includes massive neutrinos, for a given generation the mass of the neutrino is much less than that of the charged lepton, which is, in turn, less than that of the quarks of the associated family. This is illustrated in Figure 2.1, where masses of gauge bosons W and Z are also depicted to serve as reference to the top mass. The line corresponding to neutrino masses indicates an upper bound, since absolute masses are not known yet (see Sec. 3.3.4).

The physical masses measured by experiments are those created by the interactions of the mass eigenstates with the Higgs boson. On the other hand, the weak eigenstates are the members of the $SU(2)_L$ doublets that transform into each other through interaction with $W^{\pm}$ bosons (Eq. (2.12)). Thus, the mass eigenstates are not identical to the weak eigenstates. Nevertheless, the two descriptions can be related. The mass eigenstates ℓ_j, d_j and u_j are determined by the diagonalization of the mass matrices in Eq. (2.21), by means of bi-unitary transformations

$$\mathcal{M}^f = \mathcal{U}_f^{\dagger} M^f \mathcal{V}_f, \quad \text{for } f = \ell, d, u\,. \tag{2.26}$$

Where $\mathcal{U}$ and $\mathcal{V}$ are unitary matrices ($\mathcal{U}^{\dagger}\mathcal{U} = \mathcal{U}\mathcal{U}^{\dagger} = \mathbb{I}$, $\mathcal{V}^{\dagger}\mathcal{V} = \mathcal{V}\mathcal{V}^{\dagger} = \mathbb{I}$), that connect the weak interaction basis to the mass basis

$$f'_{Li} = \mathcal{U}_f f_{Li}, \quad f'_{Ri} = \mathcal{V}_f f_{Ri}. \tag{2.27}$$

Let us write the charge current interaction defined in Eq. (2.12) in the mass basis

$$\mathcal{L}_{cc} = \frac{g}{2\sqrt{2}}\left[\left(\overline{u}'_{Li}\gamma^{\mu}(1-\gamma_5)d'_{Lj} + \overline{\nu}'_{Li}\gamma^{\mu}(1-\gamma_5)\ell'_{Lj}\right)W^{+}_{\mu} + \text{H.c.}\right] \tag{2.28}$$

$$= \frac{g}{2\sqrt{2}}\left[\left(\overline{u}_{Li}\gamma^{\mu}(1-\gamma_5)\,\mathbf{V_{ij}}\,d_{Lj} + \overline{\nu}_{Li}\gamma^{\mu}(1-\gamma_5)\ell_{Lj}\right)W^{+}_{\mu} + \text{H.c.}\right]. \tag{2.29}$$

The purely leptonic charged current of the weak interactions is unaffected by transformations among the charged LH fields, because the transformation matrix $\mathcal{U}_\ell$ can be absorbed by the massless neutrinos. Hence, lepton flavor is conserved in the SM. Whereas, a mixing matrix $\mathbf{V}$ appears in the quark charge-current sector

$$\mathbf{V} = \mathcal{U}_u^{\dagger}\mathcal{U}_d. \tag{2.30}$$

This unitary 3×3 matrix contains all possible flavor-transitions and CP-violation. $\mathbf{V}$ is called the quark flavor mixing matrix, most commonly known as the Cabibbo-Kobayashi-Maskawa (CKM) matrix [45,46]. In order to determine the number of physical parameters of $\mathbf{V}$, we take the case of a general $n \times n$ unitary matrix, which is characterized by n^2 real parameters: $n(n-1)/2$ rotation angles and $n(n+1)/2$ phases. In the case of $\mathbf{V}$ not all phases are physical, since one can rephase the quark fields

$$u_i \to e^{i\theta_i} u_i, \quad d_j \to e^{i\theta_j} u_j \quad \Rightarrow \mathbf{V} \to \mathbf{V} e^{i(\theta_j - \theta_i)}. \tag{2.31}$$

Thus, the number of physical phases is reduced to $(n-1)(n-2)/2$. The total physical free parameters in the quark-mixing is then $(n-1)^2$. For three quark generations, the CKM matrix is described by three rotation angles and one phase. The "standard" CKM parametrization [47] is

$$\begin{aligned} \mathbf{V} &= \begin{pmatrix} 1 & 0 & 0 \\ 0 & c_{23} & s_{23} \\ 0 & -s_{23} & c_{23} \end{pmatrix} \begin{pmatrix} c_{13} & 0 & s_{13}e^{i\delta} \\ 0 & 1 & 0 \\ -s_{13}e^{i\delta} & 0 & c_{13} \end{pmatrix} \begin{pmatrix} c_{12} & s_{12} & 0 \\ -s_{12} & c_{12} & 0 \\ 0 & 0 & 1 \end{pmatrix} \\ &= \begin{pmatrix} c_{12}c_{13} & s_{12}c_{13} & s_{13}e^{i\delta} \\ -s_{12}c_{23} - c_{12}s_{23}s_{13}e^{-i\delta} & c_{12}c_{23} - s_{12}s_{23}s_{13}e^{-i\delta} & s_{23}c_{13} \\ s_{12}s_{23} - c_{12}c_{23}s_{13}e^{-i\delta} & -c_{12}s_{23} - s_{12}c_{23}s_{13}e^{-i\delta} & c_{23}c_{13} \end{pmatrix}. \end{aligned} \tag{2.32}$$

Where $c_{ij} = \cos\theta_{ij}$ and $s_{ij} = \sin\theta_{ij}$ for $i, j = 1, 2, 3$, and δ is the phase responsible for all the CP-violating phenomena [6] observed in K and B meson decays [50, 51] and just recently discovered in D mesons [52], constituting the first evidence of CP-violation in states containing only up-type quarks. The precise determination of the CKM matrix elements is of great importance. Several measurements severely constrain the magnitudes and phases of possible NP contributions to flavor-changing interactions.

Up to date, the predictions of the EW theory have been consistent with experimental data, the discovery of the Higgs particle being one of the most remarkable achievements of the model so far. Nevertheless, this framework fails to determine the number of fermion generations, their masses and their hierarchy. In total the SM contains 18 free paremeters, most of which have been pointed out in this chapter. The fermion sector depends on: six quark masses, three charged lepton masses, three quark mixing angles and one phase. In addition three coupling constants (the strong coupling from QCD included). Two parameters coming from the scalar Higgs sector, the Higgs VEV and a quartic coupling constant. Considering that neutrinos are massive particles the number of independent parameters adds up to 25. The values of all these parameters must be determined from experimental measurements. These theoretical shortcomings are unsatisfactory aspects that compel us to go beyond the SM.

[6] Reviews on CP violation can be found in [48, 49].

CHAPTER 3

Neutrino Physics

At the time the SM was constructed, parity violating experiments [53] showed results where nearly all produced and observed neutrinos had LH helicities, meaning that RH neutrino interactions are absent. Led by these observations, the electroweak theory omitted the introduction of RH components of neutrinos. This is a unique property that only neutrinos possess, since the rest of the SM fermions do have RH components, that allow to construct a mass term (see Eq. (2.18)). The lack of RH neutrinos combined with the renormalizability of the electroweak Lagrangian unables the appearance of a neutrino mass in the SM. In the decade of 1990, the paradigm on neutrino masses changed when anomalies in the solar and atmospheric neutrinos were observed by solar neutrino experiments [8, 54–56], and the neutrino observatories KamLAND [10] and SuperKamiokande (SuperK) [7], providing an indirect but strong evidence that neutrinos are massive and lepton flavors are mixed. Moreover, analysis of the cosmic microwave background anisotropy [13] in combination with other astrophysical data, set constraints on the sum of neutrino masses to be lower than 1 eV [57], indicating that neutrino masses must be very small.
In this chapter we will discuss the possible nature of the small neutrino mass term. The mixing between neutrino eigenstates and how this mixing leads to oscillations. We review the oscillation parameters and the experiments that measure them. Lastly, neutrino mass models and a phenomenological application to test neutrino models are explained.

3.1 Dirac and Majorana masses

The SM can be extended to provide a Dirac mass for the neutrinos in the same fashion the Higgs mechanism generates the masses to the known fermions. To this end, the RH component N_R of the neutrino field needs to be introduced. This field does not take part in electroweak interactions, therefore it must be a singlet under SU(2) and possesses hypercharge equal to zero. This implementation is sometimes called the "minimally extended SM". The extra Yukawa interaction for the case of one neutrino generation coupled to the Higgs is

$$\mathcal{L}^{\nu}_{Yukawa} = -y_{\nu}\overline{l_L}\tilde{H}N_R + \text{H.c.}. \tag{3.1}$$

After electroweak symmetry breaking a Dirac neutrino mass is obtained

$$\mathcal{L}^{\nu}_{m_D} = -\frac{vy_{\nu}}{\sqrt{2}}\left(\overline{\nu}_L N_R + \overline{N}_R \nu_L\right) = -m_D \overline{N}_R \nu_L + \text{H.c.}, \tag{3.2}$$

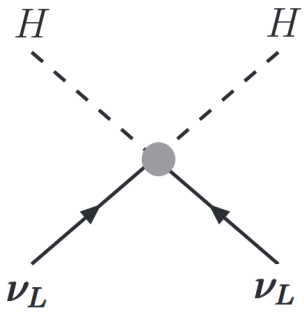

Figure 3.1: Representation of the Weinberg operator.

where $m_D = \frac{v y_\nu}{\sqrt{2}}$, which is the same relation that Dirac masses of charged leptons follow. However, unlike charged leptons, neutrinos are experimentally constrained to have masses below eV (see Sec. 3.3.4). The Yukawa couplings would need to be of the order of $y_\nu \sim 10^{-13}$ to achieve the appropriate values for neutrino masses.
There is another possibility to accomplish the neutrino mass term. Given that neutrinos are electrically neutral, a LH chiral neutrino can be transformed into a RH one under charge conjugation. To illustrate this, we take the Dirac equations for the two chiral fermionic fields $\Psi_{L,R}$

$$i\gamma^\mu \partial_\mu \Psi_L = m\Psi_R, \quad i\gamma^\mu \partial_\mu \Psi_R = m\Psi_L. \tag{3.3}$$

When charge conjugating the equation on the right

$$C\left(i\gamma^\mu \partial_\mu \Psi_R = m\Psi_L\right) \rightarrow i\gamma^\mu \partial_\mu \Psi_R^c = m\Psi_L^c\,, \tag{3.4}$$

it turns out to be identical to the equation on the left if

$$\Psi_L^c = C\bar{\Psi}_L^T \equiv \Psi_R, \tag{3.5}$$

where the C symbol stands for the Lorentz charge conjugation matrix $C = i\sigma^2$. The relation above is called the Majorana condition, which can only be satisfied by electrically uncharged particles. Assuming that neutrinos follow the Majorana condition in Eq. (3.5), a Majorana mass term for the neutrino is allowed by Lorentz symmetry. It can be derived from Eq. (3.2) by replacing N_R for ν_L^c,

$$\mathcal{L}^\nu_{m_M} = -\frac{1}{2} m_M \overline{\nu_L^c} \nu_L + \text{H.c.} \tag{3.6}$$

The factor of $1/2$ is introduced to avoid double counting given that a Majorana fermion is in fact its own antiparticle. This implies that a Majorana mass term for neutrinos breaks any global U(1) symmetry under which ν_L is charged. In particular, it violates lepton number by two units.

3.1.1 The Weinberg operator

The Majorana mass term presented in Eq. (3.6) carries hypercharge equal to -1. Thus, it is not gauge invariant, and cannot be introduced directly in the SM Lagrangian. Nevertheless, there is a possibility to generate an invariant mass term while using SM fields. This is realized through the non-renormalizable 5-dimensional Weinberg operator [58], which is the lowest order operator that generates Majorana neutrino masses. The effective Weinberg operator can be written as follows

$$\mathcal{L}_5 = \frac{C^{(5)}}{\Lambda}\left(\overline{l_L^c}\tilde{H}^*\right)\left(\tilde{H}^\dagger l_L\right) + \text{H.c.}, \tag{3.7}$$

where $C^{(5)}$ is a coupling constant, and Λ is a parameter with dimensions of mass, which can be interpreted as the NP energy scale at which this operator is induced. After electroweak symmetry breaking, the Majorana mass term comes to be

$$\mathcal{L}_{\text{eff}} = \frac{1}{2}C^{(5)}\frac{v^2}{\Lambda}\overline{\nu_L^c}\nu_L + \text{H.c.}, \tag{3.8}$$

where the Majorana mass is identified as

$$m_M = C^{(5)}\frac{v^2}{\Lambda}. \tag{3.9}$$

In order to accomodate $m_\nu < 1$ eV neutrino masses, if $C^{(5)} \sim 1$, Λ must come from a NP scale of the order of 10^{14} GeV, which is close to the unification scale of electroweak and strong interactions. Although the Majorana mass term for neutrinos generated through the Weinberg operator conserves electric charge, it still breaks the total lepton number conservation. This might be interpreted as a consequence of the SM being an effective low-energy theory of a much more general theory at higher energies [59–61].
The Majorana and Dirac descriptions have different phenomenological consequences, making a Majorana neutrino distinguishable from a Dirac one. Most of the theories beyond the SM have considered neutrinos as Majorana particles, but so far no experimental proof supports this assumption. The most promising way to find the nature of the neutrino is from the search of neutrinoless double beta decay detection [15, 16, 62, 63].

3.2 Neutrino oscillations

Neutrino flavor oscillations are a consequence of the existence of nonzero neutrino masses and lepton flavor mixing. Speculations of neutrino mixing date from 1957 when B. Pontecorvo [64] motivated by Gell-Mann and Pais theory of $K^0 - \bar{K}^0$ mixing and oscillations [65], considered a transition of a mesonium bound system (μ^+e^-) into antimesonium (μ^-e^+) intermediated by neutrino-antineutrino mixed states. Hints on additional global lepton charge sparked from Davis radiochemical experiment [66]. Thus, Pontecorvo suggested a more realistic case of oscillations between two different types of neutrinos [67]. A couple of years later, in 1959 Pontecorvo proposed that the two types of neutrinos are associated to different reactions [68]. Considering the muon decay as example

$$\mu^- \to e^- + \bar{\nu}_e + \nu_\mu, \tag{3.10}$$

it was required for the resulting neutrinos to not be identical. One of them was asociated to the electron (ν_e) and the other to the muon (ν_μ). A direct proof of the existence of the muon neutrino was obtained in the first experiment with accelerator neutrinos in 1962 in the Brookhaven experiment [69]. With this discovery the concept of lepton flavor number appeared, with $L_e = 1$ for e^- and ν_e, and $L_\mu = 1$ for μ^- and ν_μ. The first intuitive understanding of two-flavored neutrino mixing and oscillations was presented by Z. Maki, M. Nakagawa, S. Sakata [70] in 1962 and Pontecorvo [71] in 1967.
To understand how neutrinos oscillate, it is convenient to start with the simplest scenario, the two-neutrino mixing. Suppose a neutrino ν_α produced in a certain source travels a path with length L until it reaches a detector, the neutrino reacts with the detector and produces a charged lepton ℓ_β. Thus, the final state of

the neutrino is ν_β (Fig. 3.2). If $\alpha \neq \beta$, the neutrino has suffered a flavor change in its journey $\nu_\alpha \rightarrow \nu_\beta$, and one can find out the probability of this transition. To this end, let us describe the neutrino ν_α as a superposition of the mass eigenstates ν_i

$$|\nu_\alpha\rangle = \sum_i U_{\alpha i}|\nu_i\rangle, \tag{3.11}$$

where U is a unitary 2×2 mixing matrix

$$U = \begin{pmatrix} \cos\theta & \sin\theta \\ -\sin\theta & \cos\theta \end{pmatrix}. \tag{3.12}$$

After a time t the initial state evolves as described by the plane wave solution

$$|\nu_\alpha(t)\rangle = \sum_i U_{\alpha i} e^{-iE_i t}|\nu_i(0)\rangle \tag{3.13}$$

$$= e^{-iE_1 t}\cos\theta|\nu_1\rangle + e^{-iE_2 t}\sin\theta|\nu_2\rangle. \tag{3.14}$$

Then, the probability of ν_α oscillating into ν_β after a time t has elapsed is,

$$P_{\nu_\alpha \rightarrow \nu_\beta}(t) = |\langle\nu_\beta|\nu_\alpha(t)\rangle|^2 \tag{3.15}$$

$$= \sin^2(2\theta)\sin^2\left(\frac{E_2 - E_1}{2}t\right). \tag{3.16}$$

Here E_i is the energy of ν_i in the detector frame. Assuming all mass eigenstates have the same momentum, in the ultrarelativistic limit $p \gg m_i$, E_i is given by the relativistic energy-momentum relation

$$E_i = \sqrt{p^2 + m_i^2} = p + \frac{m_i^2}{2p} \approx E + \frac{m_i^2}{2E}. \tag{3.17}$$

Since in this limit $t \sim L$, and $E_2 - E_1 = \Delta m^2/2E$, where $(m_2^2 - m_1^2) \equiv \Delta m^2$, the oscillation probability is rewritten as

$$P_{\nu_\alpha \rightarrow \nu_\beta}(t) = \sin^2(2\theta)\sin^2\left(\frac{\Delta m^2 L}{4E}\right) \tag{3.18}$$

$$= \sin^2(2\theta)\sin^2\left(1.27\frac{\Delta m^2\left[\mathrm{eV}^2\right]L\,[\mathrm{Km}]}{4E\,[\mathrm{GeV}]}\right), \tag{3.19}$$

where the former equation has been expressed in natural units, whereas the latter in SI units. From this probability equation we note that neutrino oscillation is dictated by the angle θ, the mass squared difference Δm^2, the neutrino energy E and the distance between the neutrino source and the detector. The angle θ defines how mixed the flavor states are in the mass states. If $\theta = 0$, no mixing occurs, thus neutrinos cannot oscillate. Moreover, at least one of the neutrinos must have mass in order to generate oscillations. For neutrino oscillation experiments, knowledge of the flux of each neutrino and antineutrino flavor at production is needed for planning and designing the experiment, analyzing the data, and estimating systematic errors. The ratio L/E can be controlled in experiments with terrestrial neutrino sources, such as accelerators and nuclear reactors, with L/E fixed one can deduce how sensitive an experiment will be to the neutrino mass squared difference, $\min(\Delta m^2) \sim 2E/L$. If neutrinos are naturally

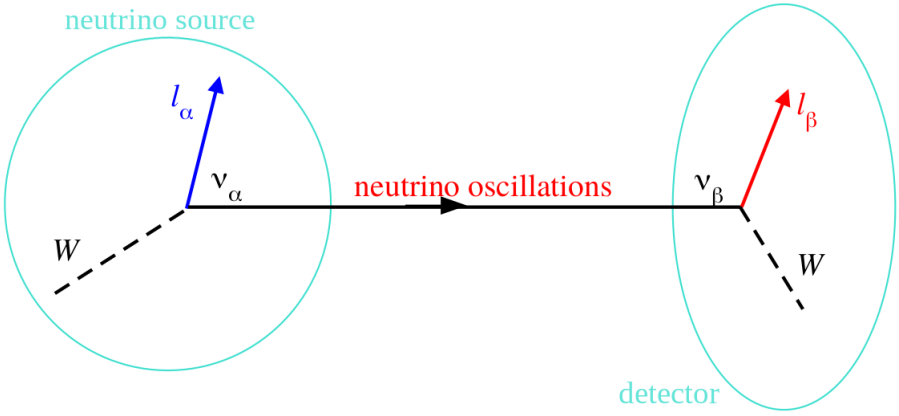

Figure 3.2: Neutrino transition $\nu_\alpha \to \nu_\beta$ from source to detector.

produced as is the case of solar and atmospheric neutrinos, their fluxes as well as the distance between the neutrino source and the detector cannot be controlled artificially. The three flavor eigenstates ν_e, ν_μ and ν_τ can be distinguished since they are produced by different reactions. However, absolute values of the neutrino masses at present are unknown, although bounds on the sum of all masses can be obtained from the observation of anisotropies in the cosmic microwave background.

When neutrinos propagate through matter the transition probabilities are changed, due to the charged current interactions between the electron neutrinos(antineutrinos) and electrons in matter. This may lead to a resonant transition that enhances the oscillation probability under certain conditions. Such effect is usually called the Mikheyev, Smirnov, Wolfenstein (MSW) effect [72, 73]. Following the 2-neutrino picture, the effect on oscillation probabilities in matter is quantified to be proportional to the number density of electrons in matter N_e. The mixing angle θ and the mass squared difference Δm^2 in Eq. (3.18) are replaced for their analog in matter θ_m and Δm^2_m

$$P_{\nu_\alpha \to \nu_\beta}(t) = \sin^2(2\theta_m)\sin^2\left(\frac{\Delta m^2_m L}{4E}\right). \tag{3.20}$$

The expressions for the effective mixing parameters in matter are

$$\sin(2\theta_m) = \frac{\sin(2\theta)}{C}, \tag{3.21}$$

$$\Delta m^2_m = C\Delta m^2, \tag{3.22}$$

with

$$C = \sqrt{(\cos(2\theta) - A)^2 + \sin^2(2\theta)}, \qquad \text{and} \quad A = \pm\frac{2\sqrt{2}G_F N_e E}{\Delta m^2}, \tag{3.23}$$

where G_F is the Fermi constant. The positive sign in A applies to electron-neutrino transitions, whereas the negative sign to the electron-antineutrino ones. In three-flavor neutrino oscillations, the transition probabilities are dependent of the δ CP-phase. [7] The probabilities of $\nu_\alpha \to \nu_\beta$ and the antineutrino pair $\bar{\nu}_\alpha \to \bar{\nu}_\beta$ are related as [74]

$$P_{\bar{\nu}_\alpha \to \bar{\nu}_\beta} = P_{\nu_\alpha \to \nu_\beta}(\delta \to -\delta, A \to -A). \tag{3.24}$$

[7] δ is a parameter of the 3×3 leptonic mixing matrix U that we will derive in Sec. 3.2.1.

The effect on neutrino and antineutrino oscillations caused by matter can be significant in long-baseline experiments with sufficiently high energies, making them sensitive to the neutrino mass ordering.
A more detailed description of neutrino experiments, oscillation parameters and neutrino mass ordering is exhibited in Sec. 3.3. First, we dedicate the next section to the construction of the unitary matrix that mixes the neutrino flavor eigenstates into the three physical neutrino mass states.

3.2.1 Leptonic mixing matrix

To derive a more general leptonic mixing matrix U, a parameter counting analogous to the quark mixing in Sec. 2.2 is performed. In the case of n neutrino flavors and n massive neutrinos, the $n \times n$ unitary mixing matrix U can be parameterized by $n(n-1)/2$ rotation angles and $n(n+1)/2$ phases. If the massive neutrinos ν_i are Dirac particles, only $(n-1)(n-2)/2$ phases are physical and can be responsible for CP violation (CPV) in the lepton sector. For $n = 3$ there is just one CPV phase in U, which is usually called the "Dirac CP violating phase". If, however, the massive neutrinos are Majorana fermions, the mixing matrix U contains $n(n-1)/2$ CPV phases [75, 76]. In contrast to Dirac fields, the massive Majorana neutrino fields cannot absorb phases. In this case U can be cast in the form [75]

$$U \;=\; V\,P, \tag{3.25}$$

where the matrix V contains $(n-1)(n-2)/2$ Dirac CPV phases, while P is a diagonal matrix with the additional $(n-1)$ Majorana CPV phases

$$P = \mathrm{diag}(1, e^{i\frac{\alpha_{21}}{2}}, e^{i\frac{\alpha_{31}}{2}}, ..., e^{i\frac{\alpha_{n1}}{2}}) \tag{3.26}$$

In the case of $n = 3$ there are altogether 3 CPV phases: one Dirac and two Majorana. The 3 neutrino mixing matrix U can be constructed by considering rotations between the mass eigenstates $\nu_1 - \nu_2$, $\nu_2 - \nu_3$ and $\nu_1 - \nu_3$ by the angles θ_{12}, θ_{23} and θ_{13} respectively

$$U = \begin{pmatrix} c_{12}c_{13} & s_{12}c_{13} & s_{13}e^{i\delta} \\ -s_{12}c_{23} - c_{12}s_{23}s_{13}e^{-i\delta} & c_{12}c_{23} - s_{12}s_{23}s_{13}e^{-i\delta} & s_{23}c_{13} \\ s_{12}s_{23} - c_{12}c_{23}s_{13}e^{-i\delta} & -c_{12}s_{23} - s_{12}c_{23}s_{13}e^{-i\delta} & c_{23}c_{13} \end{pmatrix} \begin{pmatrix} 1 & 0 & 0 \\ 0 & e^{i\alpha} & 0 \\ 0 & 0 & e^{i\beta} \end{pmatrix}. \tag{3.27}$$

Here the Dirac CPV phase is labeled as δ, and the Majorana phases as α and β. We denote $c_{ij} = \cos\theta_{ij}$ and $s_{ij} = \sin\theta_{ij}$ for $i, j = 1, 2, 3$.
The U matrix in Eq. (3.27) is the standard leptonic mixing matrix [8], which contains all the existing data on neutrino oscillations, and diagonalizes the neutrino mass matrix m_ν as

$$U^T\, m_\nu\, U = \widehat{m}_\nu \equiv \begin{pmatrix} m_1 & 0 & 0 \\ 0 & m_2 & 0 \\ 0 & 0 & m_3 \end{pmatrix}. \tag{3.28}$$

3.3 Neutrino parameters and experiments

Different experiments aim to determine different neutrino properties. Measurements of the mixing angles θ_{12}, θ_{23}, θ_{13}, the mass parameters Δm^2_{21}, $|\Delta m^2_{31}|$, [9] and the Dirac phase δ are accessible to neutrino

[8] This parametrization of U is commonly known as Pontecorvo-Maki-Nakagawa-Sakata (PMNS) matrix.
[9] Experiments show that $\Delta m^2_{21} \ll \Delta m^2_{32}$ so that the third square mass difference is $\Delta m^2_{32} \approx \Delta m^2_{31}$ [77].

oscillation experiments. The absolute scale of neutrino masses is searched in beta decay experiments and in cosmological observations. Neutrinoless double beta decay experiments, sensitive to lepton number violation, can yield information about the Majorana phases α and β in the case of Majorana neutrinos, as well as determination of the lightest neutrino mass state. Experiments in astrophysics and cosmology have the potential to unveil more neutrino properties. Table 3.1 summarizes the most relevant neutrino experiments currently, and the parameters they can measure.

Parameters	Experiments
$\Delta m^2_{21}, \theta_{12}$	Solar: SAGE [78], SuperK [79–82], SNO [83, 84], GALLEX [85], Borexino [86] Earth: KamLAND [87]
$\Delta m^2_{31}, \theta_{23}$	Atmos.: SuperK [88], ANTARES [89], IceCube-DeepCore [90] Acce.: K2K [91], MINOS [92], OPERA [93], T2K [12], NOνA [94]
$\Delta m^2_{31}, \theta_{13}$	Reactors: Daya Bay [95], Double CHOOZ [96], RENO [97] T2K [98], NOνA
δ	NOνA [99], T2K, SuperKamiokande
sign$\left(\Delta m^2_{31}\right)$	NOνA, T2K, SuperKamiokande
m_i, (absolute nuetrino masses)	$0\nu\beta\beta$: HM [100], GERDA [101], CUORE [102], KamLAND-Zen [103], EXO-200 [104], MAJORANA [105] β decay: MAINZ [106], TROITSK [107], KATRIN [108, 109] Cosmology: Planck [13]
N_ν, (# of active and light neutrinos)	LEP [42]
n_s, (# of neutrinos)	LSND [110], MiniBooNE [111], Cosmology

Table 3.1: List of current experiments for the detection of neutrino properties.

3.3.1 Measurement of Δm^2_{21} and θ_{12}

Nuclear reactions in the interior of the sun produce neutrinos continuously. These solar neutrinos are electron neutrinos characterized by different energy spectra depending on the reaction they are being produced by. The $p + p \rightarrow d + e^+ + \nu_e$ reaction generates the largest contribution of ν_e neutrinos, but with quite a small energy, $E < 0.42$ MeV. The reaction with the largest energy spectrum, extending up to more than 10 MeV, is the boron-8 beta-decay into beryllium-8, ${}^8B \rightarrow {}^8 Be^* + e^+ + \nu_e$. However, this is the reaction with the smallest flux. The SuperK and Sudbury Neutrino Observation (SNO) are the only neutrino experiments that detect the B solar neutrinos, based on the reactions of electrons in water. Historically, the chlorine based radiochemical detector in the mine of Homestake [56] was the first experiment to notice the neutrino deficit in the solar neutrino flux, which contradicted the predictions made by the standard solar model [112], and consequently led to consider the oscillation of neutrinos. Nowadays, it is mainly through SuperK [79–82] and SNO [83, 84], together with Borexino [86] and KamLAND [87] liquid scintillation detectors, that Δm^2_{21} and θ_{12} are experimentally determined. Though, KamLAND uses terrestrial antineutrinos ($\bar{\nu}_e$) emitted by nuclear reactors.

3.3.2 Measurement of $|\Delta m^2_{31(32)}|$ and θ_{23}

The collision of cosmic rays with nuclei in the upper atmosphere produces charged pions $\pi^{\pm}$, which chain decay into neutrinos

$$\pi^{\pm} \rightarrow \mu^{\pm} + \nu_{\mu}(\bar{\nu}_{\mu}) \tag{3.29}$$
$$\rightarrow e^{\pm} + \nu_e(\bar{\nu}_e) + \bar{\nu}_{\mu}(\nu_{\mu}) + \nu_{\mu}(\bar{\nu}_{\mu}). \tag{3.30}$$

Charged pion decays are the main production channel of atmospheric neutrinos. Almost all atmospheric neutrino experiments are placed deep underground to shield from cosmic ray muons. In the case of accelerator neutrino beams, the pulsed nature of the beam provides additional background suppression. [10] If neutrinos are not distinguished from antineutrinos, two ν_{μ} are expected for each ν_e in first approximation, $R_{e\mu} \equiv \frac{N(\nu_{\mu})}{N(\nu_e)} \simeq 2$. In 1998, SuperK provided a measurement of the ratio $R_{e\mu}$ being about 0.6 times the theoretical expectation, indicating that the ν_{μ} deficit was a consequence of ν_{μ} transitioning into ν_{τ}. This result became the first compelling evidence of neutrino oscillation. The experimental values of $|\Delta m^2_{31(32)}|$ and θ_{23} obtained in the atmospheric oscillations discovery needed a confirmation by accelerator neutrino experiments in which the neutrino beam is tunable and has high purity. Independent confirmation came from K2K [91] (KEK to Kamioka), MINOS [92] (Main Injector Neutrino Oscillations), and T2K [12] (Tokai to Kamioka). The most recent confirmation comes from the NOνA [94] (NuMI Off-Axis ν_e Appearance) collaboration results. The most precise measurements of $|\Delta m^2_{31}|$ and θ_{23} are currently obtained by T2K [98].

3.3.3 Measurement of θ_{13}

After the discoveries of solar and atmospheric neutrino oscillations, the determination of θ_{13} seemed a natural step towards the completion of the 3-ν mixing picture. Above that, a not too small θ_{13}, enhances the opportunity to measure the unknown Dirac CPV phase δ. First hints for θ_{13} came from solar experiments. However, they were confirmed until recently by reactors. In 2012, the reactor neutrino oscillation experiments Daya Bay [95], Double CHOOZ [96] and RENO [97], obtained θ_{13} from the measurements of reactor $\bar{\nu}_e$ disappearance.

The results of the global fit on neutrino oscillation parameters reported in [77], are displayed in Tables 3.2 and 3.3. This analysis fits data of the solar, atmospheric, reactors and long-baseline of most of the experiments mentioned in Table 3.1.

Parameter	Best fit $\pm 1\sigma$	2σ	3σ
$\Delta m^2_{21}[10^{-5}\text{eV}^2]$	$7.55^{+0.20}_{-0.16}$	7.20 – 7.94	7.05 – 8.14
$\Delta m^2_{31}[10^{-3}\text{eV}^2]$ (NO)	2.50 ± 0.03	2.44 – 2.57	2.41 – 2.60
$\Delta m^2_{31}[10^{-3}\text{eV}^2]$ (IO)	$2.42^{+0.03}_{-0.04}$	2.34 – 2.47	2.31 – 2.51

Table 3.2: Neutrino mass square differences from global data [77].

[10] Telescopes for high-energy neutrinos (TeV~PeV) such as ANTARES [89] and IceCube-DeepCore [90] have a depth of 2500 m and 1450-2450 m respectively.

Parameter	Best fit $\pm 1\sigma$	2σ	3σ
$\sin^2\theta_{12}$	$0.320^{+0.020}_{-0.016}$	0.289 – 0.359	0.273 – 0.379
$\sin^2\theta_{23}$ (NO)	$0.547^{+0.020}_{-0.030}$	0.467 – 0.583	0.445 – 0.599
$\sin^2\theta_{23}$ (IO)	$0.551^{+0.018}_{-0.030}$	0.491 – 0.584	0.453 – 0.598
$\sin^2\theta_{13}$ (NO)	$0.0216^{+0.00083}_{-0.00069}$	0.0203 – 0.0234	0.0196 – 0.0241
$\sin^2\theta_{13}$ (IO)	$0.0222^{+0.00074}_{-0.00076}$	0.0207 – 0.0236	0.0199 – 0.0244
δ/π (NO)	$1.32^{+0.21}_{-0.15}$	1.01 – 1.75	0.87 – 1.94
δ/π (IO)	$1.56^{+0.13}_{-0.15}$	1.27 – 1.82	1.12 – 1.94

Table 3.3: Leptonic mixing parameters from global data [77].

3.3.4 The absolute mass scale

Neutrino oscillation phenomena do not depend on the absolute values of neutrino masses but on their squared mass differences. The two independent mass squared differences between the neutrino mass eigenstates can be found from solar (Δm^2_{21}) and atmospheric (Δm^2_{31}) neutrino observations (Table 3.2). Since the mass spectrum of charged leptons exhibit the hierarchy $m_{e_1} < m_{e_2} < m_{e_3}$, which is followed in a similar way in the quark sector (Fig 2.1), this arrangement is considered to be "normal". In the neutrino sector, by definition, we call ν_1 and ν_2 the two neutrinos whose masses are closer in value, with $m_1 < m_2$. The third mass eigenstate has a larger separation in mass from $\nu_{1,2}$. In view of the lack of information about the absolute values of the mass states, two mass orderings are possible, ν_3 can be either heavier or lighter than $\nu_{1,2}$:

- $m_1^2 < m_2^2 < m_3^2$ Normal ordering (NO).
- $m_3^2 < m_1^2 < m_2^2$ Inverse ordering (IO).

There are several methods for the determination of neutrino mass ordering. In the following we summarize each of them and present their current bounds on the neutrino mass scale.

i) Endpoint of beta spectrum

Beta decay experiments are based on the idea that non-vanishing neutrino masses cause kinematic effects that are reflected in the electron spectrum, more specifically in its endpoint. Tritium $\left({}^3H\right)$ is often used as decaying nucleus in beta decay experiments

$$ {}^3H \rightarrow {}^3He + e^- + \bar{\nu}_e. \tag{3.31} $$

The decay spectrum depends in general on the mass of the effective eletron neutrino ν_e which is composed of the three mass eigenstates and their masses

$$ m^2_{\nu_e} = \sum_{i=1}^{3} |U_{ei}|^2 m_i^2 = c_{13}^2 \left(m_1^2 c_{12}^2 + m_2^2 s_{12}^2\right) + m_3^2 s_{13}^2. \tag{3.32} $$

The present bounds for the effective electron neutrino mass comes from the Mainz [106] and Troitsk [107] experiments

$$ m_{\nu_e} < \begin{cases} 2.30 \text{ eV} & (95\% \text{ C.L.}) \quad \text{MAINZ} \\ 2.05 \text{ eV} & (95\% \text{ C.L.}) \quad \text{TROITSK} \end{cases} \tag{3.33} $$

The KATRIN experiment [109] expects to obtain a sensitivity of 0.2 eV at 90% confidence level.

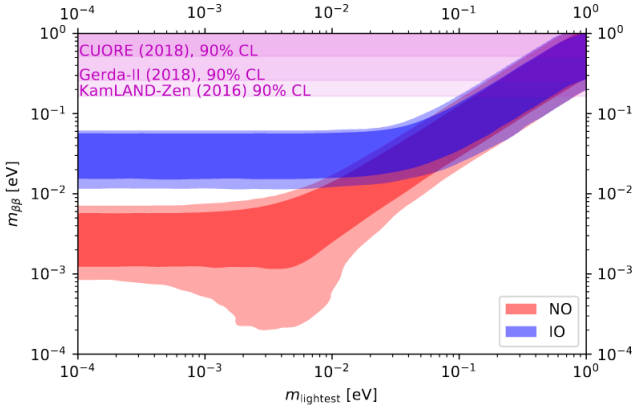

Figure 3.3: Effective Majorana neutrino mass $m_{\beta\beta}$ as function of the mass of m_{light} for the two mass ordering schemes in contrast with the most competitive upper bounds [114].

ii) $0\nu2\beta$ experiments

Neutrinoless double beta decays are only possible if neutrinos are Majorana particles. These decays are lepton number violating processes of the type

$$(A, Z) \to (A, Z + 2) + 2e^{-}, \tag{3.34}$$

with no neutrinos emitted. This signal would allow to measure the combination

$$m_{\beta\beta} = \sum_{i=1}^{3} U_{ei}^2 m_i = c_{13}^2 \left(m_1 c_{12}^2 + m_2 s_{12}^2 e^{2i\alpha} \right) + m_3 s_{13}^2 e^{2i(\beta-\delta)}, \tag{3.35}$$

where $m_{\beta\beta}$ is the first element of the light neutrino mass matrix in the flavor basis. These experiments are particularly challenging. Furthermore, the extraction of $m_{\beta\beta}$ from a positive signal would have large theoretical errors due to uncertaties in the computation of the nuclear matrix elements [113]. The experiments with the most stringent bounds are currently GERDA [101], CUORE [102] and KamLAND-Zen [103], using the isotopes ^{76}Ge, ^{130}Te and ^{136}Xe, respectively.

$$m_{\beta\beta} < \begin{cases} 0.12 - 0.26 \text{ eV} & (90\% \text{ C.L.}) \quad \text{GERDA} \\ 0.11 - 0.52 \text{ eV} & (90\% \text{ C.L.}) \quad \text{CUORE} \\ 0.061 - 0.165 \text{ eV} & (90\% \text{ C.L.}) \quad \text{KamLAND-Zen} \end{cases} \tag{3.36}$$

The ranges account for different theoretical calculations of the nuclear matrix elements. Figure 3.3 shows the effective Majorana neutrino mass $m_{\beta\beta}$ as function of the mass of the lightest neutrino m_{light}. Taking into account the current uncertainties on the neutrino mixing angles and phases for three neutrinos, the red(blue) region corresponds to normal(inverted) ordering. The horizontal lines indicate the upper bounds from the experiments in (3.36), where the disfavored value for the nuclear matrix element of each process is assumed.

iii) Cosmology

Cosmological effects of massive neutrinos are present in the Cosmic Microwave Background (CMB) and in the formation of Large Scale Structures (LSS) in the universe. Neutrinos that turn non-relativistic

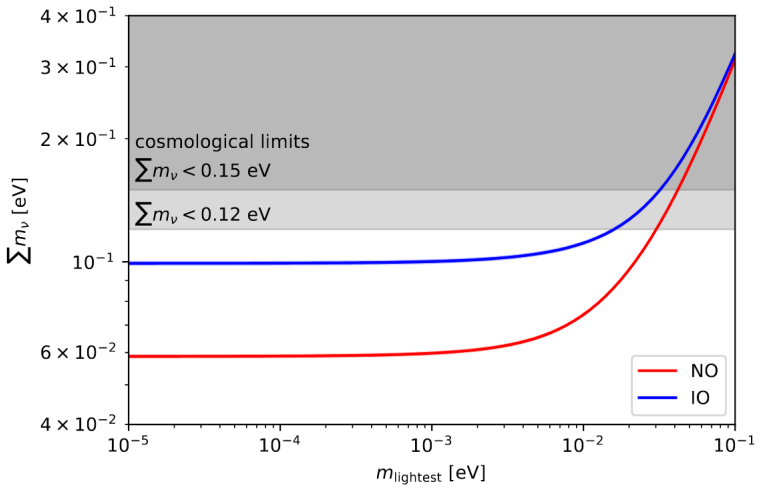

Figure 3.4: Values of $\sum m_\nu$ as function of the lightes neutrino mass for the two possible ordering schemes and the two representative bounds on the sum of the neutrino masses from cosmology [114].

around the decoupling period contribute to the mass density of the universe. With their energy density given by $\rho_\nu \simeq n_\nu \sum m_\nu$, where n_ν is the neutrino number density and $\sum m_\nu$ the sum of non-relativistic neutrino masses, the total neutrino density today can be computed using measurements of the CMB temperature [115]. Thus, one can obtain an upper bound for the sum of neutrino masses. Some additional constraints to take into account are data from CMB lensing, Baryon Acoustic Oscillations, Supernovae Ia luminosity distance and also direct measurements of the Hubble constant. Stronger bounds are set by combining the available data on CMB and the LSS cosmological model. For different scenarios [57, 116–121] the upper limits on the sum of neutrino masses range as

$$\sum m_\nu \lesssim 0.12 - 0.15 \text{ eV} \qquad (95\% \text{ C.L.}). \tag{3.37}$$

Figure 3.4 shows the sum of neutrino masses $\sum m_\nu$ as a function of m_{light}, with $m_1 = m_{\text{light}}$ for normal ordering represented in red and $m_3 = m_{\text{light}}$ for inverted ordering in blue. The (indistiguishable) width of the lines correspond to the 3σ values of Δm^2_{ij} from table 3.2. The horizontal bands illustrate the two upper limits given in Eq. (3.37). With stronger cosmological measurements ($\sum m_\nu \lesssim 0.1$ eV) the inverted ordering can be ruled out.

iv) Neutrino oscillation facilities

Global fits to neutrino oscillation data from long-baseline and atmospheric neutrino experiments are sensible to the neutrino mass ordering, since it is highly correlated to the true value of the δ CP phase. A 3.4σ preference in favor of NO is obtained by the global fit in [77]. Combining more precise data from NOνA, T2K and SuperK experiments can lead to even higher sensitivities.

For a more in depth discussion on future prospects for the determination of neutrino mass ordering and the absolute mass scale we suggest the review [114].

3.4 Models for neutrino mass generation at tree-level

As we have pointed out in Sec. 3.1.1, the Weinberg operator is the lowest order operator that generates Majorana neutrino masses. Throughout Sec. 3.3 we presented the up to date experimental data of neutrino squared mass differences and mixing angles, and how several methods constrain the absolute neutrino masses to be very small. In this section we will show a scheme that generates small neutrino masses through the Weinberg operator described in Eq. (3.7) at tree level with renormalizable interactions. It consists in adding a new heavy state to the SM, which acts as a messenger between the leptons and Higgs. The heaviness of the new state is what enables neutrinos to get light masses. Such a mechanism receives the name of *seesaw* [76, 122–126].
The idea around the seesaw mechanism is illustrated in the following. Assuming right-handed neutrinos N_R, the most general neutrino mass term involves the mass of Dirac m_D defined in Eq. (3.2) and the Majorana mass M_R of the RH neutrinos N_R. In the basis $n_L^T = (\nu_L, N_R^c)$ the total mass term is expressed as

$$\mathcal{L}_{m_{D+M}} = -\frac{1}{2} n_L^T \, C \, \mathcal{M}_n \, n_L + \text{H.c.} \tag{3.38}$$

$$= -\frac{1}{2} (\nu_L \, N_R^c) \begin{pmatrix} 0 & m_D \\ m_D^T & M_R \end{pmatrix} \begin{pmatrix} \nu_L^c \\ N_R \end{pmatrix} + \text{H.c.}. \tag{3.39}$$

Assuming $m_D \ll M_R$, the neutrino mass matrix $\mathcal{M}_n$ can be block-diagonalized to obtain

$$W^T \mathcal{M}_n W \simeq \begin{pmatrix} m_{\text{light}} & 0 \\ 0 & m_{\text{heavy}} \end{pmatrix}, \tag{3.40}$$

with

$$W \simeq \begin{pmatrix} 1 - \frac{1}{2} m_D^\dagger (M_R M_R^\dagger)^{-1} m_D & (M_R^{-1} m_D)^\dagger \\ -M_R^{-1} m_D & 1 - \frac{1}{2} M_R^{-1} m_D m_D^\dagger (M_R^\dagger)^{-1} \end{pmatrix}. \tag{3.41}$$

Substituing the expression above in the Eq. (3.40) one finds m_{light} and m_{heavy} in terms of m_D and M_R

$$m_{\text{light}} \approx -m_D^T M_R^{-1} m_D \approx \frac{v^2}{2} y_\nu^T m_N^{-1} y_\nu, \tag{3.42}$$

$$m_{\text{heavy}} \approx M_R. \tag{3.43}$$

The heavy masses are given by the eigenvalues of M_R, whereas the masses of the light neutrinos are given by the eigenvalues of the 3×3 matrix m_{light} , whose elements are suppressed by M_R^{-1}. The order of magnitude of the mass m_D cannot surpass the electroweak scale 10^2 GeV, whereas the size of the mass M_R is not subject to any SM symmetry because N_R is a singlet. Hence, M_R can be much higher than m_D producing light neutrinos. The name seesaw, serves as a metaphore to visualize what happens in this mechanism: while one mass goes up, another goes down.
The seesaw mechanism is classified in three types, depending on the kind of heavy state that induces the effective vertex:

- **Type-I seesaw:** N_R fermion singlet with Y=0.
- **Type-II seesaw:** Δ scalar triplet with Y=1.
- **Type-III seesaw:** Σ fermion triplet with Y=0.

The type-I seesaw is essentially what we have explained. The other two types are detailed next.

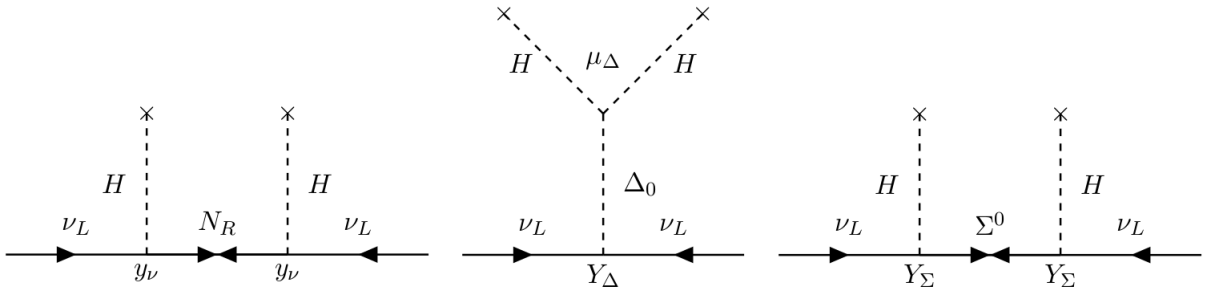

Figure 3.5: Representation of tree level type-I, type-II and type-III seesaws.

Type-II seesaw

In the seesaw type II [124], a new SU(2) scalar triplet Δ couples to the SM leptons as described by the new Yukawa term

$$\mathcal{L}_\Delta = -Y_\Delta \overline{l_L^c} \Delta l_L + \text{H.c.} \tag{3.44}$$

where Y_Δ is a symmetric matrix. The SU(2) triplet Δ can be represented in a 2×2 matrix by mapping $\vec{\Delta} = (\Delta_1, \Delta_2, \Delta_3)$ to the Pauli matrix basis $\vec{\sigma} = (\sigma_1, \sigma_2, \sigma_3)$

$$\Delta = \frac{1}{\sqrt{2}} \vec{\sigma} \vec{\Delta} = \begin{pmatrix} \frac{\Delta^+}{\sqrt{2}} & \Delta^{++} \\ \Delta^0 & -\frac{\Delta^+}{\sqrt{2}} \end{pmatrix}. \tag{3.45}$$

The elements Δ^{++}, Δ^+ and Δ^0 are defined as

$$\Delta^{++} = \frac{1}{\sqrt{2}}(\Delta_1 - i\Delta_2), \quad \Delta^+ = \Delta_3, \quad \Delta^0 = \frac{1}{\sqrt{2}}(\Delta_1 + i\Delta_2), \tag{3.46}$$

being their third component of isospin $I_3 = 1, 0 - 1$ respectively. The new terms of the scalar potential involving Δ interactions are

$$V(H, \Delta) \quad \supset \quad m_\Delta^2 \text{Tr}\left(\Delta\Delta^\dagger\right) + \left(\mu_\Delta \tilde{H}^\dagger \Delta^\dagger H + \text{H.c.}\right). \tag{3.47}$$

The parameter μ_Δ breaks lepton number explicitly if Δ^0 acquires a VEV when EWSB takes place. In the limit $v \ll m_\Delta$, the VEV of Δ^0 is determined to be

$$\langle \Delta^0 \rangle \equiv v_\Delta \simeq -\frac{\mu_\Delta v^2}{2m_\Delta^2}. \tag{3.48}$$

Therefore, the neutrino mass is

$$m_\nu = -2Y_\Delta v_\Delta = Y_\Delta \frac{v^2 \mu_\Delta}{m_\Delta^2}. \tag{3.49}$$

Comparing this result to the one obtained in Eq. (3.9) through the Weinberg operator, taking $\Lambda = m_\Delta$, one identifies

$$C^{(5)} = Y_\Delta \frac{\mu_\Delta}{m_\Delta}. \tag{3.50}$$

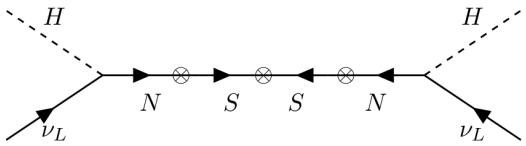

Figure 3.6: Representation of tree-level inverse seesaw.

Given that the triplet scalar VEV contributes to the ρ parameter, [11] the v_Δ is very well constrained by electroweak precision tests to not be larger than ~ 3 GeV [127].

Type-III seesaw

The type III seesaw [128] can be seen as an extension of type I, where a fermion triplet with zero hypercharge is used instead of a singlet. The fermion triplet Σ is represented in matrix form as:

$$\Sigma = \frac{1}{\sqrt{2}}\vec{\sigma}\cdot\vec{\Sigma} = \begin{pmatrix} \frac{\Sigma_0}{\sqrt{2}} & \Sigma^+ \\ \Sigma^- & -\frac{\Sigma_0}{\sqrt{2}} \end{pmatrix}, \tag{3.51}$$

where

$$\Sigma^\pm = \frac{1}{\sqrt{2}}(\Sigma_1 \mp i\Sigma_2), \quad \Sigma^0 = \Sigma_3. \tag{3.52}$$

The relevant renormalizable Lagrangian for the triplet Σ involves the Yukawa interaction with the leptons and Higgs scalar as well as Σ mass term

$$\mathcal{L}_\Sigma = -Y_\Sigma \overline{l_L}\Sigma\tilde{H} - \frac{1}{2}M_\Sigma\overline{\Sigma^c}\Sigma + \text{H.c.}. \tag{3.53}$$

After EWSB, a neutrino mass relation similar to the one in type-I seesaw is found

$$m_\nu \approx \frac{Y_\Sigma^2 v^2}{M_\Sigma}. \tag{3.54}$$

The charged components of $\Sigma^\pm$ are combined into a Dirac field $E^\pm$ with mass M_Σ. Charged leptons mix with $E^\pm$ giving rise to tree-level FCNC, making type-III seesaw more restricted than type-I.

Inverse seesaw

Contrary to the large mass scale needed in the standard seesaw mechanism to suppress neutrino masses, in the inverse seesaw (ISS) [129–131] the energy scale of the NP is reduced, due to the suppresion produced by a new parameter. For this scheme besides of the right-handed neutrinos N_R included by the standard seesaw, three SU(2) singlets S_i are introduced. The mass terms of the neutral fields are described in the following Lagangian

$$\mathcal{L}_{m_n} = -\overline{\nu_L}m_D N_R - \overline{S_L}M_R N_R - \frac{1}{2}\overline{S_L}\mu_S S_L^c + \text{H.c.} \tag{3.55}$$

[11] The electroweak ρ parameter is define as $\rho \equiv m_W^2/(m_Z^2\cos^2\theta_W)$. In a model containing a new scalar with $Y = 1$, the VEV of such field contributes to the mass of the W boson, affecting ρ. However, ρ is experimentally well measured to be approximately 1, constraining the value of the new VEV.

with m_D being the Dirac mass term given in (3.2). In the basis $n_L \equiv (\nu_L, N_R^c, S_L)^T$, the neutrino mass term reads

$$\mathcal{L}_{m_n} = -\frac{1}{2} n_L^T C \mathcal{M}_n n_L + \text{H.c.}, \tag{3.56}$$

where $\mathcal{M}_n$ is a 9×9 mass matrix. $\mathcal{M}_n$ is represented in a 3×3 matrix form as

$$\mathcal{M}_n = \begin{pmatrix} 0 & m_D^T & 0 \\ m_D & 0 & M_R \\ 0 & M_R^T & \mu_S \end{pmatrix}. \tag{3.57}$$

The three lightest eigenstates of $\mathcal{M}_n$ correspond to the physical neutrinos. When the condition $\mu_S \ll m_D \ll M_R$ is ensured, the diagonalization of $\mathcal{M}_n$ can be carried out through perturbative methods, leading to the neutrino mass matrix approximated expression

$$m_\nu \approx m_D^T \left(M_R^T\right)^{-1} \mu_S \, M_R^{-1} \, m_D \approx \frac{v^2}{2} y_\nu^T \left(M_R^T\right)^{-1} \mu_S \, M_R^{-1} \, y_\nu \, . \tag{3.58}$$

M_R is still a large Dirac mass scale suppressing light neutrino masses. However, the energy scale is not as large as in the seesaw case. This is due to the extra suppression coming from the Majorana parameter μ_S. When $\mu_S \to 0$ the neutrino masses are zero and lepton number is restored. Thus, it is technically natural to set μ_S to be very small [132], allowing to have $y_\nu \approx O(1)$.

The seesaw was the first mechanism proposed to explain the tiny masses of neutrinos, and is still the most popular. We have reviewed some of the most minimalist versions of seesaw at tree-level, however one can go to higher orders for the realization of the Weinberg operator. For instance, at 1-loop level one finds schemes such as the Zee model [133], in which neutrino masses have some extra suppresion. This is due to the (natural) small coupling constant $C^{(5)}$ which is affected by a factor of $1/(4\pi)^2$ thanks to the loop. Thus, one can achieve masses in agreement with neutrino data with the introduction of not so heavy fields with masses of the order of TeV.
Overall, the Weinberg operator parameterizes a large class of models in which the common denominator is the violation of lepton number by two units. Therefore, it can only generate Majorana neutrinos. A way to test Majorana neutrino mass models is through their effects on charged lepton flavor violating observables. This kind of analysis does not seem straightforward, though it can be facilitated by the Casas-Ibarra parametrization which is described in the upcoming section.

3.5 Casas-Ibarra parametrization

Many model that induces Majorana neutrino masses generates a mass matrix for the light neutrinos that is proportional to the Yukawa coupling product $y_\nu^T y_\nu$. Furthermore, these models induce effects in the charge lepton sector such as $\ell_\alpha \to \ell_\beta \gamma$ decays [12] whose branching depends on the y_ν matrix. In order to make predictions for these branching ratios, it is necessary to determine the most general form of y_ν, compatible with neutrino oscillation data. A description for y_ν in terms of the neutrino mixing matrix U, presented in Eq. (3.27), and the diagonal mass matrices of light m_ν and heavy M_R Majorana neutrinos is feasible in the type-I seesaw realization. This is displayed in the Casas-Ibarra parametrization [134, 135]. Without loss of generality, one usually chooses the basis with the leptonic Yukawa couplings y_ℓ and the

[12] Lepton Flavor Violating observables including $\ell_\alpha \to \ell_\beta \gamma$ decays are discussed in Chap. 4.

heavy neutrino mass matrix M_R being diagonal, real and positive

$$M_\ell = \text{Diag}(m_e, m_\mu, m_\tau), \qquad M_R = \Lambda^{-1} \equiv \text{Diag}(M_1, M_2, M_3). \tag{3.59}$$

In this basis, Casas and Ibarra proposed an interesting parametrization of y_ν

$$y_\nu = U^* \sqrt{\widehat{m}_\nu}\, R\, \sqrt{\Lambda^{-1}}. \tag{3.60}$$

Here R is any complex orthogonal 3×3 matrix $R^T R = \mathbb{I}_3$, where $\mathbb{I}_3$ is the 3×3 unit matrix, and $\widehat{m}_\nu$ is determined using U as in Eq. (3.28). It is straight forward to obtain

$$y_\nu^\dagger y_\nu = \sqrt{\Lambda^{-1}}\, R^\dagger\, \widehat{m}_\nu R\, \sqrt{\Lambda^{-1}}. \tag{3.61}$$

Eq. (3.60) has the freedom to accommodate both neutrino spectra, the ordering NO or IO, and the form of the complex R is the only parameter that depends on the mass ordering choice [135].
In Chap. 5 we will make use of an adapted parametrization [13] for the Yukawa couplings of a model that generates neutrino masses at 1-loop, to fix the neutrino data parameters and explore the lepton flavor violating phenomenology.

[13] The Casas-Ibarra parametrization can be generalized to be applied not only into seesaw type-I models, but to any Majorana neutrino mass model by means of the *Master parametrization* [136].

CHAPTER 4

Charged Lepton Flavor Violation

The imposition of individual lepton flavors being conserved in the neutral and charged sectors have been proven violated, at least in the neutral sector, after the detection of neutrino oscillations. This has established a clear need to construct physics beyond the SM, in which the lepton flavor symmetry is broken, permitting not only neutrino flavor transitions, but also processes with charged lepton flavor violation (cLFV). Processes with cLFV include $\ell_\alpha \to \ell_\beta\gamma$, $\ell_\alpha \to \ell_\beta\ell_\gamma\bar{\ell}_\sigma$, $\ell_\alpha + X \to \ell_\beta + X$ and $X \to \ell_\alpha\bar{\ell}_\beta$, where $\alpha,\beta,\ldots \in \{e,\mu,\tau\}$ and X are states that carry no lepton flavor number.
Different models may lead to different rates for a given cLFV observable. For instance in the minimally extended SM where a right-handed neutrino for each flavor is introduced, the process $\mu \to e\gamma$ takes place as illustrated in Figure 4.3. The predicted branching ratio for this decay is [137–142]

$$\mathrm{Br}(\mu \to e\gamma) = \frac{3\alpha}{32\pi}\left|\sum_{k=2,3} U^*_{\mu k}U_{ek}\frac{\Delta m^2_{k1}}{M^2_W}\right|^2 \lesssim 10^{-54}, \tag{4.1}$$

where $U_{\alpha k}$ are elements of the leptonic mixing matrix, Δm^2_{k1} are the neutrino mass squared differences, α is the fine structure constant, and M_W is the mass of the W boson. In this example the rate is extremely suppressed due to the small masses of neutrinos, making it totally inaccesible to any experiment.
Even though the rate of cLFV processes cannot be estimated model-independently, the adoption of an effective field theory applied to (charged and neutral) LFV transitions, permits a model independent study of NP interactions. This approach is discussed in Section 4.2.
Experimentally, numerous high-intensity facilities are dedicated to look for low-energy NP signals. For many years the searches for cLFV have focused on the radiative process $\ell_\alpha \to \ell_\beta\gamma$. For radiative muon decays, $\mu^+ \to e^+\gamma$, searches date back to the 1940's, when muons were considered to be mesons. The

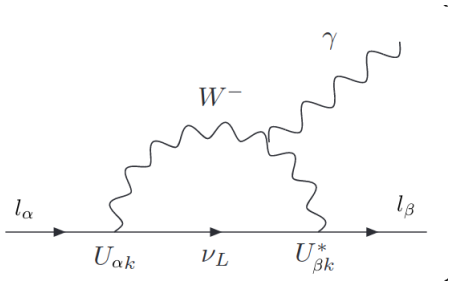

Figure 4.1: CLFV process $\ell_\alpha \to \ell_\beta\gamma$ in the minimal SM.

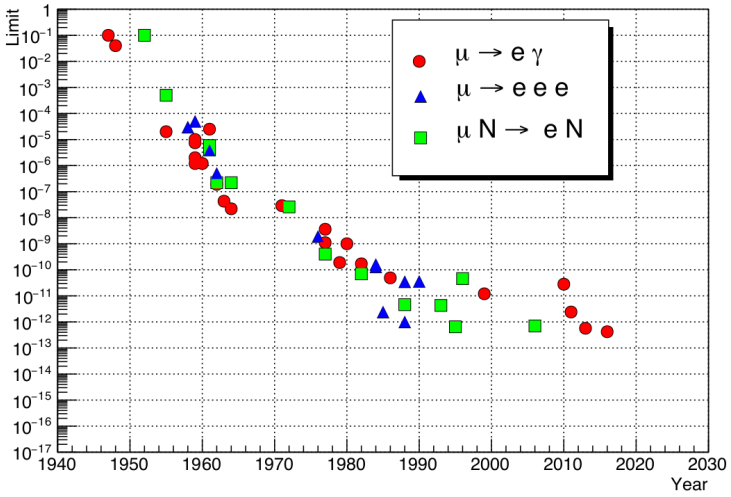

Figure 4.2: The history of cLFV searches in muons [17].

Fermi theory predicted a branching ratio of $\mathrm{BR}\left(\mu^+ \to e^+\gamma\right) \sim 10^{-4}$ [143]. However, this decay had been searched in 1954 resulting in an upper limit of 2×10^{-5} [144], and improved to 7×10^{-7} by 1959 [145]. Accelerator experiments increased the evidence of muons not behaving like mesons. Given that muons can decay into a neutrino-antineutrino pair, it was proposed that the neutrino associated with the muon decay $\mu \to e\nu\bar{\nu}$, was a different particle than the neutrino associated with beta decay [146], in order to overcome the non-observation of the radiative muon decay. This led to the conception of lepton flavor number [68]. Research on $\mu \to e\gamma$ continue up to date. Along with two other rare muon processes, $\mu \to 3e$ decays and $\mu \to e$ conversion in nuclei, their experimental searches provide the most stringent current bounds on cLFV, as well as the most promising future experimental sensitivities. Figure 4.2 shows the history of the branching ratios improvement for the three rare muon decays. The current status of cLFV searches and future sensitivities are exhibit next.

4.1 Current experimental status and future projects

No observation of a flavor violating process involving charged leptons has ever been made. This has been used by many experiments to set strong limits on the most relevant cLFV observables, usually translated into stringent bounds on the parameter space of many new physics models. In what concerns the radiative decay $\ell_\alpha \to \ell_\beta\gamma$, the experimental search is led by the MEG collaboration. This experiment searches for the process $\mu \to e\gamma$ and recently announced the limit $\mathrm{BR}(\mu \to e\gamma) < 4.2 \times 10^{-13}$ [147]. The 3-body LFV decay $\mu \to 3\,e$ was also searched for long ago by the SINDRUM experiment [148], which obtained the limit $\mathrm{BR}(\mu \to 3\,e) < 1.0 \times 10^{-12}$, still not improved by any experiment after almost 30 years. Another $\mu - e$ LFV process of interest due to the existing bounds is $\mu - e$ conversion in nuclei. Among the experiments involved in this search we may mention SINDRUM II, which searched for $\mu - e$ conversion in muonic gold and obtained the impressive limit $\mathrm{CR}(\mu - e, \mathrm{Au}) < 7 \times 10^{-13}$ [149]. Finally, the current experimental limits for τ lepton observables are less stringent, with branching ratios bounded to be below $\sim 10^{-8}$.

In addition to the active cLFV searches, some of them with planned upgrades, several promising upcoming

LFV Process	Present Bound	Future Sensitivity
$\mu \to e\gamma$	4.2×10^{-13} [147]	6×10^{-14} [18]
$\tau \to e\gamma$	3.3×10^{-8} [160]	$\sim 3 \times 10^{-9}$ [155]
$\tau \to \mu\gamma$	4.4×10^{-8} [160]	$\sim 3 \times 10^{-9}$ [155]
$\mu \to eee$	1.0×10^{-12} [148]	$\sim 10^{-16}$ [19]
$\tau \to \mu\mu\mu$	2.1×10^{-8} [161]	$\sim 10^{-9}$ [155]
$\tau^- \to e^-\mu^+\mu^-$	2.7×10^{-8} [161]	$\sim 10^{-9}$ [155]
$\tau^- \to \mu^-e^+e^-$	1.8×10^{-8} [161]	$\sim 10^{-9}$ [155]
$\tau \to eee$	2.7×10^{-8} [161]	$\sim 10^{-9}$ [155]
$\mu^-, \mathrm{Ti} \to e^-, \mathrm{Ti}$	4.3×10^{-12} [162]	$\sim 10^{-18}$ [163]
$\mu^-, \mathrm{Au} \to e^-, \mathrm{Au}$	7×10^{-13} [149]	
$\mu^-, \mathrm{Al} \to e^-, \mathrm{Al}$		$10^{-15} - 10^{-18}$
$\mu^-, \mathrm{SiC} \to e^-, \mathrm{SiC}$		10^{-14} [26]

Table 4.1: Current experimental bounds and future sensitivities for the most important LFV observables.

experiments will join the effort in the next few years. [14] Although, the MEG experiment completed data-taking in 2013, upgrades on the components of this experiment together with new components give place to the MEG II detector, which will allow to reach a sensitivity to branching ratios as low as 6×10^{-14} [18]. Despite significant improvements are also expected for τ observables from searches in B factories [155–158], the expected sensitivities are still less spectacular than those for μ observables. Regarding the new projects, the most promising ones are expected in searches for $\mu \to 3\,e$ and $\mu - e$ conversion in nuclei. The Mu3e experiment, which plans to start data taking soon, announces a sensitivity for $\mu \to 3\,e$ branching ratios of the order of $\sim 10^{-16}$ [19]. In case no discovery is made, this would imply an impressive improvement of the current bound by 4 orders of magnitude. Regarding $\mu - e$ conversion in nuclei, the competition will be shared by several experiments, with expected sensitivities for the conversion rate ranging from 10^{-14} to an impressive 10^{-18}. These include Mu2e [20–24], DeeMe[25, 26], COMET [27–29] and, in the long term, the future PRISM/PRIME [30].
Colliders can also play a relevant role in the search for cLFV. Data from LEP and LHC has allowed to constrain cLFV decays of SM neutral bosons $Z \to \ell_\alpha \ell_\beta$ and Higgs $h \to \ell_\alpha \ell_\beta$ [159]. For reference, in Tab. 4.1 we collect present bounds and expected sensitivities for the most popular low-energy LFV observables.

4.2 Standard model effective field theory

Experimental bounds on cLFV transitions can be used to constrain NP contributions in a model-independent way, by means of the effective approach [164, 165]. The SM is commonly assumed to be merely an effective theory valid up to some scale Λ. NP enters in the energy scale above Λ and additional dynamic degrees of freedom become relevant. The effective SM Lagrangian consists of a systematic dimensional expansion in $1/\Lambda$ that respects the SM gauge symmetries and all operators are constructed from SM fields. Besides, this effective Lagrangian must be reduced to the SM at low energies. The reduction to the SM occurs via decoupling of the heavy particles with masses $M_Z \ll \Lambda$ in most of beyond SM theories. Such decoupling at the perturbative level is allowed by the Appelquist-Carazzone

[14] See [17, 150–154] for recent reviews.

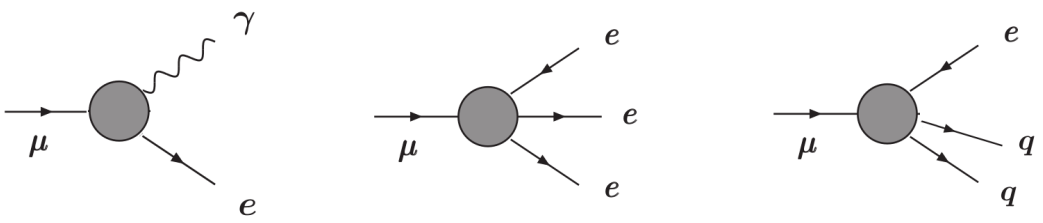

Figure 4.3: CLFV processes generated from 6-dimensional operators.

theorem [166]. Higher-dimensional operators suppressed by powers of Λ appear as new contributions in the effective SM Lagrangian

$$\mathcal{L}_{\text{eff}} = \mathcal{L}^{(4)}_{\text{SM}} + \frac{1}{\Lambda}\sum_k C^{(5)}_k O^{(5)}_k + \frac{1}{\Lambda^2}\sum_k C^{(6)}_k O^{(6)}_k + \sum_{n\geq 7}\frac{1}{\Lambda^{n-4}} C^{(n)}_k O^{(n)}_k. \tag{4.2}$$

Here $\mathcal{L}^{(4)}_{\text{SM}}$ is the usual renormalizable part of the SM Lagrangian containing operators up to dimension-4. The unique Weinberg operator described in Sec. 3.1.1 makes its appearence in $O^{(5)}_k$, dimension-6 operators are denoted by $O^{(6)}_k$, and $C^{(n)}_k$ stand for the corresponding dimensionless coupling constants, i.e. the Wilson coefficients. It is possible to parameterize the NP effects at the electroweak scale in terms of these operators and the associated Wilson coefficients. One can find the effective higher dimensional operators in a model independent way. When choosing a specific model, the Wilson coefficients can be calculated as a function of model parameters by matching the NP model under consideration on the effective SM [167]. [15]

As we know, the dimension-5 Weinberg operator provides neutrino mass terms and LFV in the neutrino sector in the minimal SM. Beyond tree level, it can also cause cLFV (Fig. 4.3). However, the amount of cLFV provided by the Weinberg operator is far below any foreseeable experimental capability (see Eq. (4.1)). Hence, we turn to dimension-6 operators [168–171] looking for possible cLFV signals. The low energy cLFV observables with the most stringent experimental current bounds on cLFV, as well as the most near-future sensitivity (Table 4.1), are those listed below

- Neutrinoless radiative decay , i.e. $\ell_\alpha \to \ell_\beta\gamma$.
- Neutrinoless three-body decay, i.e. $\ell_\alpha \to 3\ell_\beta$.
- $\mu - e$ conversion in nuclei.

The aforementioned cLFV observables are generated via dimension-6 operators of the following type:

$$O^{(6)}_{2\ell\gamma} \sim \left(\bar{l}_\alpha \sigma^{\mu\nu} e_\beta\right) H\, B_{\mu\nu}, \tag{4.3}$$

$$O^{(6)}_{4\ell} \sim \left(\bar{l}_\alpha \Gamma_{\text{S,V,T}}\, P_{L,R} l_\beta\right)\left(\bar{l}_\gamma \Gamma_{\text{S,V,T}}\, P_{L,R} l_\delta\right), \tag{4.4}$$

$$O^{(6)}_{2\ell 2d,u} \sim \left(\bar{l}_\alpha \Gamma_{\text{S,V,T}}\, P_{L,R} l_\beta\right)\left(\bar{d}_\gamma \Gamma_{\text{S,V,T}}\, P_{L,R}\, d_\delta\right), \quad \left(\bar{l}_\alpha \Gamma_{\text{S,V,T}}\, P_{L,R} l_\beta\right)\left(\bar{u}_\gamma \Gamma_{\text{S,V,T}}\, P_{L,R}\, u_\delta\right). \tag{4.5}$$

Where $P_{L,R} = \frac{1}{2}(1 \mp \gamma_5)$ are the usual chirality projectors, and we have defined $\Gamma_{\text{S}} = 1$, $\Gamma_{\text{V}} = \gamma_\mu$ and $\Gamma_{\text{T}} = \sigma_{\mu\nu}$. Figure 4.3 depicts the realization of these operators for the case of muon decays. At low

[15] In analogy to the electroweak theory matching with the intermediate vector boson theory at low energies, $\Lambda \ll M_W$.

energies one can better use an effective Lagrangian which is not gauge invariant. Such a Lagrangian is presented in Appendix A, and it gives rise to each of the aforementioned operators above. The description of their branching ratios can be found in Appendix B.

4.3 Computational tools

Theoretical efforts for the study of processes with flavor transitions conglomerate numerous models, with all kinds of symmetries and particle content. Given the current accuracy level delivered by the experiments, it is necessary to analize the phenomenology of these models, in order to shed light to the undelying structure of NP. The systematics study of NP scenarios can be very challenging. Nevertheless, many of the required tasks can nowadays be automatized by computer tools such as SARAH, SPheno or FlavorKit, making it possible to run precise calculations of flavor observables, and thus test our theoretical expectations.

4.3.1 SARAH

A very useful computational tool for analyzing particle physics models is the Mathematica package SARAH [172–176]. Despite the original concept of SARAH to tackle supersymmetric models only, implementations of non-supersymmetric ones have been allowed after version 3. SARAH derives a lot of analytical information about the given model. [16] It calculates all vertices, mass matrices, tadpoles equations, 1-loop corrections for tadpoles and self-energies, and 2-loop renormalization group equations (RGEs). Furthermore, SARAH can export these analytical expressions into LaTeX files. Concerning numerical calculations, SARAH can be use to generate the required input files for other high-energy physics tools, of which the most popular are:

- SPheno: To compute the mass spectrum, decay rates and flavor observables [179, 180].
- MicrOmegas: To compute the dark matter relic density and other related observables [181–183].
- MadGraph: To run Monte Carlo simulations for collider studies [184].

4.3.2 SPheno

SPheno [179, 180] is a spectrum calculator written in Fortran. Similar to the origins of SARAH, the SPheno code was created for the study of supersymmetric phenomenology. The development of SARAH 3 made it possible to implement new supersymmetric and non-supersymmetric models in SPheno without the need to write any Fortran code by hand. The modules created by SARAH for SPheno calculate the full 1-loop and partially 2-loop corrected mass spectrum, branching ratios and decays widths of all states, and many flavor and precision observables. The user only needs to define input values for the parameters of the model of interest either at some high-energy scale ('GUT' version) or at the electroweak scale (low scale version). [17]

4.3.3 FlavorKit

The FlavorKit [185] functionality is an extension of SARAH for the study of flavor observables in models beyond the SM. FlavorKit provides routines for the calculation of a large number of lepton and quark

[16] For a pedagogical overview about model implementation we recommend [177, 178].
[17] For instructions about how to create the GUT and low energy versions we refer to [177] and [178] respectively.

flavor observables. These files can be easily edited/extended by the user to define his own operators and/or observables. Generic expresions of the Wilson coefficients associated to 5- and 6-dimensional operators are derived from all the contributing Feynman diagrams, making use of `FeynArts/FormCalc` [186–191]. Numerous tree and 1-loop topologies for processes of 2-fermions-1-boson and 4-fermions are considered in the routines. For each topology the amplitudes with all possible generic insertions are included. In the case of 1-loop diagrams, not only all possible particles in the loop are considered, but also all different propagators for penguin diagrams are taken into account. Meaning that, besides the photonic penguins (which are often considered to be dominant in many processes), also all Higgs, Z and -if existing- Z' penguins are generated. In the same way, all possible combinations of box diagrams are also calculated. An output with all the generic formulas for the Wilson coefficients is passed to `SARAH`, which generates the `Fortran` code that allows to calculate numerically the values of these Wilson coefficients with `SPheno`, and are then combined to calculate the observables.

CHAPTER 5

Lepton Flavor Violation in the singlet-triplet scotogenic model

Although the SM of particle physics is supported by a vast amount of experimental evidence, it is also known to be incomplete due to its lack of solution for two central problems of modern physics: neutrino masses and the DM of the universe. Several SM extensions aiming at a common explanation for these two issues have been put forward in recent years. The scotogenic model, proposed by Ernest Ma in [192], constitutes one of the most attractive proposals. In this model, the SM particle content is enlarged with the introduction of a second scalar doublet and N_N (with $N_N \geq 2$) singlet fermions, all charged under a $\mathbb{Z}_2$ parity. This discrete symmetry forbids the usual tree-level contribution to neutrino masses, which are induced at the 1-loop level, and gives rise to a stable state, a weakly-interacting dark matter candidate. The phenomenology of this model has been studied in great detail, see [193–214], and several theoretical aspects have been discussed in recent literature, such as renormalization group running effects [215–217] as well as new model building directions [218–223].
In this work we will concentrate on a simple extension [18] of the minimal setup introduced in [192]: the singlet-triplet scotogenic model [35]. In this variant of the scotogenic model, the fermion sector includes the $SU(2)_L$ triplet Σ, which can mix with the singlet fermions via the VEV of a real scalar, Ω, also triplet under $SU(2)_L$. The most relevant features of the minimal model, radiative neutrino masses and a stable dark matter candidate, are kept in this variant, while the singlet-triplet mixing allows one to *interpolate* between pure singlet DM [192] and pure triplet DM [225], when the dark matter candidate is fermionic. This leads to a richer phenomenology, in particular to better prospects in direct DM detection experiments [35].

We study LFV in the singlet-triplet scotogenic model [37], in the spirit of previous works for the singlet [206] and triplet [226] models. [19] We will show that the model contains large regions of parameter space with observable LFV rates and hence will be probed in the near round of LFV experiments. Furthermore, we will explore some aspects of the LFV phenomenology of the model, such as the relative weight of the dipole operators with respect to other contributions to the LFV amplitudes, and determine that the most promising experimental perspectives are found for the LFV 3-body decays $\mu \to 3\,e$ and for coherent $\mu - e$ conversion in nuclei.

This chapter is organized as follows: in Sec. 5.1 we introduce the model whereas in Sec. 5.2 we obtain approximate expressions for the observables of interest. Sec. 5.3 contains our phenomenological analysis

[18] See [224] for a general classification of scotogenic models leading to radiative neutrino masses and viable dark matter candidates.

[19] See also [214] for a general study of LFV in scotogenic models with higher $SU(2)_L$ representations.

	generations	$SU(2)_L$	$U(1)_Y$	$\mathbb{Z}_2$
H	1	**2**	1/2	+
η	1	**2**	1/2	-
Ω	1	**3**	0	+
l_L	3	**2**	−1/2	+
ℓ_R	3	**1**	−1	+
N	1	**1**	0	-
Σ	1	**3**	0	-

Table 5.1: Matter content and charge assignment of the singlet-triplet scotogenic model.

of the model. Finally, we summarize our results and draw our conclusions in Sec. 5.4.

5.1 The singlet-triplet scotogenic model

We consider the model introduced in [35]. The matter content of the model, as well as the charge assignment under $SU(2)_L$, $U(1)_Y$ and $\mathbb{Z}_2$, is shown in Table 5.1. The quark sector, not included in this table, is SM-like and has $\mathbb{Z}_2 = +1$. The new fields beyond the SM particle content include two fermions: the singlet N and the triplet Σ, both with vanishing hypercharge and odd under the discrete $\mathbb{Z}_2$. Regarding the new scalars, these are the doublet η, also odd under $\mathbb{Z}_2$, and the real triplet Ω. The $SU(2)_L$ doublets H and η can be decomposed as

$$H = \begin{pmatrix} H^+ \\ H^0 \end{pmatrix}, \quad \eta = \begin{pmatrix} \eta^+ \\ \eta^0 \end{pmatrix}, \tag{5.1}$$

and can be identified with the usual SM Higgs doublet and a new *inert* doublet. Regarding the $SU(2)_L$ triplets, Σ and Ω, they are decomposed using the standard 2×2 matrix notation as

$$\Sigma = \begin{pmatrix} \frac{\Sigma^0}{\sqrt{2}} & \Sigma^+ \\ \Sigma^- & -\frac{\Sigma^0}{\sqrt{2}} \end{pmatrix}, \quad \Omega = \begin{pmatrix} \frac{\Omega^0}{\sqrt{2}} & \Omega^+ \\ \Omega^- & -\frac{\Omega^0}{\sqrt{2}} \end{pmatrix}. \tag{5.2}$$

With the charge assignment in Table 5.1, the most general $SU(3)_c \times SU(2)_L \times U(1)_Y$, Lorentz and $\mathbb{Z}_2$ invariant Yukawa Lagrangian is given by

$$-\mathcal{L}_Y = y_e^{\alpha\beta}\, \overline{l_\alpha}\, H\, \ell_\beta + y_N^\alpha\, \overline{l_\alpha}\, \tilde{\eta}\, N + y_\Sigma^\alpha\, \overline{l_\alpha}\, \tilde{\eta}\, \Sigma + y_\Omega\, \overline{\Sigma}\, \Omega\, N + \text{H.c.}\,. \tag{5.3}$$

Here we indicate the flavor indices $\alpha, \beta = 1, 2, 3$ explicitly and denote $\tilde{\eta} = i\sigma_2 \eta^*$, as usual. Gauge contractions are omitted for the sake of clarity. The Σ and N fermions have Majorana mass terms,

$$-\mathcal{L}_M = \frac{1}{2}\, M_\Sigma\, \overline{\Sigma^c}\Sigma + \frac{1}{2}\, M_N\, \overline{N^c} N + \text{H.c.}\,. \tag{5.4}$$

Finally, the scalar potential can be written as [20]

$$\begin{aligned}\mathcal{V} &= -m_H^2 H^\dagger H + m_\eta^2 \eta^\dagger \eta + \frac{\lambda_1}{2}\left(H^\dagger H\right)^2 + \frac{\lambda_2}{2}\left(\eta^\dagger \eta\right)^2 + \lambda_3 \left(H^\dagger H\right)\left(\eta^\dagger \eta\right) \\ &+ \lambda_4 \left(H^\dagger \eta\right)\left(\eta^\dagger H\right) + \frac{\lambda_5}{2}\left[\left(H^\dagger \eta\right)^2 + \text{H.c.}\right] - \frac{m_\Omega^2}{2}\,\Omega^\dagger \Omega \\ &+ \frac{\lambda_1^\Omega}{2}\left(H^\dagger H\right)\left(\Omega^\dagger \Omega\right) + \frac{\lambda_2^\Omega}{4}\left(\Omega^\dagger \Omega\right)^2 + \frac{\lambda^\eta}{2}\left(\eta^\dagger \eta\right)\left(\Omega^\dagger \Omega\right) \\ &+ \mu_1\, H^\dagger\, \Omega\, H + \mu_2\, \eta^\dagger\, \Omega\, \eta\,. \end{aligned} \tag{5.5}$$

5.1.1 Symmetry breaking and scalar sector

We will assume that the scalar potential in Eq. (5.5) is such that

$$\langle H^0 \rangle = \frac{v}{\sqrt{2}}\,, \quad \langle \Omega^0 \rangle = v_\Omega\,, \quad \langle \eta^0 \rangle = 0\,, \tag{5.6}$$

with $v, v_\Omega \neq 0$. These VEVs are determined by means of the minimization conditions

$$t_H = -m_H^2\, v + \frac{1}{2}\lambda_1 v^3 + \frac{1}{2}\lambda_1^\Omega v v_\Omega^2 - \frac{1}{\sqrt{2}}\, v v_\Omega\, \mu_1 = 0\,, \tag{5.7}$$

$$t_\Omega = -m_\Omega^2\, v_\Omega + \lambda_2^\Omega v_\Omega^3 + \frac{1}{2}\lambda_1^\Omega v^2 v_\Omega - \frac{1}{2\sqrt{2}} v^2\, \mu_1 = 0\,, \tag{5.8}$$

where $t_i \equiv \frac{\partial \mathcal{V}}{\partial v_i}$ is the tadpole of v_i. The VEVs v and v_Ω break the electroweak symmetry and induce masses for the gauge bosons,

$$m_W^2 = \frac{1}{4}\, g^2 \left(v^2 + 4\, v_\Omega^2\right)\,, \tag{5.9}$$

$$m_Z^2 = \frac{1}{4}\left(g^2 + g'^2\right) v^2\,. \tag{5.10}$$

We note that the triplet VEV v_Ω contributes to the W boson mass, thus receiving constraints from electroweak precision tests. We estimate that this VEV cannot be larger than about 4.5 GeV (at 3σ).

The scalar spectrum of the model contains the $\mathbb{Z}_2$-even scalars H^0, Ω^0, $H^\pm$ and $\Omega^\pm$, and the $\mathbb{Z}_2$-odd scalars η^0 and $\eta^\pm$. In the basis $S = \text{Re}\left(H^0\,,\, \Omega^0\right)$, the mass matrix for the $\mathbb{Z}_2$-even neutral scalars is given by

$$\mathcal{M}_S^2 = \begin{pmatrix} -m_H^2 + \frac{3}{2}\lambda_1 v^2 + \frac{1}{2}\lambda_1^\Omega v_\Omega^2 - \frac{1}{\sqrt{2}} v_\Omega\, \mu_1 & \lambda_1^\Omega v v_\Omega - \frac{1}{\sqrt{2}} v\, \mu_1 \\ \lambda_1^\Omega v v_\Omega - \frac{1}{\sqrt{2}} v\, \mu_1 & -m_\Omega^2 + \frac{1}{2}\lambda_1^\Omega v^2 + 3\lambda_2^\Omega v_\Omega^2 \end{pmatrix}. \tag{5.11}$$

The lightest of the S mass eigenstates, S_1, can be identified with the SM Higgs boson with a mass $m_{S_1} = m_{\text{Higgs}} \simeq 126$ GeV, whereas the heaviest mass eigenstate, S_2, is a new heavy Higgs boson not present in the SM. Regarding the $\mathbb{Z}_2$-even charged scalars, their mass matrix in the basis $\mathfrak{H}^\pm = \left(H^\pm\,,\, \Omega^\pm\right)$

[20] The Lagrangian in Eqs. (5.3), (5.4) and (5.5) differs from the one in Ref. [35] in two details: (i) some redundant terms in the scalar potential have been removed and the remaining ones have been renamed, and (ii) some couplings and mass terms have been normalized differently. The $\text{SU}(2)_L$ triplets Σ and Ω also have a different normalization, see Eq. (5.2).

takes the form

$$\mathcal{M}^2_{\mathfrak{H}^\pm} = \begin{pmatrix} -m_H^2 + \frac{1}{2}\lambda_1 v^2 + \frac{1}{2}\lambda_1^\Omega v_\Omega^2 + \frac{1}{\sqrt{2}} v_\Omega \mu_1 + \frac{1}{4} g^2 v^2 \xi_{W^\pm} & \frac{1}{\sqrt{2}} v \mu_1 - \frac{1}{2} g^2 v v_\Omega \xi_{W^\pm} \\ \frac{1}{\sqrt{2}} v \mu_1 - \frac{1}{2} g^2 v v_\Omega \xi_{W^\pm} & -m_\Omega^2 + \frac{1}{2}\lambda_1^\Omega v^2 + \lambda_2^\Omega v_\Omega^2 + g^2 v_\Omega^2 \xi_{W^\pm} \end{pmatrix}. \tag{5.12}$$

One of the $\mathfrak{H}^\pm$ mass eigenstates is the Goldstone boson that becomes the longitudinal component of the W boson, whereas the other is a physical charged scalar. In what concerns the $\mathbb{Z}_2$-odd scalars $\eta^{0,\pm}$, we first express the neutral η^0 field in terms of its CP-even and CP-odd components as

$$\eta^0 = \frac{1}{\sqrt{2}} \left(\eta^R + i \eta^I \right). \tag{5.13}$$

The conservation of the $\mathbb{Z}_2$ symmetry implies that the $\eta^{R,I,\pm}$ fields do not mix with the rest of scalars. Their masses are given by [21]

$$m^2_{\eta^R} = m_\eta^2 + \frac{1}{2}(\lambda_3 + \lambda_4 + \lambda_5) v^2 + \frac{1}{2}\lambda^\eta v_\Omega^2 - \frac{1}{\sqrt{2}} v_\Omega \mu_2, \tag{5.14}$$

$$m^2_{\eta^I} = m_\eta^2 + \frac{1}{2}(\lambda_3 + \lambda_4 - \lambda_5) v^2 + \frac{1}{2}\lambda^\eta v_\Omega^2 - \frac{1}{\sqrt{2}} v_\Omega \mu_2, \tag{5.15}$$

$$m^2_{\eta^\pm} = m_\eta^2 + \frac{1}{2}\lambda_3 v^2 + \frac{1}{2}\lambda^\eta v_\Omega^2 + \frac{1}{\sqrt{2}} v_\Omega \mu_2 . \tag{5.16}$$

We point out that the mass difference between the neutral η scalars is controlled by the λ_5 coupling, $m^2_{\eta^R} - m^2_{\eta^I} = \lambda_5 v^2$, and thus vanishes if $\lambda_5 = 0$. This will be relevant for the generation of neutrino masses, as shown in Sec. 5.1.2.

Finally, we emphasize that the vacuum in Eq. (5.6) breaks $\mathrm{SU}(2)_L \times \mathrm{U}(1)_Y \to \mathrm{U}(1)_Q$ but preserves the $\mathbb{Z}_2$ discrete symmetry. As we will discuss below, this gives rise to the existence of a stable neutral particle which may play the role of the dark matter of the universe.

5.1.2 Neutrino masses

Before discussing neutrino masses we must comment on the $\mathbb{Z}_2$-odd neutral fermions. The $\mathbb{Z}_2$-odd fields Σ^0 and N get mixed by the Yukawa coupling Y_Ω and the non-zero VEV v_Ω. In the basis $\left(\Sigma^0, N\right)$, their Majorana mass matrix takes the form

$$\mathcal{M}_\chi = \begin{pmatrix} M_\Sigma & y_\Omega v_\Omega \\ y_\Omega v_\Omega & M_N \end{pmatrix}. \tag{5.17}$$

The mass eigenstates $\chi_{1,2}$ are determined by the 2×2 orthogonal matrix $V(\alpha)$,

$$\begin{pmatrix} \chi_1 \\ \chi_2 \end{pmatrix} = \begin{pmatrix} \cos\alpha & \sin\alpha \\ -\sin\alpha & \cos\alpha \end{pmatrix} \begin{pmatrix} \Sigma^0 \\ N \end{pmatrix} = V(\alpha) \begin{pmatrix} \Sigma^0 \\ N \end{pmatrix}, \tag{5.18}$$

such that

$$\tan(2\alpha) = \frac{2\, y_\Omega v_\Omega}{M_\Sigma - M_N}. \tag{5.19}$$

[21] Although we provide analytical expressions for the masses in full generality, our analysis will assume CP conservation in the scalar sector, allowing us to consider that η^R and η^I do not mix.

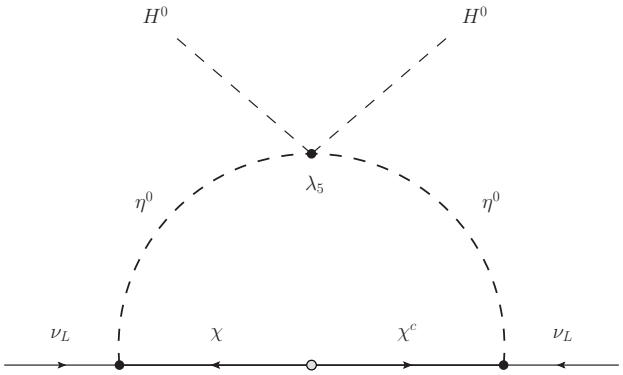

Figure 5.1: 1-loop neutrino masses in the singlet-triplet scotogenic model. Here $\eta^0 \equiv \left(\eta^R, \eta^I\right)$ and $\chi \equiv (\chi_1, \chi_2)$.

The singlet-triplet scotogenic model generates Majorana neutrino masses at the 1-loop level. This is shown in Fig. 5.1, which actually includes four loop diagrams, since $\eta^0 \equiv \left(\eta^R, \eta^I\right)$ and $\chi \equiv (\chi_1, \chi_2)$. The resulting neutrino mass matrix can be written as [22]

$$\begin{aligned}(m_\nu)_{\alpha\beta} &= \sum_{\sigma=1}^{2} \left(\frac{i h_{\alpha\sigma}}{\sqrt{2}}\right)\left(\frac{-i h_{\beta\sigma}}{\sqrt{2}}\right)\left[I(M^2_{\chi_\sigma}, m^2_{\eta^R}) - I(M^2_{\chi_\sigma}, m^2_{\eta^I})\right] \\ &= \sum_{\sigma=1}^{2} \frac{h_{\alpha\sigma}\, h_{\beta\sigma}\, M_{\chi_\sigma}}{2\,(4\pi)^2}\left[\frac{m^2_{\eta^R} \ln\left(\frac{M^2_{\chi_\sigma}}{m^2_{\eta^R}}\right)}{M^2_{\chi_\sigma} - m^2_{\eta^R}} - \frac{m^2_{\eta^I} \ln\left(\frac{M^2_{\chi_\sigma}}{m^2_{\eta^I}}\right)}{M^2_{\chi_\sigma} - m^2_{\eta^I}}\right],\end{aligned} \tag{5.20}$$

where h is a 3×2 matrix defined as

$$h = \begin{pmatrix} \frac{y^1_\Sigma}{\sqrt{2}} & y^1_N \\ \frac{y^2_\Sigma}{\sqrt{2}} & y^2_N \\ \frac{y^3_\Sigma}{\sqrt{2}} & y^3_N \end{pmatrix} \cdot V^T(\alpha)\,, \tag{5.21}$$

and $I(m_1^2, m_2^2)$ is a Passarino-Veltman function evaluated in the limit of zero external momentum. We note that $m^2_{\eta^R} = m^2_{\eta^I}$ leads to vanishing neutrino masses due to an exact cancellation between the η^R and η^I loops. This was indeed expected, since $m^2_{\eta^R} = m^2_{\eta^I}$ implies $\lambda_5 = 0$ and a definition of a conserved lepton number would be possible in this case. Furthermore, this justifies the choice $\lambda_5 \ll 1$, which is natural in the sense of 't Hooft [132], given that the limit $\lambda_5 \to 0$ increases the symmetry of the model. It proves convenient to write the neutrino mass matrix in Eq. (5.20) as

$$m_\nu = h\,\Lambda\,h^T\,, \tag{5.22}$$

[22] We correct this expression by including a factor of 1/2 missing in [35].

where

$$\Lambda = \begin{pmatrix} \Lambda_1 & 0 \\ 0 & \Lambda_2 \end{pmatrix}, \quad \Lambda_\sigma = \frac{M_{\chi_\sigma}}{2\,(4\pi)^2}\left[\frac{m^2_{\eta^R}\ln\left(\frac{M^2_{\chi_\sigma}}{m^2_{\eta^R}}\right)}{M^2_{\chi_\sigma}-m^2_{\eta^R}} - \frac{m^2_{\eta^I}\ln\left(\frac{M^2_{\chi_\sigma}}{m^2_{\eta^I}}\right)}{M^2_{\chi_\sigma}-m^2_{\eta^I}}\right]. \tag{5.23}$$

A neutrino mass matrix as the one in Eq. (5.22) formally resembles that obtained in the standard type-I seesaw with two generations of right-handed neutrinos. In this case we can make use of an adapted Casas-Ibarra parameterization explained in Sec. 3.5, to obtain an expression for the Yukawa matrix h,

$$h = U^* \sqrt{\widehat{m}_\nu}\, R\, \sqrt{\Lambda}^{-1}. \tag{5.24}$$

Here R is a 3×2 complex matrix such that $RR^T = \mathbb{I}_3$, and the neutrino mass matrix is diagonalized as Eq. (3.28), where U is the standard leptonic mixing matrix defined in Eq. (3.27). Similarly to the type-I seesaw with two right-handed neutrinos, the singlet-triplet scotogenic model predicts a vanishing mass for the lightest neutrino. The ordering NO or IO depends on the choice of R

$$R = \begin{pmatrix} 0 & 0 \\ \cos\gamma & \sin\gamma \\ -\sin\gamma & \cos\gamma \end{pmatrix} \quad \textbf{for NO} \quad (m_1 = 0), \tag{5.25}$$

$$R = \begin{pmatrix} \cos\gamma & \sin\gamma \\ -\sin\gamma & \cos\gamma \\ 0 & 0 \end{pmatrix} \quad \textbf{for IO} \quad (m_3 = 0). \tag{5.26}$$

We can finally make use of the previous expressions and write the Yukawa couplings h in terms of the leptonic mixing matrix matrix U, the eigenvalues m_i and the complex angle γ. In case of NO, one obtains

$$h_{\alpha 1} = \frac{1}{\sqrt{\Lambda_1}}\left(\cos\gamma\,\sqrt{m_2}\,U^*_{\alpha 2} - \sin\gamma\,\sqrt{m_3}\,U^*_{\alpha 3}\right), \tag{5.27}$$

$$h_{\alpha 2} = \frac{1}{\sqrt{\Lambda_2}}\left(\sin\gamma\,\sqrt{m_2}\,U^*_{\alpha 2} + \cos\gamma\,\sqrt{m_3}\,U^*_{\alpha 3}\right), \tag{5.28}$$

whereas for IO one finds

$$h_{\alpha 1} = \frac{1}{\sqrt{\Lambda_1}}\left(\cos\gamma\,\sqrt{m_1}\,U^*_{\alpha 1} - \sin\gamma\,\sqrt{m_2}\,U^*_{\alpha 2}\right), \tag{5.29}$$

$$h_{\alpha 2} = \frac{1}{\sqrt{\Lambda_2}}\left(\sin\gamma\,\sqrt{m_1}\,U^*_{\alpha 1} + \cos\gamma\,\sqrt{m_2}\,U^*_{\alpha 2}\right). \tag{5.30}$$

5.1.3 Dark matter in the model

The lightest state charged under the conserved $\mathbb{Z}_2$ parity is stable and hence, if electrically neutral, it constitutes a standard weakly-interacting dark matter candidate. Therefore, in what concerns dark matter, the singlet-triplet scotogenic model contains two distinct scenarios: (i) scalar dark matter, when the candidate is the lightest neutral η state, η_R or η_I, and (ii) fermion dark matter, when the candidate is χ_1, the lightest χ state. Even though we will not be concerned about dark matter in this thesis, we find it worth summarizing the main features of these two scenarios:

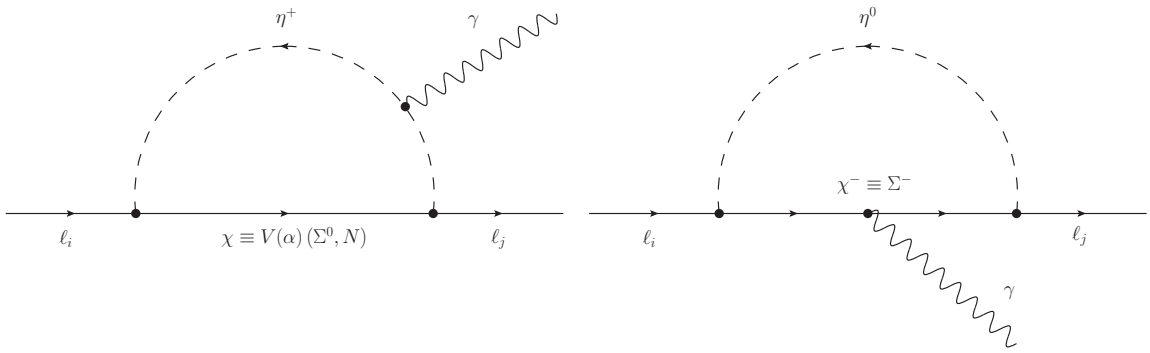

Figure 5.2: Photon penguin diagrams leading to the dominant Wilson coefficients K_1^L and K_2^R.

- **Scalar dark matter:** In this case the dark matter phenomenology resembles that of the inert doublet model [227] (see also [228–230] for some recent works on dark matter in the inert doublet model). Since in this scenario dark matter production in the early universe is driven by gauge interactions, there is no direct relation with LFV (driven by Yukawa interactions).

- **Fermion dark matter:** This scenario presents some of the most interesting features of the singlet-triplet scotogenic model [35]. The phenomenology dramatically depends on the nature of the dark matter candidate. In the two extreme cases this can be a pure $\mathrm{SU}(2)_L$ singlet (when $\chi_1 \equiv N$) or a pure $\mathrm{SU}(2)_L$ triplet (when $\chi_1 \equiv \Sigma$), while in general it will be an admixture of these two gauge eigenstates. When χ_1 is mostly singlet, the dark matter phenomenology is determined by Yukawa interactions and one expects a direct link between dark matter and LFV, as in the minimal scotogenic model [211]. In contrast, the DM phenomenology of a mostly triplet dark matter candidate is driven by the known gauge interactions. This case has little impact on LFV and predicts a dark matter candidate with a mass of about $\sim$ 2.7 TeV in order to reproduce the observed dark matter relic density. The parameter Y_Ω, which determines the $N - \Sigma$ mixing, interpolates between these two cases, in a way completely analogous to DM in R-parity conserving supersymmetry.

5.2 LFV observables

5.2.1 Approximate expressions for the observables

We use the `FlavorKit` [185] functionality of `SARAH` [172–176] (see sec. 4.3) for the analytical computation of the LFV Wilson coefficients and observables. This allows us to automatically obtain complete analytical results for the LFV observables as well as robust numerical routines to be combined with `SPheno` [179, 180]. For the conventions used in this analysis, the definition of the relevant LFV operators and the generic expressions for the LFV observables we refer to Appendices A and B. Even though we will make use of the complete analytical results for the numerical exploration of the phenomenology of the model, we find it convenient to present simple approximate expressions for the observables of interest.

Our numerical analysis reveals that the LFV phenomenology is mainly driven by two Wilson coefficients, both generated by photon penguin diagrams: the monopole K_1^L and the dipole K_2^R. Box diagrams also lead to sizable contributions, mainly to the Wilson coefficients A_{LL}^V, B_{LL}^V and C_{LL}^V, but we have found

them to be always subdominant compared to the photonic monopole and dipole contributions. Therefore, we can obtain simple approximate expressions for the LFV observables in terms of only K_1^L and K_2^R.

The most relevant photon penguin diagrams in the singlet-triplet scotogenic model are shown in Fig. 5.2. The diagram with the neutral fermions $\chi \equiv (\chi_1, \chi_2)$ running in the loop is common to the scotogenic model [206], whereas the diagram with the charged Σ^- state is only present in the singlet-triplet variant. This difference has an impact on the phenomenology, as we will see below. Let us first consider the dipole coefficient K_2^R, which induces the radiative LFV decay $\ell_\alpha \to \ell_\beta \gamma$. It can be written as

$$K_2^R = \frac{1}{16\pi^2}\left(D^0 + D^-\right), \tag{5.31}$$

where the contributions from the two diagrams in Fig. 5.2 are approximately given by

$$\begin{aligned} D^0 = {} & \frac{1}{2\,m_{\eta^+}^2} \times \\ & \left[\left(\frac{1}{\sqrt{2}}\cos\alpha\sin\alpha\left(\left(y_\Sigma^i\right)^* y_N^j + \left(y_N^i\right)^* y_\Sigma^j\right) + \frac{1}{2}\left(y_\Sigma^i\right)^* y_\Sigma^j \cos^2\alpha + \left(y_N^i\right)^* y_N^j \sin^2\alpha\right) F_2(\xi_1)\right. \\ & \left.+\left(\frac{-1}{\sqrt{2}}\cos\alpha\sin\alpha\left(\left(y_\Sigma^i\right)^* y_N^j + \left(y_N^i\right)^* y_\Sigma^j\right) + \frac{1}{2}\left(y_\Sigma^i\right)^* y_\Sigma^j \sin^2\alpha + \left(y_N^i\right)^* y_N^j \cos^2\alpha\right) F_2(\xi_2)\right], \end{aligned} \tag{5.32}$$

$$D^- = -\frac{1}{2\,m_{\eta^0}^2}\left(y_\Sigma^i\right)^* y_\Sigma^j\, G_2(\rho)\,. \tag{5.33}$$

Similarly, the monopole coefficient K_1^L can be split as

$$K_1^L = \frac{1}{16\pi^2}\left(M^0 + M^-\right), \tag{5.34}$$

and the two contributions from the penguin diagrams in Fig. 5.2 are given by

$$\begin{aligned} M^0 = {} & -\frac{1}{6\,m_{\eta^+}^2} \times \\ & \left[\left(\frac{1}{\sqrt{2}}\cos\alpha\sin\alpha\left(\left(y_\Sigma^i\right)^* y_N^j + \left(y_N^i\right)^* y_\Sigma^j\right) + \frac{1}{2}\left(y_\Sigma^i\right)^* y_\Sigma^j \cos^2\alpha + \left(y_N^i\right)^* y_N^j \sin^2\alpha\right) F_1(\xi_1)\right. \\ & \left.+\left(\frac{-1}{\sqrt{2}}\cos\alpha\sin\alpha\left(\left(y_\Sigma^i\right)^* y_N^j + \left(y_N^i\right)^* y_\Sigma^j\right) + \frac{1}{2}\left(y_\Sigma^i\right)^* y_\Sigma^j \sin^2\alpha + \left(y_N^i\right)^* y_N^j \cos^2\alpha\right) F_1(\xi_2)\right], \end{aligned} \tag{5.35}$$

$$M^- = \frac{1}{6\,m_{\eta^0}^2}\left(y_\Sigma^i\right)^* y_\Sigma^j\, G_1(\rho)\,. \tag{5.36}$$

Here we have defined

$$\xi_i = \frac{m_{\chi_i}^2}{m_{\eta^+}^2}, \quad \rho = \frac{m_{\chi^-}^2}{m_{\eta^0}^2}, \tag{5.37}$$

and used $m^2_{\eta^R} \simeq m^2_{\eta^I} \equiv m^2_{\eta^0}$. Finally, the loop functions appearing in these expressions are given by

$$F_1(x) = \frac{2 - 9x + 18x^2 - 11x^3 + 6x^3 \log x}{6(1-x)^4}, \tag{5.38}$$

$$G_1(x) = \frac{-16 + 45x - 36x^2 + 7x^3 + 6(3x-2)\log x}{6(1-x)^4}, \tag{5.39}$$

$$F_2(x) = \frac{1 - 6x + 3x^2 + 2x^3 - 6x^2 \log x}{6(1-x)^4}, \tag{5.40}$$

$$G_2(x) = \frac{2 + 3x - 6x^2 + x^3 + 6x \log x}{6(1-x)^4}. \tag{5.41}$$

We find that in the limit $M_\Sigma \to \infty$ our analytical results are in good agreement with those obtained in the scotogenic model [206]. [23] Finally, we emphasize that the numerical results discussed in the next section are based on the full 1-loop evaluation of the LFV observables and not on these approximate expressions, only presented to gain insight.

5.3 Phenomenological analysis

Our phenomenological analysis uses a SARAH-generated SPheno [179, 180] module for the numerical evaluation of the LFV observables. We solve the tadpole equations for the squared mass terms m^2_H and m^2_Ω and use an adapted Casas-Ibarra parameterization for neutrino masses to compute the Yukawa couplings y_N and y_Σ. For this purpose, the results of the global fit to neutrino oscillation data [231] will be used. Furthermore, given the little impact on the LFV phenomenology, we fix the following parameters in the scalar potential,

$$\lambda_{2,3,4} = \lambda^\Omega_{1,2} = \lambda^\eta = 0.1\,, \quad \lambda_5 = 10^{-8}\,, \tag{5.42}$$

$$\mu_1 = 50\,\text{GeV}\,, \quad \mu_2 = 1\,\text{TeV}\,. \tag{5.43}$$

We have explicitly checked that these parameters only affect the LFV observables indirectly, due to their influence on the scalar spectrum. The parameter λ_5 does indeed have a strong impact on the LFV observables, but only due to the scaling of the Yukawa couplings, y_N and y_Σ, induced via the neutrino mass relation in Eq. (5.20). All our numerical results have been obtained with $\lambda_5 = 10^{-8}$, except those for the τ lepton observables, obtained with $\lambda_5 = 10^{-10}$. The large value chosen for the trilinear coupling μ_2 ensures the conservation of the $\mathbb{Z}_2$ symmetry up to high energy scales [232]. We also fix $v_\Omega = 1$ GeV. This choice leads to a negligible deviation from $\rho = 1$, thus respecting limits from electroweak precision data. Finally, the doublet VEV v is fixed so that m_W is correctly obtained, see Eq. (5.9), and the quartic coupling λ_1 so that the lightest CP-even state in the model has a mass compatible with that of the recently discovered Higgs boson. This leaves us with four free model parameters,

$$y_\Omega\,, \quad m^2_\eta\,, \quad M_N\,, \quad M_\Sigma\,,$$

as well as the usual free choices in the implementation of the Casas-Ibarra parametrization: the R matrix angle γ, the Dirac CP-violating phase δ and Normal/Inverted Ordering for the light neutrino spectrum.

[23] Notice that the loop functions have been renamed with respect to [206].

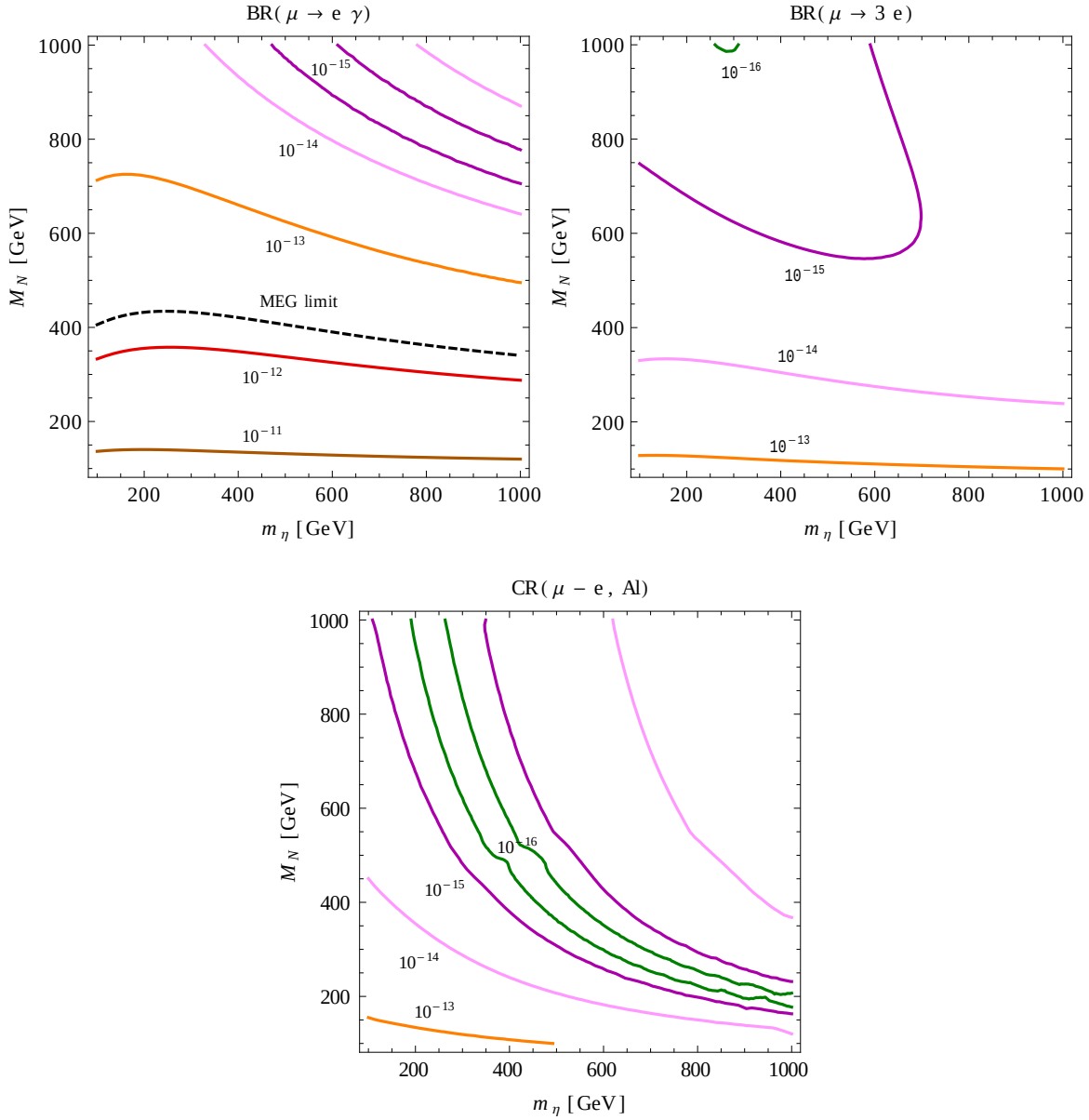

Figure 5.3: Contours of BR($\mu \to e\gamma$), BR($\mu \to 3\,e$) and CR($\mu - e$, Al) in the m_η-M_N plane. Figures obtained with fixed $y_\Omega = 0.1$ and $M_\Sigma = 500$ GeV, see text for more details.

General predictions of the model

We will now explore some aspects of the LFV phenomenology of the singlet-triplet scotogenic model. First of all, Fig. 5.3 shows contours of BR($\mu \to e\gamma$) (upper left panel), BR($\mu \to 3\,e$) (upper right panel) and CR($\mu - e$, Al) (lower panel) in the m_η-M_N plane, obtained with the setup introduced above and the choices $y_\Omega = 0.1$, $M_\Sigma = 500$ GeV, $\gamma = \delta = 0$, normal ordering for the light neutrino spectrum and taking best-fit values for the neutrino oscillation parameters. The first conclusion one can draw from this figure is that the singlet-triplet scotogenic model will be probed in the next round of LFV experiments: one easily finds parameter points where the three observables, BR($\mu \to e\gamma$), BR($\mu \to 3\,e$) and CR($\mu - e$, Al), are within the reach of the MEG and Mu3e experiments, respectively. In fact, the particular choice of

	Point 1	**Point 2**
y_Ω	0.1	0.1
m_η^2 [GeV^2]	$2.5 \cdot 10^5$	$2.5 \cdot 10^5$
M_N [GeV]	500	500
M_Σ [GeV]	800	300
BR($\mu \to e\gamma$)	$4.7 \cdot 10^{-13}$	$1.3 \cdot 10^{-15}$
BR($\mu \to 3\,e$)	$3.2 \cdot 10^{-15}$	$6.1 \cdot 10^{-15}$
CR($\mu - e$, Al)	$1.1 \cdot 10^{-15}$	$5.4 \cdot 10^{-14}$

Table 5.2: Benchmark points, parameter values and LFV observables. In addition to the four input values in this table, we take the parameter choices in Eqs. (5.42) and (5.43), use $\gamma = 0$, best-fit values for the neutrino oscillation parameters, as obtained in [231], normal ordering for the light neutrino spectrum and $\delta = 0$.

parameters made in this figure rules out low M_N values ($\lesssim 400$ GeV) as they would imply a too large $\mu \to e\gamma$ rate, in conflict with the current bound set by the MEG experiment [233]. [24] In the case of $\mu \to 3\,e$, the spectacular Mu3e sensitivity to branching ratios as low as $\sim 10^{-16}$ would allow one to probe the complete m_η-M_N plane explored in Fig. 5.3, with mass values up to the TeV scale and even higher in some cases. This also happens for $\mu - e$ conversion in Aluminum. In this observable, however, a strong cancellation takes place for a narrow band of the m_η-M_N plane, where the resulting negligible conversion rates cannot be probed in the near future. Qualitatively similar results are found for $\mu - e$ conversion rates in other nuclei, where analogous cancellations take place as well.

Figure 5.3 also shows that in the long term the processes $\mu \to 3\,e$ and $\mu - e$ conversion in nuclei will be more stringent than $\mu \to e\gamma$. Currently, only the MEG experiment sets relevant constraints in the explored m_η-M_N, ruling out a small portion with low M_N values, while the current bounds for $\mu \to 3\,e$ and $\mu - e$ conversion in nuclei do not imply any relevant restrictions. Given the expected experimental sensitivities in the search for these two observables, this fact will certainly change in the future. We find that the reach of experiments such as Mu3e (in case of $\mu \to 3\,e$) and Mu2e or COMET (in case of $\mu - e$ conversion in nuclei), clearly supersedes that of MEG, even after the planned upgrade.

Before moving to the discussion of the BR($\mu \to e\gamma$)/BR($\mu \to 3\,e$) ratio, we would like to make some additional comments about Figure 5.3. We have explicitly checked that our numerical results reproduce the expected decoupling behavior, namely that all LFV observables go to zero when m_η and $M_{N,\Sigma}$, the masses of the particles involved in their generation, go to infinity. However, this is not completely apparent when looking at Figure 5.3. There are two reasons for this: (i) some regions of the parameter space lead to cancellations among diagrams that strongly reduce some of the Wilson coefficients (see below for details), and (ii) the fit to neutrino oscillation data that leads to an increase in the Yukawa couplings when m_η or $M_{N,\Sigma}$ increase.

The BR($\mu \to 3\,e$)/BR($\mu \to e\gamma$) ratio

We also observe in Fig. 5.3 that for most points in the selected m_η-M_N plane, one obtains BR($\mu \to e\gamma$) $\gg$ BR($\mu \to 3\,e$). However, this is not a general prediction of the model, as we proceed to discuss now. Let us consider the benchmark points in Table 5.2. The results for the LFV observables have been obtained making the same choices as for Fig. 5.3, but using specific values for m_η^2, M_N and M_Σ. First, we observe

[24] The limit of MEG available at the time this analysis took place was 5.7×10^{-13}, which is a little bit higher than the actual value presented in Table 4.1.

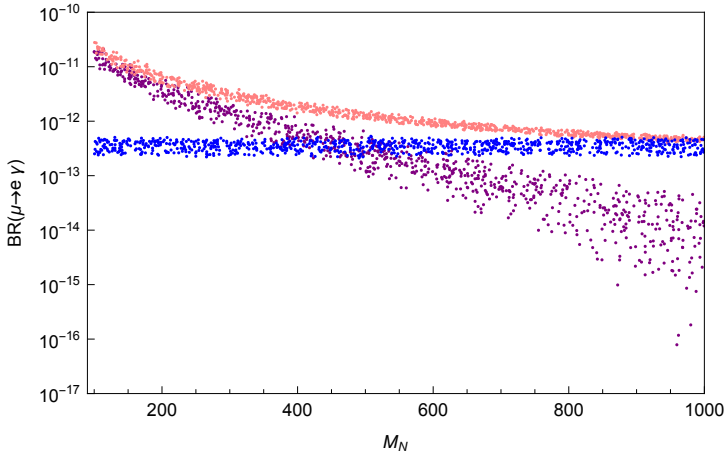

Figure 5.4: BR($\mu \to e\gamma$) as a function of M_N for fixed values $y_\Omega = 0.1$, $m_\eta^2 = 2.5 \cdot 10^5$ GeV^2 and $M_\Sigma = 500$ GeV. The purple dots display the total branching ratio, whereas the pink and blue dots show partial results obtained with only the D^0 and D^- contributions, respectively.

that the ratio

$$R_{\mu e} = \frac{\mathrm{BR}(\mu \to 3\, e)}{\mathrm{BR}(\mu \to e\gamma)}\,, \tag{5.44}$$

can vary by orders of magnitude between different benchmark points just by changing a single parameter, M_Σ. In fact, while **point 1** predicts LFV rates within the reach of future experiments searching for $\mu \to e\gamma$, $\mu \to 3\, e$ and $\mu - e$ conversion in nuclei, **point 2** leads to a BR($\mu \to e\gamma$) below the foreseen MEG sensitivity and can only be probed by $\mu \to 3\, e$ and $\mu - e$ conversion in nuclei experiments. Moreover, we note that only BR($\mu \to e\gamma$) varies substantially between point 1 and point 2, with a decrease of more than two orders of magnitude, while the other $\mu - e$ flavor violating observables are slightly larger in point 2.

The strong dependence of the $\mu \to e\gamma$ rate on M_Σ can be understood as follows. When $M_\Sigma < M_N$, as in point 2, one expects the dominant LFV Feynman diagrams to be those with triplet fermions, Σ^0 and Σ^-, running in the loop. Furthermore, when the mixing between singlet and triplet fermions is small ($\alpha \simeq 0$) one of the neutral χ states is mainly composed of Σ^0 and is mass degenerate with the charged $\chi^- \equiv \Sigma^-$. In this case, a cancellation between the D^0 and D^- contributions in Eqs. (5.32) and (5.33) takes place. Using these equations, it is straightforward to show that for $\alpha \simeq 0$, the fermion triplet loops lead to $K_2^R \propto F_2(\xi_1) - 2\, G_2(\rho)$, both loop functions being positive. Therefore, one naturally expects to find parameter points where this cancellation in the dipole coefficient is effective, leading to a reduction in the $\mu \to e\gamma$ rate.

This is explicitly shown in Fig. 5.4, where we plot our numerical results for BR($\mu \to e\gamma$) as a function of M_N for the fixed values $y_\Omega = 0.1$, $m_\eta^2 = 2.5 \cdot 10^5$ GeV^2 and $M_\Sigma = 500$ GeV. The purple dots display the total branching ratio, whereas the pink and blue dots show partial results obtained with only the D^0 and D^- contributions, respectively. This figure has been obtained by allowing the neutrino oscillation parameters to vary randomly within the preferred $3\,\sigma$ ranges found by the global fit of [231], which explains the spread of the points. We observe that the D^0 and D^- contributions approach a common value for large M_N values, whereas the total branching ratio drops. This is due to the abovementioned cancellation in the Σ^0-Σ^- loops. For low M_N values the singlet contributions to D^0 dominate and the cancellation in the triplet contributions is not relevant. However, as M_N increases and the N contribution to D^0 gets smaller, the cancellation in the triplet contributions becomes visible. We point out that a similar cancellation in the monopole coefficient takes place, again due to the relative sign between M^0

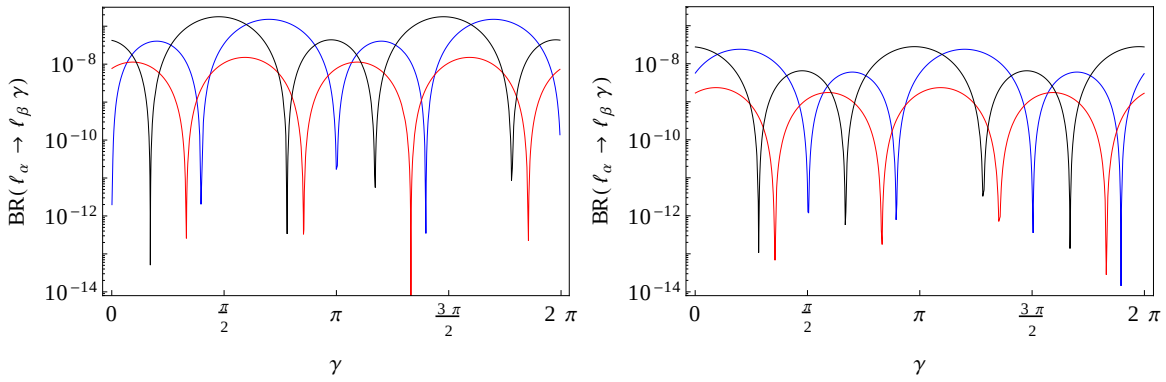

Figure 5.5: BR($\ell_\alpha \to \ell_\beta \gamma$) as a function of the R matrix angle γ for $M_\Sigma = 300$ GeV (left) and $M_\Sigma = 800$ GeV (right). The color code is as follows: $(\alpha,\beta) = (2,1)$ in blue, $(\alpha,\beta) = (3,1)$ in red and $(\alpha,\beta) = (3,2)$ in black. See text for more details.

and M^-, see Eqs. (5.35) and (5.36). However, typically this cancellation has little impact on the LFV observables which receive contributions from the monopole operator due to the interplay with the other contributions (e.g. dipole).

LFV τ decays

So far we have concentrated on $\mu - e$ violating processes. Now we turn our attention towards LFV processes involving the τ lepton. Given the worse experimental limits, these can only be phenomenologically relevant when they have rates much larger than those for the μ lepton. For example, in the benchmark points 1 and 2 presented above one finds branching ratios for the radiative decays $\tau \to \ell_\alpha \gamma$, with $\ell_\alpha = e, \mu$, in the $\sim 10^{-13} - 10^{-12}$ ballpark, clearly below the expected experimental sensitivity in the near future.

The results shown in Tab. 5.2 for points 1 and 2 were obtained with a vanishing R matrix angle γ. This parameter has a direct impact on the Yukawa couplings y_N and y_Σ, see Eqs. (5.27) - (5.30), and can lead to cancellations in the amplitudes of specific flavor violating transitions. This is illustrated in Fig. 5.5, where we show our numerical results for BR($\ell_\alpha \to \ell_\beta \gamma$) as a function of the R matrix angle γ (assumed to be real for simplicity) for $M_\Sigma = 300$ GeV (on the left) and $M_\Sigma = 800$ GeV (on the right). The rest of the parameters are fixed to the same values as in points 1 and 2, with the exception of a smaller λ_5 coupling ($\lambda_5 = 10^{-10}$) in order to increase the resulting Yukawa couplings and get larger LFV rates. We see in these figures that even though most points are experimentally excluded due to a $\mu \to e\gamma$ rate above the MEG bound, for certain γ values a strong cancellation takes place, leading to a tiny BR($\mu \to e\gamma$) and BR($\tau \to e\gamma$) $\sim 10^{-9} - 10^{-8}$ within reach of B factories.

Therefore, we conclude that the singlet-triplet scotogenic model can also be probed via τ observables. However, the scenarios that would be experimentally explored in this way are not generic and require a certain level of tuning in the Yukawa parameters in order to suppress the $\mu \to e$ rates.

5.4 Summary and conclusions

We have investigated the lepton flavor violating phenomenology of the singlet-triplet scotogenic model, a well-motivated scotogenic neutrino mass model in which neutrinos acquire their masses at the 1-loop level. The same symmetry that forbids the tree-level generation of neutrino masses stabilizes a weakly-

interacting dark matter candidate, thus providing a natural solution for another fundamental problem of current physics.

Our main findings can be summarized as follows:

- The model will be probed in the next generation of LFV experiments. In fact, we have found that parts of the parameter space are already ruled out by $\mu \to e\gamma$ searches. This of course depends on the value of the λ_5 parameter, which sets the global size of the Yukawa parameters and is expected to be naturally small due to its crucial role in the violation of lepton number.

- Currently, the most stringent LFV bound on the model is the one set by the MEG experiment on BR($\mu \to e\gamma$). However, this will soon change due to the impressive expected sensitivity in the forthcoming experiments. Experiments such as Mu3e (searching for $\mu \to 3\,e$) and Mu2e or COMET (searching for $\mu - e$ conversion in nuclei) will soon probe larger portions of the parameter space of the model.

- The operators with the largest contributions to the LFV amplitudes are the monopole and dipole ones. These are induced by photon penguin diagrams with scotogenic states running in the loop. Box diagrams have a subdominant role.

- One naturally finds points of the parameter space with BR($\mu \to 3\,e$), CR($\mu - e$, Nucleus) $\gg$ BR($\mu \to e\gamma$). This is caused by cancellations in the dipole coefficient which take place when the dominant contributions are generated by Σ^0-Σ^- loops. When this happens, MEG is usually unable to constrain the model.

- The singlet-triplet scotogenic model can also be probed via τ observables, but the scenarios where these have values close to the current or near future sensitivities require a certain tuning of the Yukawa parameters. Nevertheless, this can be achieved by properly choosing the γ angle of the Casas-Ibarra matrix R.

Finally, there are other ways to probe the parameter space of the singlet-triplet scotogenic model. As already explained, scotogenic models have a potential interplay between DM physics and LFV in scenarios with fermionic DM. In this case, the application of LFV bounds combined with the Planck result for the DM relic density and constraints from direct DM detection experiments (an attractive feature of the singlet-triplet scotogenic model), would help obtain very stringent constraints on the model and, eventually, rule out large fractions of the parameter space. Regarding collider phenomenology, the Σ and Ω triplets can be pair-produced in Drell-Yan processes at the LHC. In case of the Σ fermions, their subsequent decays lead to final states including DM particles, hence to signatures with missing energy, in a way analogous to the standard R-parity conserving supersymmetric signals [234].

CHAPTER 6

Lepton Flavor Violation in a Z' model for the b → s anomalies

In Section 4 LFV is pointed out as one of the most promising probes for NP searches. As observations of neutrino oscillations confirm LFV in the neutral lepton sector, motivations to search for LFV obsevables in the charged lepton sector emerge. Moreover, the deviation between the SM predictions and experimental measurements of observables associated to semileptonic $b \to s$ processes give hints of Lepton Flavor Universality violation. However, most of the models in the literature which account for such effects do not explain the observed neutrino masses and mixings. It is the aim of this chapter to explore the LFV phenomenology of a model that includes a non-universal interaction associated to the $b \to s$ anomalies and NP associated to the neutrino mass generation. An analysis of which of the aforementioned sources of LFV possesses the most relevant effects is performed. The model under consideration is introduced in [36]. This model includes a massive Z' boson whose interactions with SM particles result in new contributions that explain the anomalies in $b \to s$ transitions. For our purposes, we extend the model with a non-trival *embedding* of neutrino masses [38].
The chapter is organized as follows. In Sec. 6.1 we briefly review Lepton Flavor Universality and the current status of the $b \to s$ anomalies. In Sec. 6.2 we explain Z' model building. In Sec. 6.3 we introduce the model and discuss its most relevant features. Our setup for the phenomenological analysis as well as our results are described in detail in Sec. 6.4. Finally, a summary of the results and conclusions is drawn in Sec. 6.5.

6.1 Lepton Flavor Universality and the B-anomalies

In the SM, gauge bosons couple with the same strength to all three lepton families. As a consequence, one expects the branching ratio of a weak process mediated by a SM gauge boson and leptons as final states to be more or less the same no matter the lepton family. Deviations from this rule are only expected for the tau lepton due to non-negligible mass effects.
In 2013 the LHCb collaboration reported several observables associated to semileptonic decays involving $b \to s$ quark flavor transition. The measurements showed a decrease in many branching ratios of B mesons decays with respect to the SM predictions [235], as well as anomalies in angular observables, most notoriously in P_5' [236]. These anomalies persisted in the analysis of 2015 using the full LHC dataset collected in run I [237]. LHCb improved the measurement of the branching ratio for $B \to K\mu\mu$ at the beginning of 2014. After a couple of months, hints of LFU violation sparked when R_K, measured in the dilepton mass range q^2 from 1 to 6 GeV^2, appeared to have a value lower than 1 [238]. R_K represents

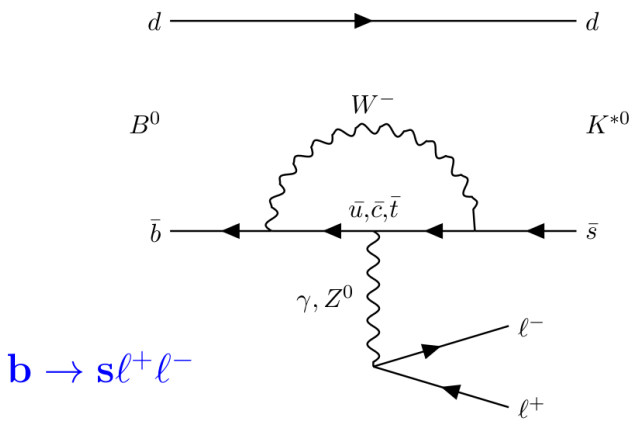

Figure 6.1: SM contribution to flavor changing neutral currents of semileptonic decays of B mesons at loop level.

the ratio between $B \to K\mu^+\mu^-$ and $B \to Ke^+e^-$ decays

$$R_{K^{(*)}} = \frac{\int_{q^2_{\min}}^{q^2_{\max}} \frac{d\Gamma(B\to K^{(*)}\mu^+\mu^-)}{dq^2}\, dq^2}{\int_{q^2_{\min}}^{q^2_{\max}} \frac{d\Gamma(B\to K^{(*)}e^+e^-)}{dq^2}\, dq^2}\,. \tag{6.1}$$

The SM predicts $R_K \approx 1$ to a very good accuracy; hence, the measurement of R_K made by LHCb represents a deviation of 2.6σ away from the SM [239].
Another test of LFU in $B \to K^*\ell^+\ell^-$ decays was carried out by the Belle collaboration in 2016 [240,241]. The results of the analysis on the measurement of angular observables showed a discrepancy from the SM prediction for P_5' in the muon modes with a local significance of 2.6σ, corroborating previews LHCb results. [25] More indications of universality violation were reported by LHCb in 2017 [243], this time, coming from B decays to K^*. The ratio R_{K^*} (6.1) was measured in two regions of the dilepton invariant mass squared q^2. The following expressions summarize the experimental hints in favor of the violation of LFU

$$\begin{aligned} R_K &= 0.745^{+0.090}_{-0.074} \pm 0.036\,, \quad q^2 \in [1,6]\ \text{GeV}^2\,, \\ R_{K^*} &= 0.660^{+0.110}_{-0.070} \pm 0.024\,, \quad q^2 \in [0.045, 1.1]\ \text{GeV}^2\,, \\ R_{K^*} &= 0.685^{+0.113}_{-0.069} \pm 0.047\,, \quad q^2 \in [1.1, 6.0]\ \text{GeV}^2\,. \end{aligned} \tag{6.2}$$

It is worth mentioning that there are also anomalies in the case of $b \to c$ quark transitions which were first reported by BaBar in 2012 [244], and seen later by LHCb and Belle collaborations. However, for this work we are only focusing in the anomalies coming from $b \to s$ transitions. Fig. 6.1 shows an example to a SM contribution to quark flavor transitions for the case of neutral currents.

In order to interpret the available data on $b \to s$ transitions it proves convenient to adopt an effective

[25] In March of 2019, an updated measured on the ratio R_K was presented by the LHCb collaboration with a value of $R_K = 0.846^{+0.060+0.016}_{-0.054-0.014}$ in the dilepton mass-squared region $1.1 < q^2 < 6.0\ \text{GeV}^2/c^4$. This ratio is in agreement with the SM prediction at the 2.5σ [242].

field theory language. The effective Hamiltonian for $b \to s$ transitions is

$$\mathcal{H}_{\text{eff}} = -\frac{4G_F}{\sqrt{2}} V_{tb} V_{ts}^* \frac{e^2}{16\pi^2} \sum_k \left(C_k O_k + C'_k O'_k \right) + \text{H.c.}\,. \tag{6.3}$$

Here G_F is the Fermi constant, e the electric charge and V the Cabibbo-Kobayashi-Maskawa (CKM) matrix. O_k and O'_k are the effective operators that contribute to $b \to s$ transitions, and C_k and C'_k their Wilson coefficients. It is usually convenient to split the Wilson coefficients into the SM and the NP contributions, $C_k = C_k^{\text{SM}} + C_k^{\text{NP}}$. In the following we will indicate their leptonic flavor indices explicitly. The operators that will be relevant for our discussion are

$$O_9^{\ell_i \ell_j} = \left(\bar{s} \gamma_\mu P_L b \right) \left(\bar{\ell}_i \gamma^\mu \ell_j \right) \quad , \quad O_{10}^{\ell_i \ell_j} = \left(\bar{s} \gamma_\mu P_L b \right) \left(\bar{\ell}_i \gamma^\mu \gamma_5 \ell_j \right) . \tag{6.4}$$

Primed operators are obtained by replacing P_L by P_R in the quark current and $\ell_{i,j} = e, \mu, \tau$ are the three lepton flavors. Several independent global fits have used data on $b \to s$ transitions to constrain the Wilson coefficients of these operators, following the model independent approach [245–253]. From these fits, a wide range of NP scenarios emerge with significances higher rather than the SM. It is noticeable how the favoured LFU-violating NP predominantly affects $b \to s\mu\mu$ more than $b \to see$. Moreover, it is found that the semileptonic operator $O_{9\mu}$ encloses the dominant NP contribution. This observation leads to the associated Wilson coefficient $C_{9\mu\mu} = C_{9\mu\mu}^{\text{SM}} + C_{9\mu\mu}^{\text{NP}}$ to play a central role in the explanation of the $b \to s$ anomalies. In order to improve the fits, a large negative contribution coming from $C_{9\mu\mu}^{\text{NP}}$ is required, typically of the order of 25% with respect to the SM value. The NP scenarios that properly accommodate the experimental data with a single parameter are found to be

1. $\left(C_{9\mu\mu}^{\text{NP}} = -C'_{9\mu\mu}, C_{10\mu\mu}^{\text{NP}} = C'_{10\mu\mu} \right)$,
2. $\left(C_{9\mu\mu}^{\text{NP}} = -C'_{9\mu\mu}, C_{10\mu\mu}^{\text{NP}} = -C'_{10\mu\mu} \right)$,
3. $\left(C_{9\mu\mu}^{\text{NP}} = -C_{10\mu\mu}^{\text{NP}}, C'_{9\mu\mu} = C'_{10\mu\mu} \right)$,
4. $\left(C_{9\mu\mu}^{\text{NP}} = -C_{10\mu\mu}^{\text{NP}}, C'_{9\mu\mu} = -C'_{10\mu\mu} \right)$.

Such scenarios can be achieved for instance, in models with leptoquarks or in Z' models with vector-like fermions. For the purposes of this chapter we will focus on the third scenario which involves the pattern $C_{9\mu\mu}^{\text{NP}} = -C_{10\mu\mu}^{\text{NP}}$. For this case, the global fit [246] estimates a value of

$$C_{9\mu\mu}^{\text{NP}} \to [-0.88, -0.37] \text{ at } 2\sigma. \tag{6.5}$$

Furthermore, one may wonder about the implications of the NP in other FCNC processes that involve mainly leptons. It has been pointed out that the violation of LFU generically implies LFV [31]. Although there are several explicit counterexamples to this rule [32, 33], this connection does indeed exist in most of the models introduced to explain the $b \to s$ anomalies. In fact, this connection may be used to learn about neutrino oscillation parameters [34]. However, since many of these models do not account for the observed neutrino masses and mixings, one may question whether the most relevant LFV effects are generally induced by the non-universal interactions associated to the $b \to s$ anomalies or by the NP associated to the generation of neutrino masses. Furthermore, even if the explanation to the $b \to s$ anomalies also involves LFV, the resulting rates could perhaps be too low to be observed by the experiments taking place in the near future. It is the goal of this chapter to address these questions in a particular model that involves couplings to a new gauge boson Z'.

6.2 Z' generalities

Several approaches have been considered in order to explain the $b \to s$ anomalies. One of the simple ways to reconcile theory predictions with experimental data involves additional $U(1)'$ gauge symmetries and associated Z' gauge bosons.
The NP contribution coming from the effective operator O_9 can be realized thanks to a massive Z' boson. The Z' boson must have flavor violating couplings to quarks and also must couple differently to electrons and muons. These features are embedded in the Lagrangian parametrized as [254, 255]

$$\mathcal{L} \supset \bar{f}_i \gamma^\mu \left(\Delta_L^{f_i f_j} P_L + \Delta_R^{f_i f_j} P_R \right) f_j Z'_\mu \,. \tag{6.6}$$

In our setup, a left handed scenario with $\Delta_L^{bs} \neq 0$, $\Delta_L^{\mu\mu} \neq 0$ and $\Delta_R^{\mu\mu} = 0$ will be considered, thus the rest of the Z' boson couplings to SM fermions will be set to zero.

6.2.1 Z' and dark matter

Besides the flavor physics implications that models with Z' bosons have, they can also prompt implications for cosmology, since in many models they serve as mediators between the dark and visible sectors to account for the dark matter of the Universe [36, 256–275]. The model introduced in [36] was the first NP model addressing the $b \to s$ anomalies with a dark sector. This is accomplished by adding the complex scalar χ, with charges $(\mathbf{1}, \mathbf{1}, 0, -1)$ under $\mathrm{SU(3)_c} \times \mathrm{SU(2)_L} \times \mathrm{U(1)_Y} \times \mathrm{U(1)'}$. Assuming that this scalar does not get a VEV, the breaking of the $\mathrm{U(1)'}$ gauge symmetry leaves a remnant $\mathbb{Z}_2$ parity, under which χ is odd. This mechanism [276–278] automatically stabilizes χ and makes it a valid dark matter candidate. Furthermore, the heavy Z' boson, crucial for the explanation of the $b \to s$ anomalies, serves as a portal between the SM and dark sectors. This establishes a non-trivial link between these two phenomenological directions in the model. We refer to [36] for a detailed discussion of the dark matter phenomenology of the model and to [279] for a recent review on the possible connection between the $b \to s$ anomalies and the dark matter of the Universe.

6.3 The model

We consider an extended version of the model introduced in [36] that also accounts for the existence of non-zero neutrino masses. A sketch of this version of the model was presented in Sec. III.B of [36].

The gauge group of the model is $\mathrm{SU(3)_c} \times \mathrm{SU(2)_L} \times \mathrm{U(1)_Y} \times \mathrm{U(1)_X}$, hence extending the SM gauge symmetry with an additional $\mathrm{U(1)_X}$ factor. The gauge coupling associated to this symmetry will be denoted by g_X and the gauge boson by Z'. Besides the usual SM fields, neutral under $\mathrm{U(1)_X}$, the matter content of the model is composed by one generation of vector-like (VL) quark doublets and two generations of vector-like lepton doublets

$$L_{L,R} = \begin{pmatrix} N \\ E \end{pmatrix}_{L,R}, \qquad Q_{L,R} = \begin{pmatrix} U \\ D \end{pmatrix}_{L,R}. \tag{6.7}$$

The model also includes the electroweak singlets ϕ and S and two generations of vector-like singlet fermions F. All new fields are charged under $\mathrm{U(1)_X}$. The complete scalar and fermion particle content of the model is given in Table 6.1. The number of new fermion generations has been chosen following the principle of minimality. More generations are possible, but they are not required to accommodate the solar and atmospheric neutrino mass scales at tree-level.

	generations	$SU(3)_c$	$SU(2)_L$	$U(1)_Y$	$U(1)_X$
H	1	**1**	**2**	1/2	0
ϕ	1	**1**	**1**	0	2
S	1	**1**	**1**	0	−4
q_L	3	**3**	**2**	1/6	0
u_R	3	**3**	**1**	2/3	0
d_R	3	**3**	**1**	−1/3	0
l_L	3	**1**	**2**	−1/2	0
e_R	3	**1**	**1**	−1	0
$Q_{L,R}$	1	**3**	**2**	1/6	2
$L_{L,R}$	2	**1**	**2**	−1/2	2
$F_{L,R}$	2	**1**	**1**	0	2

Table 6.1: Scalar and fermion particle content of the model.

The new Yukawa terms in the model are

$$-\mathcal{L}_Y = \lambda_Q\,\overline{Q_R}\,\phi\,q_L + \lambda_L\,\overline{L_R}\,\phi\,\ell_L + y\,\overline{L_L}\,H\,F_R + \widetilde{y}\,\overline{L_R}\,H\,F_L + h\,S\,\overline{F_L^c}\,F_L + \widetilde{h}\,S\,\overline{F_R^c}\,F_R + \text{H.c.}\,, \tag{6.8}$$

where λ_L is a 2×3 matrix, y and $\widetilde{y}$ are 2×2 matrices and h and $\widetilde{h}$ are 2×2 symmetric matrices. The λ_Q and λ_L couplings are the only ones involving the SM fermions, and thus play a crucial role in the resolution of the $b\to s$ anomalies. Furthermore, the vector-like fermions Q, L and F have gauge invariant Dirac mass terms

$$-\mathcal{L}_m = m_Q\,\overline{Q_L}Q_R + m_L\,\overline{L_L}L_R + m_F\,\overline{F_L}F_R + \text{H.c.}\,. \tag{6.9}$$

Both m_L and m_F are 2×2 matrices. The scalar potential of the model can be split as

$$\mathcal{V} = \mathcal{V}_{\text{SM}} + \Delta\mathcal{V}\,. \tag{6.10}$$

Here $\mathcal{V}_{\text{SM}} = m_H^2|H|^2 + \dfrac{\lambda}{2}|H|^4$ is the usual SM scalar potential. The new terms involving the $U(1)_X$ charged scalars are

$$\begin{aligned}-\Delta\mathcal{V} = {}& m_\phi^2\,|\phi|^2 + m_S^2\,|S|^2 + \frac{\lambda_\phi}{2}\,|\phi|^4 + \frac{\lambda_S}{2}\,|S|^4 \\ & + \lambda_{H\phi}\,|H|^2|\phi|^2 + \lambda_{HS}\,|H|^2|S|^2 + \lambda_{\phi S}\,|\phi|^2|S|^2 + \left(\mu'\,\phi^2 S + \text{H.c.}\right).\end{aligned} \tag{6.11}$$

We will assume that the minimization of the potential leads to non-zero VEVs for all scalars,

$$\langle H^0\rangle = \frac{v}{\sqrt{2}}\,, \qquad \langle\phi\rangle = \frac{v_\phi}{\sqrt{2}}\,, \qquad \langle S\rangle = \frac{v_S}{\sqrt{2}}\,. \tag{6.12}$$

Here H^0 is the neutral component of the SM Higgs doublet H. The ϕ and S fields will be responsible for the spontaneous breaking of $U(1)_X$, giving a mass to the Z',

$$m_{Z'}^2 = 4g_X^2\left(v_\phi^2 + 4v_S^2\right). \tag{6.13}$$

In addition, v_ϕ will induce mixings between the vector-like fermions and their SM counterparts thanks to

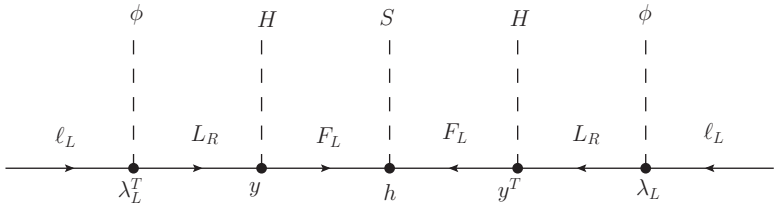

Figure 6.2: Neutrino mass generation. We note that the model under discussion provides a specific ultraviolet completion to the dimension-8 operator $O_\nu = \frac{1}{\Lambda_\nu^5}\ell\ell HH\phi\phi S$ pointed out in [36].

the λ_Q and λ_L Yukawa interactions in Eq. (6.8). As we will show below, this mixing plays a crucial role in the phenomenology of the model.

6.3.1 Neutrino masses

The definition of a conserved lepton number is not possible if S gets a non-zero VEV. Indeed, $\langle S \rangle = \frac{v_S}{\sqrt{2}} \neq 0$ breaks lepton number, leading to Majorana neutrino masses. Note, however, that lepton number conservation was actually enforced by the $U(1)_X$ gauge symmetry. For instance, Majorana mass terms like $\overline{F_L^c} F_L$ were forbidden. For this reason, the spontaneous breaking of lepton number does not lead to the existence of a physical Goldstone boson, which is instead absorbed by the Z' boson. In order to find an expression for the light neutrino masses, one must diagonalize the complete 11×11 neutral fermion mass matrix (Eq. (C.1)). In the basis $\mathcal{N} = \{\nu_L, N_R^c, N_L, F_R^c, F_L\}$, this matrix takes the form

$$\mathcal{M}_\mathcal{N} = \begin{pmatrix} 0 & -\frac{1}{\sqrt{2}} v_\phi \lambda_L^T & 0 & 0 & 0 \\ -\frac{1}{\sqrt{2}} v_\phi \lambda_L & 0 & m_L^T & 0 & \frac{1}{\sqrt{2}} v \widetilde{y} \\ 0 & m_L & 0 & -\frac{1}{\sqrt{2}} v\, y & 0 \\ 0 & 0 & -\frac{1}{\sqrt{2}} v\, y^T & \sqrt{2}\, v_S\, \widetilde{h} & m_F^T \\ 0 & \frac{1}{\sqrt{2}} v \widetilde{y}^T & 0 & m_F & \sqrt{2}\, v_S\, h \end{pmatrix}. \tag{6.14}$$

The diagonalization of this matrix can be performed in *seesaw approximation* by assuming $v_S\, h, v_S\, \widetilde{h} \ll v\, y, v\widetilde{y}, v_\phi\, \lambda_L \ll m_{L,F}$. [26] Importantly, we note that in the absence of the Yukawa couplings y and h, $\widetilde{y}$ and $\widetilde{h}$ would not contribute to the generation of neutrino masses at leading order, participating only at higher orders in perturbation theory. For this reason, we will take the simplifying assumption $\widetilde{y} = \widetilde{h} = 0$ in the following. The resulting 3×3 mass matrix for the light neutrinos is found to be

$$m_\nu \simeq \frac{v^2 v_\phi^2 v_S}{2\sqrt{2}}\, \lambda_L^T\, m_L^{-1}\, y\, m_F^{-1}\, h \left(m_F^{-1}\right)^T\, y^T \left(m_L^{-1}\right)^T \lambda_L\,, \tag{6.15}$$

where higher order terms in $h \ll 1$ have been neglected. A diagrammatic representation of the mechanism for neutrino mass generation in this model is shown in Fig. 6.2.

A neutrino mass matrix as the one in Eq. (6.15) formally resembles that obtained in the inverse seesaw [129]. Indeed, neutrino masses get suppresed due to the smallness of the hv_S term, which allows for a

[26] The explicit diagonalization of $\mathcal{M}_\mathcal{N}$ can be found in appendix C.

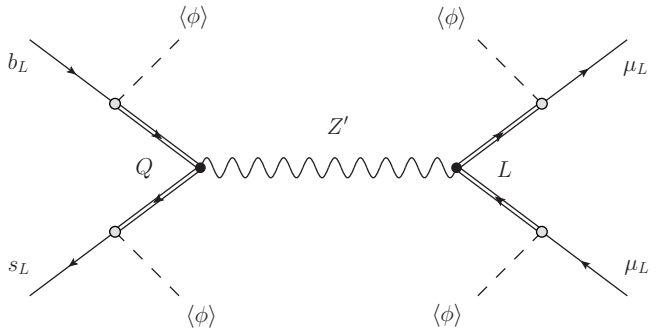

Figure 6.3: Generation of O_9 and O_{10}. The mixing between the SM fermions and the VL ones induce semileptonic four-fermion interactions.

low mass scale for the states that participate in the generation of neutrino masses. This justifies the choice $h \ll 1$, which is natural in the sense of 't Hooft [280], since the limit $h \to 0$ increases the symmetry of the model protecting this choice against quantum corrections. [27]

Given a specific texture for the λ_L Yukawa matrices, one can always find a matrix h that reproduces the observed neutrino masses and mixing angles. This matrix can be easily derived by inverting Eq. (6.15),

$$h = \bar{v}^{-5}\, m_F\, y^{-1}\, m_L\, \bar{\lambda}_L^T\, m_\nu\, \bar{\lambda}_L\, m_L^T \left(y^{-1}\right)^T\, m_F^T\,, \tag{6.16}$$

where $\bar{\lambda}_L$ is a 3×2 matrix such that $\lambda_L \bar{\lambda}_L = \mathbb{I}_2$, $\mathbb{I}_2$ being the 2×2 unit matrix, and we have defined $\bar{v}^5 = \dfrac{v^2 v_\phi^2 v_S}{2\sqrt{2}}$. The neutrino mass matrix is diagonalized as Eq. (3.28) where U is the standard leptonic mixing matrix (Eq. (3.27)).
We note that the similarity to the usual inverse seesaw mass matrix would also allow one to use an adapted Casas-Ibarra parameterization [134], as previously done in [282–284]. In this case, one solves Eq. (6.15) for the λ_L matrix, obtaining the general expression

$$\lambda_L = \bar{v}^{-5/2}\, V_X^\dagger\, D_{\sqrt{X}}\, R\, D_{\sqrt{m_\nu}}\, U^\dagger, \tag{6.17}$$

where $D_{\sqrt{m_\nu}} = \mathrm{diag}(\sqrt{m_{\nu_i}})$, $D_{\sqrt{X}} = \mathrm{diag}\left(\sqrt{\hat{X}_i}\right)$, with $\hat{X}_i$ the eigenvalues of $X = m_L^T \left(y^{-1}\right)^T m_F^T\, h^{-1}\, m_F\, y^{-1}\, m_L$, and V_X is the matrix that diagonalizes X as $V_X X V_X^T = \hat{X}$. R is a 2×3 complex matrix such that $R R^T = \mathbb{I}_2$.

6.3.2 Solving the b → s anomalies

The solution to the $b \to s$ anomalies follows the same lines as in [36]. The spontaneous breaking of the $\mathrm{U(1)_X}$ gauge symmetry by the ϕ VEV induces mixings between the SM and VL fermions due to the λ_Q and λ_L Yukawa couplings. Defining the bases $\mathcal{D}_{L,R} = \{d, D\}_{L,R}$ and $\mathcal{E}_{L,R} = \{\ell, E\}_{L,R}$, the Lagrangian after symmetry breaking includes the terms

$$-\mathcal{L} \supset \overline{\mathcal{D}_L} \mathcal{M}_\mathcal{D} \mathcal{D}_R + \overline{\mathcal{E}_L} \mathcal{M}_\mathcal{E} \mathcal{E}_R + \mathrm{H.c.}\,. \tag{6.18}$$

[27] We refer to [281] for a comprehensive exploration of possible inverse seesaw realizations.

The 4×4 down-quark mass matrix is given by

$$\mathcal{M}_{\mathcal{D}} = \begin{pmatrix} \frac{1}{\sqrt{2}} v Y_d & \frac{1}{\sqrt{2}} v_\phi \lambda_Q^T \\ 0 & -m_Q \end{pmatrix}, \tag{6.19}$$

whereas the 5×5 charged lepton mass matrix is

$$\mathcal{M}_{\mathcal{E}} = \begin{pmatrix} \frac{1}{\sqrt{2}} v Y_e & \frac{1}{\sqrt{2}} v_\phi \lambda_L^T \\ 0 & -m_L \end{pmatrix}, \tag{6.20}$$

with the SM Yukawa couplings defined as $Y_d \, H \, \overline{q_L} \, d_R$ and $Y_e \, H \, \overline{\ell_L} \, \ell_R$. These two fermion mass matrices can be diagonalized by means of the following biunitary transformations

$$\mathcal{D}_L = V_d \, \widehat{\mathcal{D}_L}, \qquad \mathcal{D}_R = U_d \, \widehat{\mathcal{D}_R}, \tag{6.21}$$

$$\mathcal{E}_L = V_e \, \widehat{\mathcal{E}_L}, \qquad \mathcal{E}_R = U_e \, \widehat{\mathcal{E}_R}, \tag{6.22}$$

where $V_{d,e}$ and $U_{d,e}$ are unitary matrices and $\widehat{\mathcal{D}_{L,R}}$ and $\widehat{\mathcal{E}_{L,R}}$ denote the physical mass eigenstates. With these definitions, the diagonal mass matrices $\widehat{\mathcal{M}_{\mathcal{D}}}$ and $\widehat{\mathcal{M}_{\mathcal{E}}}$ are obtained as $\widehat{\mathcal{M}_{\mathcal{D}}} = V_d^\dagger \, \mathcal{M}_{\mathcal{D}} \, U_d$ and $\widehat{\mathcal{M}_{\mathcal{E}}} = V_e^\dagger \, \mathcal{M}_{\mathcal{E}} \, U_e$, respectively.

The SM-VL mixing leads to the generation of Z' effective couplings to the SM fermions. If these are parametrized as Eq. (6.6), the $Z' - b - s$ and $Z' - \mu - \mu$ couplings, relevant for the explanation of the $b \to s$ anomalies, are given by

$$\Delta_L^{bs} = -2 \, g_X \, (V_d)_{42}^* \, (V_d)_{43} \, , \tag{6.23}$$

$$\Delta_L^{\mu\mu} = -2 \, g_X \sum_{k=4,5} (V_e)_{k2}^* \, (V_e)_{k2} \, . \tag{6.24}$$

These couplings lead to a tree-level contribution to the four-fermion operators O_9 and O_{10}, as shown in Fig. 6.3. In fact, since the SM fermions participating in the effective vertices are purely left-handed, the operators O_9 and O_{10} are generated simultaneously, with their Wilson coefficients fulfilling [255]

$$C_{9\mu\mu}^{\text{NP}} = -C_{10\mu\mu}^{\text{NP}} = -\frac{\Delta_L^{bs} \Delta_L^{\mu\mu}}{V_{tb} V_{ts}^*} \left(\frac{\Lambda_v}{m_{Z'}} \right)^2 , \tag{6.25}$$

where we have defined

$$\Lambda_v = \left(\frac{\pi}{\sqrt{2} G_F \alpha} \right)^{1/2} \simeq 4.94 \, \text{TeV} \, , \tag{6.26}$$

with $\alpha = \frac{e^2}{4\pi}$ the electromagnetic fine structure constant. With these ingredients at hand, it is straightforward to check that the model under discussion can reproduce the required value for $C_{9\mu\mu}^{\text{NP}}$ found by the global fits to $b \to s$ data. In our numerical analysis we will always consider parameter values that do so. Furthermore, analogous operators with violation of lepton flavor are also induced. Generalizing Eq. (6.24) to

$$\Delta_L^{\ell_i \ell_j} = -2 \, g_X \sum_{k=4,5} (V_e)_{ki}^* \, (V_e)_{kj} \, , \tag{6.27}$$

one also has

$$C^{\text{NP}}_{9\ell_i\ell_j} = -\frac{\Delta_L^{bs}\Delta_L^{\ell_i\ell_j}}{V_{tb}V_{ts}^*}\left(\frac{\Lambda_v}{m_{Z'}}\right)^2 . \tag{6.28}$$

The $C^{\text{NP}}_{9\ell_i\ell_j}$ LFV Wilson coefficients are the source of the B-meson LFV decays discussed in this work.

6.4 Phenomenological analysis

Just as in Sec. 5.2.1, our phenomenological analysis uses the `FlavorKit` functionality of `SARAH` in combination with `SPheno` for the analytical and numerical computation of the purely leptonic LFV observables. For the calculation of the B-meson LFV branching ratios we follow [285].

Let us now explain our parameter choices. Without loss of generality, the matrices m_L and m_F will be taken to be diagonal. We will also further assume a diagonal form for the y matrix. Regarding the fit to neutrino oscillation data, we will consider a specific structure for the λ_L matrix with $(\lambda_L)_{i1} = 0$, thus forcing the matrix h to contain flavor-violating entries. The matrix h will be obtained by using Eq. (6.16). One could also consider an alternative scenario with $h = \bar{h}\,\mathbb{I}_3$, so that the only source of flavor violation is the matrix λ_L. However, such a general λ_L matrix would potentially lead to C^{NP}_{9ee} and non-zero $\mu - e$ flavor violating amplitudes, making this scenario a very constrained one. We found that in order to avoid the stringent limits derived from flavor and, simultaneously, be compatible with neutrino oscillation data, a strong fine-tuning would be required. For this reason, we have not explored this scenario any further. Finally, we make the choice $\left(\lambda_Q\right)_1 = 0$ in order to suppress the Z' couplings to 1st generation quarks.

In what concerns the parameter ranges explored in the following analysis, we must take into account constraints derived from direct searches at the LHC. These include searches for the vector-like fermions in the model, as well as for the heavy Z' boson that mediates the NP contributions to the flavor observables. Regarding the Z' boson, one may naively think that its production cross-section would be too low to be observable at the LHC due to our choice $\left(\lambda_Q\right)_1 = 0$. However, the Z' can indeed be produced in pp collisions due to the non-vanishing heavy quark content in the protons. Due to the large couplings to muons required to explain the $b \to s$ anomalies, it is expected to decay mainly into $\mu^+\mu^-$ (and, optionally, $\tau^+\tau^-$ if the $(\lambda_L)_{i3}$ couplings take large values). ATLAS [286] and CMS [287] have searched for a Z' boson in the dimuon channel but the resulting limits are not very stringent, allowing for Z' masses as low as ~ 100 GeV, see [288] for a recent analysis. The Z' boson has also been searched for in the ditau channel. When the Z' boson belongs to a NP sector responsible for solving additional flavor anomalies in $b \to c$ transitions, a requirement that we do not have in our setup, these searches imply $m_{Z'} \gtrsim 1$ TeV unless the Z' has a very large decay width [289]. Our setup does not correspond to any of these specific scenarios and a dedicated study would be required in order to determine the actual limits on the Z' boson mass. Since this is beyond the scope of this thesis, we will adopt the conservative choice $m_{Z'} \gtrsim 1$ TeV in the following. The LHC collaborations have also searched for the vector-like fermions in the model, which provide complementary collider bounds. The vector-like quarks are colored particles and thus efficiently produced via QCD interactions at the LHC. This implies lower bounds on their mass slightly above the TeV scale [290]. Since our setup works with vector-like quark masses above this scale, the existing bounds can be easily satisfied. Finally, the vector-like leptons can also be searched for in multilepton final states. The current limits are weaker than those for vector-like quarks and allow for masses below the TeV [288]. These constraints will be taken into account in the numerical analysis that follows.

We now proceed to present the main numerical results of our analysis.

6.4.1 BR($B \to K\tau\mu$) vs BR($\tau \to 3\mu$)

We first discuss the correlation between $\mathrm{BR}(B \to K\tau\mu)$ and $\mathrm{BR}(\tau \to 3\mu)$ and how it can be used to estimate an upper bound for $\mathrm{BR}(B \to K\tau\mu)$. [28] Assuming that the dominant contributions are induced by the tree-level exchange of the Z' boson (see below for a discussion on this point), the branching ratios for the $B \to K\tau\mu$ and $\tau \to 3\mu$ decays can be written as [285]

$$\begin{aligned}\mathrm{BR}(B \to K\tau\mu) &= \mathrm{BR}(B \to K\tau^-\mu^+) + \mathrm{BR}(B \to K\tau^+\mu^-) = \\ &= 2 \cdot 10^{-9}\, A_{K\tau\mu} \left| \frac{\Delta_L^{bs}\Delta_L^{\tau\mu}}{V_{tb}V_{ts}^*} \right|^2 \left(\frac{\Lambda_v}{m_{Z'}} \right)^4 , \end{aligned} \tag{6.29}$$

$$\mathrm{BR}(\tau \to 3\mu) = \frac{m_\tau^5}{768\pi^3 \Gamma_\tau m_{Z'}^4} \left| \Delta_L^{\mu\mu}\Delta_L^{\tau\mu} \right|^2 , \tag{6.30}$$

where m_τ and Γ_τ are the tau lepton mass and decay width, respectively, and $A_{K\tau\mu} = 19.6 \pm 1.7$. This parameter has been obtained by combining the coefficients $a_{K\tau\mu} + b_{K\tau\mu}$, see [285], and adding the $a_{K\tau\mu}$ and $b_{K\tau\mu}$ errors in quadrature. We note that although Ref. [292] provides slightly different numerical values for these coefficients, they are perfectly compatible, in particular given the level of precision required for our analysis. One can now combine these expressions with Eq. (6.25) to obtain

$$\frac{\mathrm{BR}(B \to K\tau\mu)}{\mathrm{BR}(\tau \to 3\mu)} = 1.7 \cdot 10^7\ \mathrm{TeV}^4 \left(\frac{\left|\Delta_L^{bs}\right|}{m_{Z'}} \right)^4 \frac{1}{\left| C_{9\mu\mu}^{\mathrm{NP}} \right|^2} . \tag{6.31}$$

The ratio $\left|\Delta_L^{bs}\right| / m_{Z'}$ is strongly constrained by $B_s - \overline{B_s}$ mixing, which in this model would be induced via Z' tree-level exchange. Allowing for a 10% deviation in the mixing amplitude, one finds [255] [29]

$$\frac{m_{Z'}}{\left|\Delta_L^{bs}\right|} \gtrsim 244\,\mathrm{TeV} \quad \Rightarrow \quad \frac{\left|\Delta_L^{bs}\right|}{m_{Z'}} \lesssim 4 \cdot 10^{-3}\,\mathrm{TeV}^{-1} . \tag{6.32}$$

Furthermore, the current experimental upper bound on $\mathrm{BR}(\tau \to 3\mu)$ has been set by the Belle collaboration, which obtained $\mathrm{BR}(\tau \to 3\mu)_{\mathrm{max}} = 2.1 \times 10^{-8}$ [161], whereas the preferred 2σ range obtained for $C_{9\mu\mu}^{\mathrm{NP}}$ in the global fit [246] is $[-0.88, -0.37]$. With these ingredients at hand one can easily obtain the largest branching ratio for the $B \to K\tau\mu$ decay in this model, finding

$$\mathrm{BR}(B \to K\tau\mu)_{\mathrm{max}} \lesssim 8 \cdot 10^{-10} . \tag{6.33}$$

This result is clearly below the current experimental limit, $\mathrm{BR}(B \to K\tau\mu) < 4.8 \cdot 10^{-5}$ [294]. The main reason behind this result is the stringent constraint from $B_s - \overline{B_s}$ mixing. However, we would like to emphasize two points: (1) this is the largest $\mathrm{BR}(B \to K\tau\mu)$ that one expects when the Z' boson has purely left-handed couplings, as in the model under consideration, and (2) while in models with additional Z' right-handed couplings cancellations in the $B_s - \overline{B_s}$ mixing amplitude are possible [285], increasing $\mathrm{BR}(B \to K\tau\mu)_{\mathrm{max}}$ beyond the value given in Eq. (6.33) would require a significant fine-tuning of the parameters.

[28] See [291] for a scenario leading to correlations between $\mathrm{BR}(B \to K\tau\mu)$ and $\mathrm{BR}(\tau \to 3\mu)$ and R_K.

[29] The impact of stronger $B_s - \overline{B_s}$ mixing bounds has been recently explored in [293].

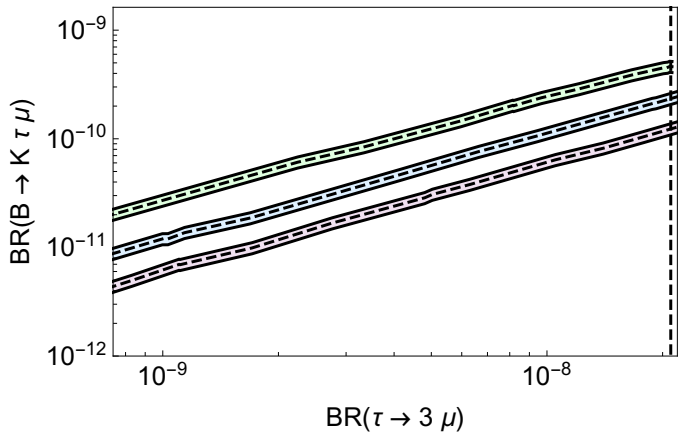

Figure 6.4: Correlation between $\mathrm{BR}(\tau \to 3\mu)$ and $\mathrm{BR}(B \to K\tau\mu)$ for three different sets of parameters. This figure has been obtained varying $(\lambda_L)_{13} = (\lambda_L)_{22}$. The vertical dashed line corresponds to the Belle experimental bound $\mathrm{BR}(\tau \to 3\,\mu)_{\mathrm{max}} = 2.1 \cdot 10^{-8}$ [161].

Figure 6.4 shows the correlation between $\mathrm{BR}(B \to K\tau\mu)$ and $\mathrm{BR}(\tau \to 3\,\mu)$ for three specific parameter choices. This figure has been obtained varying $(\lambda_L)_{13} = (\lambda_L)_{22}$. The values of the model parameters in the three different scenarios are:

- **Green:** $g_X = 0.155$, $v_S = 10.6$ GeV, $m_{Z'} = 1592$ GeV, $(m_L)_{11} = (m_L)_{22} = 1904$ GeV and $\left(\lambda_Q\right)_2 = \left(\lambda_Q\right)_3 = 0.0407$.
- **Blue:** $g_X = 0.2$, $v_S = 200$ GeV, $m_{Z'} = 1010$ GeV, $(m_L)_{11} = (m_L)_{22} = 1600$ GeV, $\left(\lambda_Q\right)_2 = \left(\lambda_Q\right)_3 = 0.055$.
- **Purple:** $g_X = 0.4$, $v_S = 34$ GeV, $m_{Z'} = 2330$ GeV, $(m_L)_{11} = (m_L)_{22} = 1007$ GeV, $\left(\lambda_Q\right)_2 = \left(\lambda_Q\right)_3 = 0.052$.

We note that higher values of $\left(\lambda_Q\right)_2 = \left(\lambda_Q\right)_3$ would be excluded due to $B_s - \overline{B_s}$ mixing constraints. The green band in Fig. 6.4 reaches $\mathrm{BR}(B \to K\tau\mu) \sim 6 \cdot 10^{-10}$, close to the upper bound estimated in Eq. (6.33). As we will show next, the strong correlations found in our analysis can be broken by loop effects, hence affecting the general conclusions derived from our phenomenological exploration. For instance, in regions of parameter space where loop corrections cancel the tree-level results for $\mathrm{BR}(\tau \to 3\,\mu)$, Eq. (6.31) would no longer hold and a larger $\mathrm{BR}(B \to K\tau\mu)$ would be allowed. This would require a fine-tuning of the masses and mixings in the charged lepton sector.

6.4.2 On the relevance of loop effects in BR($\tau \to 3\,\mu$)

So far we have discussed tree-level predictions of the model. However, one may wonder whether loop corrections might alter the results presented above. We have addressed this issue in Fig. 6.5, where we show the ratio between the tree-level expression for $\mathrm{BR}(\tau \to 3\,\mu)$ given in Eq. (6.30) and the complete numerical result including 1-loop contributions as returned by `SPheno`,

$$R_{\tau 3\mu} = \frac{\mathrm{BR}(\tau \to 3\,\mu)_{\text{tree-level}}}{\mathrm{BR}(\tau \to 3\,\mu)_{\text{1-loop}}}\,. \tag{6.34}$$

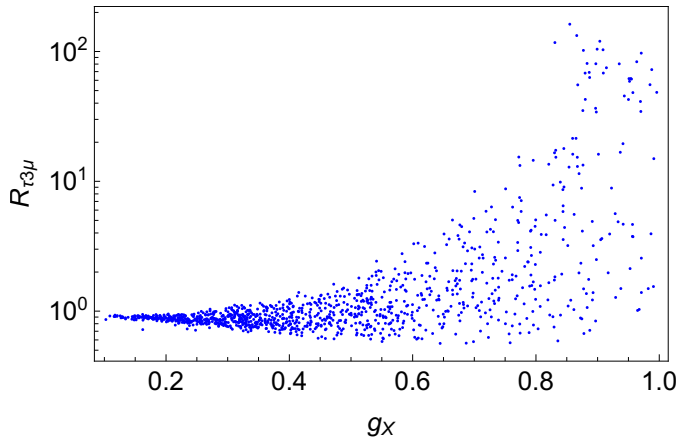

Figure 6.5: Behavior of the ratio $R_{\tau 3\mu}$ as a function of the gauge coupling g_X. Several model parameters have been randomly scanned over a wide range of numerical values, see text for details. The tree-level expression in Eq. (6.30) and the complete numerical result including 1-loop corrections can be very different for $g_X \gtrsim 0.4$.

This plot has been obtained by randomly scanning in the following ranges:

$$\begin{aligned} 0.05 &< g_X < 1.0 \\ 10\ \text{GeV} &< v_S < 500\ \text{GeV} \\ 0.01 &< \left(\lambda_Q\right)_2 = \left(\lambda_Q\right)_3 < 0.1 \\ 0.8\ \text{TeV} &< (m_L)_{11} = (m_L)_{22} < 2\ \text{TeV} \\ 1\ \text{TeV} &< m_{Z'} < 3\ \text{TeV} \end{aligned}$$

One can clearly see in Fig. 6.5 that while the tree-level expression in Eq. (6.30) and the complete numerical result including 1-loop corrections are actually very similar for low values of g_X, they can be very different for $g_X > 0.4$.

The impact of the loop corrections in $\tau \to 3\,\mu$ can be easily understood with the following considerations. In fact, it is not surprising that loop effects can be as large as the tree-level ones in $\tau \to 3\,\mu$. Fig. 6.6 shows two Feynman diagrams relevant for the calculation of the $\tau \to 3\,\mu$ amplitude. The diagram on the left constitutes the dominant tree-level contribution, whereas the diagram on the right is one of the dominant 1-loop contributions. Their contribution to the amplitude for external left-handed leptons can be generically written as

$$\mathcal{A}_{\text{tree}} = \frac{g_X^2}{m_{Z'}^2} F_{\text{tree}}\left(V_e\right) , \tag{6.35}$$

$$\mathcal{A}_{\text{loop}} = \frac{1}{16\pi^2} \frac{g_X^2\, g_{Z\ell\ell}}{m_Z^2} F_{\text{loop}}^{g_X}\left(m_{\mathcal{E}}, V_e\right) , \tag{6.36}$$

where $g_{Z\ell\ell}$ is the SM Z boson coupling to a pair of left-handed charged leptons and F_{tree} and $F_{\text{loop}}^{g_X}$ are two functions of the charged leptons (the five eigenstates) masses and mixings. F_{tree} only depends on the mixings in V_e due the Z' couplings to $\tau\mu$ and $\mu\mu$, given in Eq. (6.27). In contrast, $F_{\text{loop}}^{g_X}$ also depends on the five charged lepton masses, $m_{\mathcal{E}}$, due to the corresponding loop function. We first note that for

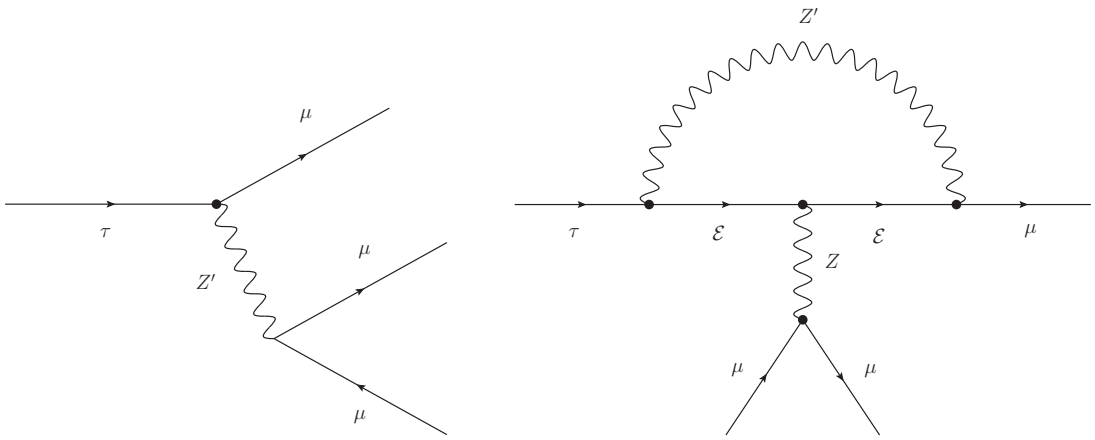

Figure 6.6: Feynman diagrams relevant for the calculation of the $\tau \to 3\mu$ amplitude. On the left, the dominant tree-level contribution is shown, whereas the diagram on the right is one of the dominant 1-loop contributions. We note that the 1-loop diagram on the right should be accompanied by two diagrams with the Z boson line attached to one of the external lepton legs.

$F_{\text{tree}} \simeq F_{\text{loop}}^{g_X}$, both contributions have comparable sizes, since

$$\frac{1}{16\pi^2}\,\frac{1}{m_Z^2} \sim \frac{1}{m_{Z'}^2} \quad , \quad \text{for } m_{Z'} \sim \text{TeV} \,. \tag{6.37}$$

Therefore, one would naively expect that loop effects in $\tau \to 3\mu$ will be generically of a size that is comparable to the tree-level ones. This is indeed what we find for large values of g_X. Moreover, we note that the 1-loop contributions may have a relative sign with respect to the tree-level ones, thus leading to cancellations in the final amplitudes, as shown in Fig. 6.5. In contrast, this is not the case for low values of g_X ($g_X \lesssim 0.4$). In this region of the parameter space we find that $F_{\text{loop}}^{g_X}$ is strongly reduced, hence suppressing loop contributions. This is due to the fact that, although $F_{\text{loop}}^{g_X}$ does not depend explicitly on g_X, there is an indirect dependence on this gauge coupling. In order to keep $m_{Z'}$ in the TeV ballpark for low values of g_X, one must introduce a large v_ϕ VEV, see Eq. (6.13), and this in turn affects the charged lepton masses and mixings as shown in Eq. (6.20). We have checked in detail that this is the reason behind the negligible loop effects for $g_X \lesssim 0.4$. However, we would like to point out that this behavior is not to be generally expected and emphasize the relevance of loop effects for a proper evaluation of $\text{BR}(\tau \to 3\mu)$ in Z' models for the $b \to s$ anomalies.

6.5 Summary and conclusions

The hints reported by the LHCb collaboration may be the first indications of a completely unexpected New Physics sector with interactions that violate lepton flavor universality. In this chapter we have explored an extension of the Z' model of [36] with a non-trivial embedding of neutrino masses and mixings. Our focus has been on the lepton flavor violating phenomenology of the resulting model, motivated by theoretical arguments that link it to the breaking of lepton flavor universality [31].

The main conclusions of our phenomenological exploration can be summarized as follows:

- The additional degrees of freedom introduced to accommodate neutrino masses and mixings play

a sub-dominant role in the lepton flavor violating predictions of the model, which are dominated by the New Physics effects induced by the states responsible for the explanation of the $b \to s$ anomalies.

- In most parts of the parameter space the rates for $B \to K\tau\mu$ and $\tau \to 3\,\mu$ are strongly correlated. This is simply due to the fact that both are dominated by tree-level Z' boson exchange. In this case, we have derived the upper limit $\mathrm{BR}(B \to K\tau\mu)_{\mathrm{max}} \lesssim 8 \cdot 10^{-10}$. This limit applies to all models with purely left-handed Z' couplings and can only be evaded by fine-tuning the contributions to $B_s - \overline{B_s}$ mixing in models with both left- and right-handed Z' couplings [285].

- Loop effects in $\tau \to 3\,\mu$ may be comparable to the tree-level ones. This is due to the strong suppression induced by the tree-level exchange of a TeV-scale Z' boson, which is absent in many 1-loop contributions. In fact, this feature is expected in generic Z' models for the $b \to s$ anomalies, although some regions of the parameter space of these models might deviate from this general expectation.

Flavor processes are clearly the most direct test of the model under discussion and crucial contributions from the Belle II experiment are expected in the long term [295]. However, the model can also be probed in several complementary ways. Direct searches at the LHC can also provide an additional handle on the model. One can have observable production rates for the vector-like lepton in the model, see [288] for a recent work in this direction, or search for the mediator of the New Physics contributions, the heavy Z' boson, see for instance [289]. If the $b \to s$ anomalies and the violation of flavor universality are finally confirmed, all these experimental approaches will be necessary to have a global picture of the new dynamics that lies beyond the Standard Model.

CHAPTER 7

Summary

In this thesis we have explored the lepton flavor violating phenomenology of two different SM extensions, employing both analytical and numerical tools. The models we have studied address the generation of small neutrino masses through different mechanisms. In Chapter 5 we presented the analysis for the singlet-triplet scotogenic model. In this setup, neutrinos acquire non-zero Majorana masses at the 1-loop level with scotogenic states running in the loop. Taking into account the data from neutrino oscillation experiments, we found that the largest contributions to the LFV amplitudes come from the monopole and dipole operators. For a certain setup, we scanned the parameter space of the LFV observables with the most stringent experimental bounds: BR($\mu \to e\gamma$), BR($\mu \to 3\,e$) and CR($\mu - e$, Al). Large part of the parameter space of BR($\mu \to e\gamma$) is already ruled out by the MEG experiment. This outcome can be changed when choosing a smaller value of the λ_5 parameter, which is expected to be naturally small due to its crucial role in the violation of lepton number.
For the model in Chapter 6 we tackle the $b \to s$ transition anomalies. The addition of a $U(1)_X$ symmetry implies the existence of an extra neutral gauge boson identified as the Z' boson. Including vector-like leptons and quarks we obtain effective interactions between the SM particles and the Z' boson, resulting in new contributions that explain the anomalies in $b \to s$ transitions and generate neutrino masses at tree-level. Given a specific texture for the λ_L Yukawa matrices that allows for flavor-violating entries, we found a matrix h that reproduces the observed neutrino masses and mixing angles. However, the values of the entries of h play a sub-dominant role in the LFV predictions of the model. The most stringent constraint comes from $B_s - \overline{B_s}$ mixing, which strongly affects the values of the Wilson coeficients that explain the $b \to s$ anomalies. The tree-level Z' boson exchange is the dominant contribution to $B \to K\tau\mu$ and $\tau \to 3\,\mu$. Such strong correlation allowed us to derived the upper limit $\text{BR}(B \to K\tau\mu)_{\text{max}} \lesssim 8 \cdot 10^{-10}$. This limit applies to all models with purely left-handed Z' couplings.

Before a significant breakthrough takes place on the theoretical side, the phenomenological approaches will keep playing a crucial role in interpreting new experimental data on quark mixing, CP violation, and neutrino oscillations. They are expected to provide useful hints towards discovering the full dynamics that lies beyond the Standard Model.

APPENDIX A

General LFV Lagrangian

The general LFV Lagrangian can be split into different pieces as [30]

$$\mathcal{L}_{\text{LFV}} = \mathcal{L}_{\ell\ell\gamma} + \mathcal{L}_{4\ell} + \mathcal{L}_{2\ell 2q}\,. \tag{A.1}$$

The first term is the $\ell - \ell - \gamma$ interaction Lagrangian, which generally leads to the following amplitude

$$T_{\ell\ell\gamma} = \bar{u}_\beta \left[q^2 \gamma^\mu \left(K_1^L P_L + K_1^R P_R \right) + i m_{\ell_\alpha} \sigma^{\mu\nu} q_\nu \left(K_2^L P_L + K_2^R P_R \right) \right] u_\alpha . \tag{A.2}$$

Here e is the electric charge, q is the photon momentum, $P_{L,R} = \frac{1}{2}(1 \mp \gamma_5)$ are the usual chirality projectors and the charged lepton spinors are denoted by $u_{\alpha,\beta}$. We omit flavor indices in the Wilson coefficients for the sake of clarity. The first and second terms in Eq. (A.2) are usually called monopole and dipole contributions, respectively. Notice that we have singled out the photonic contributions, not included in other vector operators. On the contrary, Z- and Higgs boson contributions have been included whenever possible.

The most general 4-lepton interaction Lagrangian compatible with Lorentz invariance can be written as

$$\mathcal{L}_{4\ell} = \sum_{\substack{I=S,V,T \\ X,Y=L,R}} A_{XY}^I \bar{\ell}_\beta \Gamma_I P_X \ell_\alpha \bar{\ell}_\delta \Gamma_I P_Y \ell_\gamma + \text{H.c.}\,, \tag{A.3}$$

where we have defined $\Gamma_S = 1$, $\Gamma_V = \gamma_\mu$ and $\Gamma_T = \sigma_{\mu\nu}$ and $\ell_{\alpha,\beta,\gamma,\delta}$ denote the lepton flavors. Finally, the last piece of Eq. (A.1) is the general $2\ell 2q$ 4-fermion interaction Lagrangian, given by

$$\mathcal{L}_{2\ell 2q} = \mathcal{L}_{2\ell 2d} + \mathcal{L}_{2\ell 2u} \tag{A.4}$$

where

$$\mathcal{L}_{2\ell 2d} = \sum_{\substack{I=S,V,T \\ X,Y=L,R}} B_{XY}^I \bar{\ell}_\beta \Gamma_I P_X \ell_\alpha \bar{d}_\gamma \Gamma_I P_Y d_\gamma + \text{H.c.} \tag{A.5}$$

$$\mathcal{L}_{2\ell 2u} = \mathcal{L}_{2\ell 2d}\big|_{d\to u,\, B\to C}\,, \tag{A.6}$$

and we have used d_γ to denote the d-quark flavor.

[30] We closely follow the notation and conventions used in `FlavorKit`, see [185].

APPENDIX B

Generic expressions for the LFV observables

B.1 $\ell_\alpha \to \ell_\beta \gamma$

The radiative decays $\ell_\alpha \to \ell_\beta \gamma$ only receive contributions from the dipole operators. The decay width is given by [296]

$$\Gamma\left(\ell_\alpha \to \ell_\beta \gamma\right) = \frac{\alpha m_{\ell_\alpha}^5}{4}\left(|K_2^L|^2 + |K_2^R|^2\right), \tag{B.1}$$

where α is the electromagnetic fine structure constant.

B.2 $\ell_\alpha \to 3\,\ell_\beta$

In this case, in addition to the standard dipole contributions, the decay width receives contributions from the monopole operators in Eq. (A.2) and from the 4-lepton operators in Eq. (A.3). The resulting decay width can be written as [185]

$$\begin{aligned}
\Gamma\left(\ell_\alpha \to 3\ell_\beta\right) \;=\; & \frac{m_{\ell_\alpha}^5}{512\pi^3}\left[e^4\left(\left|K_2^L\right|^2 + \left|K_2^R\right|^2\right)\left(\frac{16}{3}\log\frac{m_{\ell_\alpha}}{m_{\ell_\beta}} - \frac{22}{3}\right)\right. \\
& + \frac{1}{24}\left(\left|A_{LL}^S\right|^2 + \left|A_{RR}^S\right|^2\right) + \frac{1}{12}\left(\left|A_{LR}^S\right|^2 + \left|A_{RL}^S\right|^2\right) \\
& + \frac{2}{3}\left(\left|\hat{A}_{LL}^V\right|^2 + \left|\hat{A}_{RR}^V\right|^2\right) + \frac{1}{3}\left(\left|\hat{A}_{LR}^V\right|^2 + \left|\hat{A}_{RL}^V\right|^2\right) + 6\left(\left|A_{LL}^T\right|^2 + \left|A_{RT}^T\right|^2\right) \\
& + \frac{e^2}{3}\left(K_2^L A_{RL}^{S*} + K_2^R A_{LR}^{S*} + c.c.\right) - \frac{2e^2}{3}\left(K_2^L \hat{A}_{RL}^{V*} + K_2^R \hat{A}_{LR}^{V*} + c.c.\right) \\
& - \frac{4e^2}{3}\left(K_2^L \hat{A}_{RR}^{V*} + K_2^R \hat{A}_{LL}^{V*} + c.c.\right) \\
& \left. - \frac{1}{2}\left(A_{LL}^S A_{LL}^{T*} + A_{RR}^S A_{RR}^{T*} + c.c.\right) - \frac{1}{6}\left(A_{LR}^S \hat{A}_{LR}^{V*} + A_{RL}^S \hat{A}_{RL}^{V*} + c.c.\right)\right].
\end{aligned} \tag{B.2}$$

This expression combines the contributions from monopole operators with those of 4-lepton operators of vectorial type,

$$\hat{A}_{XY}^V = A_{XY}^V + e^2 K_1^X \qquad (X, Y = L, R), \tag{B.3}$$

and neglects the mass of the leptons in the final state, with the exception of the dipole contributions $K_2^{L,R}$, where an infrared divergence would otherwise occur due to the presence of a massless photon propagator.

B.3 $\mu - e$ conversion in nuclei

In coherent $\mu - e$ conversion in nuclei, only the scalar and vector operators in Eqs. (A.2), (A.5) and (A.6) contribute. This includes photonic monopole and dipole operators, supplemented with the standard photon vertices with the up- and down quarks, as well as $2\ell 2q$ 4-fermion operators. They induce the effective μeqq couplings

$$g_{LV(q)} = \frac{\sqrt{2}}{G_F}\left[e^2 Q_q \left(K_1^L - K_2^R\right) - \frac{1}{2}\left(C_{\ell\ell qq}^{VLL} + C_{\ell\ell qq}^{VLR}\right)\right], \tag{B.4}$$

$$g_{RV(q)} = g_{LV(q)}\big|_{L\to R}\,, \tag{B.5}$$

$$g_{LS(q)} = -\frac{\sqrt{2}}{G_F}\frac{1}{2}\left(C_{\ell\ell qq}^{SLL} + C_{\ell\ell qq}^{SLR}\right), \tag{B.6}$$

$$g_{RS(q)} = g_{LS(q)}\big|_{L\to R}\,, \tag{B.7}$$

where Q_q is the quark electric charge ($Q_d = -1/3$, $Q_u = 2/3$) and $C_{\ell\ell qq}^{IXK} = B_{XY}^K \left(C_{XY}^K\right)$ for d-quarks (u-quarks), with $X = L, R$ and $K = S, V$. These couplings at the quark level must be *dressed* to obtain the effective couplings at the nucleon level. One finds

$$g_{XK}^{(0)} = \frac{1}{2}\sum_{q=u,d,s}\left(g_{XK(q)} G_K^{(q,p)} + g_{XK(q)} G_K^{(q,n)}\right), \tag{B.8}$$

$$g_{XK}^{(1)} = \frac{1}{2}\sum_{q=u,d,s}\left(g_{XK(q)} G_K^{(q,p)} - g_{XK(q)} G_K^{(q,n)}\right), \tag{B.9}$$

where the $G_K^{(q,p)}$ and $G_K^{(q,n)}$ numerical coefficients were computed in [297] and given in [185]. For an improved calculation of the scalar coefficients we refer to [298]. Finally, the conversion rate, normalized to the standard muon capture rate Γ_{capt}, is given by [165]

$$\begin{aligned}\text{CR}(\mu - e, \text{Nucleus}) = {} & \frac{p_e\, E_e\, m_\mu^3\, G_F^2\, \alpha^3\, Z_{\text{eff}}^4\, F_p^2}{8\pi^2\, Z\, \Gamma_{\text{capt}}} \\ & \times \left\{\left|(Z+N)\left(g_{LV}^{(0)} + g_{LS}^{(0)}\right) + (Z-N)\left(g_{LV}^{(1)} + g_{LS}^{(1)}\right)\right|^2 + \right. \\ & \left. \left|(Z+N)\left(g_{RV}^{(0)} + g_{RS}^{(0)}\right) + (Z-N)\left(g_{RV}^{(1)} + g_{RS}^{(1)}\right)\right|^2\right\}. \end{aligned} \tag{B.10}$$

Z and N are the number of protons and neutrons in the nucleus under consideration and Z_{eff} is its effective atomic charge [299]. Furthermore, G_F is the Fermi constant, F_p is the nuclear matrix element and p_e and E_e ($\simeq m_\mu$) are the momentum and energy of the electron.

APPENDIX C

Diagonalization of 11 × 11 neutrino mass matrix

In Sec. 6.3.1 we introduced the 11×11 mass matrix $\mathcal{M}_\mathcal{N}$ of the neutral leptons of a model to address the $b \to s$ anomalies. In this Appendix we explain the procedure we took to find the leading order expression for the mass matrix of the three light neutrinos which are identified as the three lightest eigenvalues of $\mathcal{M}_\mathcal{N}$. In Eq. (6.14) $\mathcal{M}_\mathcal{N}$ was expressed in a simplified form where λ_L represents a 2×3 matrix, y, m_L, m_F and h are 2×2 matrices. Hence, the explicit expression for the 11×11 matrix is [31]

$$
\begin{pmatrix}
0 & 0 & 0 & -\frac{v_\phi \lambda_{L_{11}}}{\sqrt{2}} & -\frac{v_\phi \lambda_{L_{21}}}{\sqrt{2}} & 0 & 0 & 0 & 0 & 0 & 0 \\
0 & 0 & 0 & -\frac{v_\phi \lambda_{L_{12}}}{\sqrt{2}} & -\frac{v_\phi \lambda_{L_{22}}}{\sqrt{2}} & 0 & 0 & 0 & 0 & 0 & 0 \\
0 & 0 & 0 & -\frac{v_\phi \lambda_{L_{13}}}{\sqrt{2}} & -\frac{v_\phi \lambda_{L_{23}}}{\sqrt{2}} & 0 & 0 & 0 & 0 & 0 & 0 \\
-\frac{v_\phi \lambda_{L_{11}}}{\sqrt{2}} & -\frac{v_\phi \lambda_{L_{12}}}{\sqrt{2}} & -\frac{v_\phi \lambda_{L_{13}}}{\sqrt{2}} & 0 & 0 & m_{L_{11}} & m_{L_{21}} & 0 & 0 & 0 & 0 \\
-\frac{v_\phi \lambda_{L_{21}}}{\sqrt{2}} & -\frac{v_\phi \lambda_{L_{22}}}{\sqrt{2}} & -\frac{v_\phi \lambda_{L_{23}}}{\sqrt{2}} & 0 & 0 & m_{L_{12}} & m_{L_{22}} & 0 & 0 & 0 & 0 \\
0 & 0 & 0 & m_{L_{11}} & m_{L_{12}} & 0 & 0 & -\frac{v y_{11}}{\sqrt{2}} & -\frac{v y_{12}}{\sqrt{2}} & 0 & 0 \\
0 & 0 & 0 & m_{L_{21}} & m_{L_{22}} & 0 & 0 & -\frac{v y_{21}}{\sqrt{2}} & -\frac{v y_{22}}{\sqrt{2}} & 0 & 0 \\
0 & 0 & 0 & 0 & 0 & -\frac{v y_{11}}{\sqrt{2}} & -\frac{v y_{21}}{\sqrt{2}} & 0 & 0 & m_{F_{11}} & m_{F_{21}} \\
0 & 0 & 0 & 0 & 0 & -\frac{v y_{12}}{\sqrt{2}} & -\frac{v y_{22}}{\sqrt{2}} & 0 & 0 & m_{F_{12}} & m_{F_{22}} \\
0 & 0 & 0 & 0 & 0 & 0 & 0 & m_{F_{11}} & m_{F_{12}} & \sqrt{2}\, v_S\, h_{11} & -\frac{v_S (h_{12}+h_{21})}{\sqrt{2}} \\
0 & 0 & 0 & 0 & 0 & 0 & 0 & m_{F_{21}} & m_{F_{22}} & -\frac{v_S (h_{12}+h_{21})}{\sqrt{2}} & \sqrt{2}\, v_S\, h_{11}
\end{pmatrix}
= \mathcal{M}_\mathcal{N} \quad . \tag{C.1}
$$

$\mathcal{M}_\mathcal{N}$ is a symmetric matrix that can be diagonalized via $U^T \mathcal{M}_\mathcal{N} U = \text{diag}(m_1, ..., m_{11})$, where U is a unitary matrix. Using the Hermitian combination $\mathcal{M}_\mathcal{N}^\dagger \mathcal{M}_\mathcal{N}$

$$
\text{diag}\left(m_1^2, ..., m_{11}^2\right) = \left(U^T \mathcal{M}_\mathcal{N} U\right)^\dagger \left(U^T \mathcal{M}_\mathcal{N} U\right) = U^\dagger \mathcal{M}_\mathcal{N}^\dagger \mathcal{M}_\mathcal{N}\, U, \tag{C.2}
$$

U is the same matrix that diagonalizes both cases. Finding a complete analytical expression for the 11×11 matrix U using the eigenvalue equation $U^T \mathcal{M}_\mathcal{N} U$ is highly non trivial. However, one can compute a matrix U that diagonalizes $\mathcal{M}_\mathcal{N}^\dagger \mathcal{M}_\mathcal{N}$ allowing the use of perturbation theory with an inverse seesaw

[31] With $\widetilde{y}$ and $\widetilde{h}$ set to zero.

approximation [281]. In the following $\mathcal{M}_{\mathcal{N}}^{\dagger}\mathcal{M}_{\mathcal{N}}$ is taken in its 5×5 form. Assuming the ISS condition $v_S\, h \ll v\, y, v_\phi\, \lambda_L \ll m_{L,F}$, $\mathcal{M}_{\mathcal{N}} = \mathcal{M}_0 + \Delta\mathcal{M}$ is split, where $\mathcal{M}_0$ is the zeroth order matrix and $\Delta\mathcal{M}$ is the perturbation [32]

$$\mathcal{M}_{\mathcal{N}} = \underbrace{\begin{pmatrix} 0 & -v_\phi \lambda_L^T/\sqrt{2} & 0 & 0 & 0 \\ -v_\phi \lambda_L/\sqrt{2} & 0 & m_L^T & 0 & 0 \\ 0 & m_L & 0 & -vy/\sqrt{2} & 0 \\ 0 & 0 & -vy^T/\sqrt{2} & 0 & m_F^T \\ 0 & 0 & 0 & m_F & 0 \end{pmatrix}}_{\mathcal{M}_0} + \underbrace{\begin{pmatrix} 0 & 0 & 0 & 0 & 0 \\ 0 & 0 & 0 & 0 & 0 \\ 0 & 0 & 0 & 0 & 0 \\ 0 & 0 & 0 & 0 & 0 \\ 0 & 0 & 0 & 0 & \sqrt{2} v_s h \end{pmatrix}}_{\Delta\mathcal{M}}. \tag{C.3}$$

The squared mass matrix can be written as

$$\mathcal{M}_{\mathcal{N}}^{\dagger}\mathcal{M}_{\mathcal{N}} = \underbrace{\mathcal{M}_0^{\dagger}\mathcal{M}_0}_{M_0^2} + \underbrace{\Delta\mathcal{M}^{\dagger}\mathcal{M}_0 + \mathcal{M}_0^{\dagger}\Delta\mathcal{M}}_{M_I^2} + \underbrace{\Delta\mathcal{M}^{\dagger}\Delta\mathcal{M}}_{M_{II}^2}. \tag{C.4}$$

Expanding the eigenvalue equation (C.2) in series of powers

$$\left(M_0^2 + M_I^2 + M_{II}^2\right)\left(U^{(0)} + U^{(1)} + U^{(2)} + ...\right) = \mathrm{diag}\left(m_\nu^2, ..., m_5^2\right)\left(U^{(0)} + U^{(1)} + U^{(2)} + ...\right). \tag{C.5}$$

The zeroth order components for eigenvector $X_i^{(0)}$ and eigenvalues $\omega_i^{(0)}$ with $i = 1, ...5$ are the ones of the squared zeroth order mass matrix M_0^2. The first order correction to the eigenvalues $\omega_i^{(1)}$ comes from the diagonalization of M_I^2 using the unperturbed basis formed by $X_i^{(0)}$. One obtains the second order contribution $\omega_i^{(2)}$ diagonalizing M_{II}^2 with the zeroth order eigenvectors plus a term that involves the first order eigenvectors $X_i^{(1)}$,

$$\begin{aligned} \omega_i^{(0)} &= X_i^{\dagger(0)}\, M_0^2\, X_i^{(0)}, \\ \omega_i^{(1)} &= X_i^{\dagger(0)}\, M_I^2\, X_i^{(0)}, \\ \omega_i^{(2)} &= X_i^{\dagger(0)}\, M_I^2\, X_i^{(1)} + X_i^{\dagger(0)}\, M_{II}^2\, X_i^{(0)}, \quad \text{for } i = 1, ..., 5\,. \end{aligned} \tag{C.6}$$

The zeroth order eigenvalues $\omega_i^{(0)}$ are calculated

$$\omega_1^{(0)} = 0, \tag{C.7}$$

$$\omega_{2,3}^{(0)} = \frac{1}{2}\left[m_F^2 + m_L^2 + \frac{v^2}{2}y^2 + \frac{v_\phi^2}{2}\lambda_L^2 - \sqrt{\left(m_F^2 + m_L^2 + y^2 + \frac{v_\phi^2}{2}\lambda_L^2\right)^2 - 4\left(m_F^2 m_L^2 + \frac{v_\phi^2}{2}m_F^2\,\lambda_L^2 + \frac{v^2\, v_\phi^2}{4}\lambda_L^2 y^2\right)}\right],$$

$$\omega_{4,5}^{(0)} = \frac{1}{2}\left[m_F^2 + m_L^2 + \frac{v^2}{2}y^2 + \frac{v_\phi^2}{2}\lambda_L^2 + \sqrt{\left(m_F^2 + m_L^2 + y^2 + \frac{v_\phi^2}{2}\lambda_L^2\right)^2 - 4\left(m_F^2 m_L^2 + \frac{v_\phi^2}{2}m_F^2\,\lambda_L^2 + \frac{v^2\, v_\phi^2}{4}\lambda_L^2 y^2\right)}\right],$$

where the first eigenvalue $\omega_1^{(0)}$ corresponds to a 3×3 matrix with all its elements equal to zero. This matrix is identified as the zeroth order perturbative contribution to the light neutrino masses, thus we are

[32] The perturbative term violates lepton number.

only interested on finding the non-zero contributions up to second order of the lightest eigenvalues

$$m_\nu^2 \simeq \omega_1^{(0)} + \omega_1^{(1)} + \omega_1^{(2)}. \tag{C.8}$$

Given the degeneracy between $\omega_{2,3}^{(0)}$ and $\omega_{4,5}^{(0)}$ the eigenvectors $X_{2,3}^{\prime(0)}$ and $X_{4,5}^{\prime(0)}$ are not independent, these eigenvectors form a basis $U^{\prime(0)}$ under which M_I^2 is not diagonalized. Substituting $X_i^{(0)} = \sum_{j=2}^{3} a_{ij} X_j^{\prime(0)}$ for $i = 2, 3$ and $X_i^{(0)} = \sum_{j=4}^{5} a_{ij} X_j^{\prime(0)}$ for $i = 4, 5$ the system of equations to find the new basis $U^{(0)}$ is solved

$$X_i^{\dagger(0)} M_I^2 X_j^{(0)} = 0, \qquad X_i^{\dagger(0)} X_j^{(0)} = 1 \quad i \neq j. \tag{C.9}$$

Under the new basis formed by $X_i^{(0)}$ the degeneracy between the eigenvalues is lifted. Using the rotated $U^{(0)}$, we find the first order eigenvalue $\omega_1^{(1)}$ to be zero

$$\omega_1^{(1)} = X_1^{\dagger(0)} M_I^2 X_1^{(0)} = 0. \tag{C.10}$$

To obtain the second order contribution term $\omega_1^{(2)}$ according to Eq. (C.6) the first order correction to the eigenvector $X_1^{(1)}$ is needed. $X_1^{(1)}$ is given by:

$$X_1^{(1)} = \sum_{i=2}^{5} \frac{X_i^{\dagger(0)} M_I^2 X_1^{(0)}}{\omega_1^{(0)} - \omega_i^{(0)}} X_i^{(0)} = \begin{pmatrix} 0 \\ -\frac{\frac{v_s v^2 v_\phi}{2} h\, m_F\, m_L y^2 \lambda_L}{\left(\frac{v^2 v_\phi^2}{4} y^2 \lambda_L^2 + m_F^2 \left(m_L^2 + \frac{v_\phi^2}{2}\lambda_L^2\right)\right)^{3/2}} \\ 0 \\ -\frac{\frac{v_s v v_\phi}{\sqrt{2}} h\, m_F y \lambda_L \left(m_L^2 + \frac{v_\phi^2}{2}\lambda_L^2\right)}{\left(\frac{v^2 v_\phi^2}{4} y^2 \lambda_L^2 + m_F^2 \left(m_L^2 + \frac{v_\phi^2}{2}\lambda_L^2\right)\right)^{3/2}} \\ 0 \end{pmatrix}. \tag{C.11}$$

We calculate the second order contribution to be

$$\omega_1^{(2)} = \frac{\frac{v_S^2 v^4}{2} h^2 y^4 \lambda_L^4}{\left(\frac{v^2}{2} y^2 \lambda_L^2 + m_F^2 \left(\frac{2m_L^2}{v_\phi^2} + \lambda_L^2\right)\right)^2}. \tag{C.12}$$

Since $\omega_1^{(0)} = \omega_1^{(1)} = 0$, $m_\nu = \sqrt{\omega_1^{(2)}}$ would be the approximate value for the lightest eigenvalue of the 5×5 matrix $\mathcal{M}_\mathcal{N}$,

$$m_\nu \simeq \frac{\frac{v_S v^2}{\sqrt{2}} h\, y^2 \lambda_L^2}{\frac{v^2}{2} y^2 \lambda_L^2 + m_F^2 \left(\frac{2m_L^2}{v_\phi^2} + \lambda_L^2\right)}. \tag{C.13}$$

However, in the general 11×11 matrix the parameters λ_L, y, m_L, m_F and h are matrices with specific flavor indices. To translate m_ν into the correct matrix notation we rewrite it in terms of matrices

$$m_\nu \simeq \bar{v}^5\, h\, y\, y\, \lambda_L\, \lambda_L\, m_F^{-1}\, m_F^{-1}\, m_L^{-1}\, m_L^{-1}\,, \tag{C.14}$$

where the global factor $\bar{v}^5$ represents the product between of VEV's. To have the proper product of matrices we identified the flavor indices of the parameters:

$$\begin{aligned} \lambda_L &: \{L_R, \ell_L\}\,, \\ y &: \{F_R, L_L\}\,, \\ m_L &: \{L_L, L_R\}\,, \\ m_F &: \{F_R, F_L\}\,, \\ h &: \{\overline{F_L^c}, F_L\}\,. \end{aligned} \tag{C.15}$$

Rearranging the matrices in order to have the indices of m_ν which are $\{\ell_L, \ell_L\}$, we get the form

$$m_\nu \simeq \bar{v}^5\, \lambda_L^T\, m_L^{-1}\, y\, m_F^{-1}\, h\, \left(m_F^{-1}\right)^T\, y^T\, \left(m_L^{-1}\right)^T\, \lambda_L\,. \tag{C.16}$$

Substituting the global factor $\bar{v}^5 = \frac{v^2 v_\phi^2 v_S}{2\sqrt{2}}$ in to Eq. (C.16) gives us the final expression

$$m_\nu \simeq \frac{v^2 v_\phi^2 v_S}{2\sqrt{2}}\, \lambda_L^T\, m_L^{-1}\, y\, m_F^{-1}\, h\, \left(m_F^{-1}\right)^T\, y^T\, \left(m_L^{-1}\right)^T\, \lambda_L\,. \tag{C.17}$$

We have explicitly checked that the numerical values for the light neutrinos given by `SPheno`, are reproduced in a very good approximation by the neutrino mass expression obtained in this Appendix when the relation $v_S\, h \ll v\, y, v_\phi\, \lambda_L \ll m_{L,F}$ is fulfilled.

APPENDIX D

Model implementation in SARAH

D.1 TTTDM

TTTDM.m

```
Off[General::spell]

Model`Name      = "TTTDM";
Model`NameLaTeX = "Tres Tristes Tripletes DM model";
Model`Authors   = "D. Restrepo, J. Palacio, R. Lineros, M. Hirsch, A. Vicente... etc";
Model`Date      = "2014-11-24";


(* 24-11-2014 : Several changes *)
(* 04-06-2015 : Improvements in mixings *)
(* 16-09-2015 : Fixed convention for non-SUSY models *)
(* 13-10-2015 : Fixed details - full update *)
(* 26-10-2015 : Fixed sign in fermion Lagrangian terms *)
(* 27-10-2015 : Normalized triplets properly and changed numerical factors in some of their couplings *)

(*------------Particle Content---------------*)

(* Global Symmetries *)
Global[[1]] = {Z[2], Z2};

(*--------------Gauge Groups-----------------*)
Gauge[[1]]={B,   U[1], hypercharge, g1, False, 1};
Gauge[[2]]={WB, SU[2], left,        g2, True , 1};
Gauge[[3]]={G,  SU[3], color,       g3, False, 1};

(*--------------Matter Fields----------------*)
FermionFields[[1]] = {q , 3, {uL, dL},     1/6, 2,  3, 1};
FermionFields[[2]] = {l , 3, {vL, eL},    -1/2, 2,  1, 1};
FermionFields[[3]] = {d , 3, conj[dR],     1/3, 1, -3, 1};
FermionFields[[4]] = {u , 3, conj[uR],    -2/3, 1, -3, 1};
FermionFields[[5]] = {e , 3, conj[eR],       1, 1,  1, 1};
FermionFields[[6]] = {n , 1, conj[nR],       0, 1,  1,-1};
FermionFields[[7]] = {Tf, 1, {{Tf0/Sqrt[2], Tfp},{ Tfm, -Tf0/Sqrt[2] }},  0, 3,  1,-1};

ScalarFields[[1]] =  {H, 1, {Hp, H0},     1/2, 2,  1, 1};
ScalarFields[[2]] =  {Ts, 1, {{Ts0/Sqrt[2],  Tsp},{ Tsm, -Ts0/Sqrt[2] }},  0, 3,  1, 1};
ScalarFields[[3]] =  {Et, 1, {etp,et0},    1/2, 2,  1, -1};

RealScalars={Ts};
Tsm = conj[Tsp];

(*---------------DEFINITION-------------------*)

NameOfStates={GaugeES, EWSB};

(* ----- Before EWSB ----- *)

DEFINITION[GaugeES][LagrangianInput]=
{
  {LagFer    ,      {AddHC->True}},
  {LagNV     ,      {AddHC->True}},
  {LagH      ,      {AddHC->False}},
  {LagEt     ,      {AddHC->False}},
  {LagHEt    ,      {AddHC->False}},
  {LagHEtHC ,       {AddHC->True}},
  {LagT      ,      {AddHC->False}},
  {LagMu     ,      {AddHC->True}},
```

```
  {LagHT    ,      {AddHC->False}},
  {LagTEt   ,      {AddHC->False}}
};


LagFer    = -(Yd conj[H].d.q + Ye conj[H].e.l + Yu H.u.q + Yn Et.n.l + Yt Et.Tf.l + Ymix Ts.Tf.n);     (* Fermions ↪
      lagrangian *)
LagNV     = -(Mn/2 n.n + Mv/2 Tf.Tf);
(* *)
LagH      = -(- mH2 conj[H].H     + 1/2 lambda1 conj[H].H.conj[H].H );                  (* Higgs lagrangian *)
LagEt     = -(+ mEt2 conj[Et].Et  + 1/2 lambda2 conj[Et].Et.conj[Et].Et );              (* Eta lagrangian *)
LagHEt    = -(+ lambda3 conj[H].H.conj[Et].Et + lambda4 conj[H].Et.conj[Et].H );
LagHEtHC = -(+ 1/2 lambda5 conj[H].Et.conj[H].Et );
(* *)
LagT      = -(- 1/2 mT2 Ts.Ts + 1/4 lambdaT2 Ts.Ts.Ts.Ts );                              (* Triplet lagrangian and ↪
      interactions *)
LagMu     = -(+ mu1 conj[H].Ts.H  +  mu2 conj[Et].Ts.Et );
LagHT     = -(+ 1/2 lambdaT1 conj[H].H.Ts.Ts );
LagTEt    = -(+ 1/2 lambdaTet conj[Et].Et.Ts.Ts );

(* Gauge Sector *)

DEFINITION[EWSB][GaugeSector] =
{
  {{VB,VWB[3]},{VP,VZ},ZZ},
  {{VWB[1],VWB[2]},{VWp,conj[VWp]},ZW}
};

(* ----- VEVs ---- *)

DEFINITION[EWSB][VEVs]=
{
  {H0,  {v, 1/Sqrt[2]}, {Ah, \[ImaginaryI]/Sqrt[2]}, {phiH, 1/Sqrt[2]}},
  {Ts0, {v3, 1}, {TsI, 0}, {TsR, 1}},
  {et0, {0, 0}, {etI, \[ImaginaryI]/Sqrt[2]}, {etR, 1/Sqrt[2]}}
};

DEFINITION[EWSB][MatterSector]=
{
  {{phiH, TsR}, {hh, ZH}},
  {{conj[Hp], conj[Tsp]}, {Hpm, ZP}},
  {{Tf0, conj[nR]},{X0, ZX}},
  {{vL}, {VL, Vv}},
  {{{dL}, {conj[dR]}}, {{DL,Vd}, {DR,Ud}}},
  {{{uL}, {conj[uR]}}, {{UL,Vu}, {UR,Uu}}},
  {{{eL}, {conj[eR]}}, {{EL,Ve}, {ER,Ue}}}
};

(*-------------------------------------------------------*)
(* Dirac-Spinors *)
(*-------------------------------------------------------*)

DEFINITION[EWSB][DiracSpinors]=
{
  Fd  -> {  DL, conj[DR]},
  Fe  -> {  EL, conj[ER]},
  Fu  -> {  UL, conj[UR]},
  Fv  -> {  VL, conj[VL]},
  Chi -> {  X0, conj[X0] },
  Cha -> {  Tfm, conj[Tfp] }
};

DEFINITION[EWSB][GaugeES]=
{
  Fd1 ->{  FdL, 0},
  Fd2 ->{  0, FdR},
  Fu1 ->{  Fu1, 0},
  Fu2 ->{  0, Fu2},
  Fe1 ->{  Fe1, 0},
  Fe2 ->{  0, Fe2}
};
```

particles.m

```
(* ::Package:: *)
ParticleDefinitions[GaugeES] = {

      {H0,  {    PDG -> 0,
                 Width -> 0,
                 Mass -> Automatic,
                 LaTeX -> "H^0",
                 OutputName -> "H0" }},

      {Hp,  {    PDG -> 0,
                 Width -> 0,
                 Mass -> Automatic,
                 LaTeX -> "H^+",
                 OutputName -> "Hp" }},
```

```
15
16      {Ts0,  {   PDG -> 0,
17                 Width -> 0,
18                 Mass -> Automatic,
19                 LaTeX -> "\\Omega^0",
20                 OutputName -> "Ts0" }},
21
22      {Tsp,  {   LaTeX -> "\\Omega^+",
23                 OutputName -> "Tsp" }},
24
25      {Tsm,  {   LaTeX -> "\\Omega^-",
26                 OutputName -> "Tsm" }},
27
28      {Tf0,  {   PDG -> 0,
29                 Width -> 0,
30                 Mass -> Automatic,
31                 LaTeX -> "\\Sigma^0",
32                 OutputName -> "Tf0" }},
33
34      {Tfp,  {   PDG -> 0,
35                 Width -> 0,
36                 Mass -> Automatic,
37                 LaTeX -> "\\Sigma^+",
38                 OutputName -> "Tfp" }},
39
40      {Tfm,  {   PDG -> 0,
41                 Width -> 0,
42                 Mass -> Automatic,
43                 LaTeX -> "\\Sigma^-",
44                 OutputName -> "Tfm" }},
45
46      {et0, {    PDG -> 0,
47                 Width -> 0,
48                 Mass -> Automatic,
49                 LaTeX -> "\\eta^0",
50                 OutputName -> "et0" }},
51
52      {etp, {    PDG -> 0,
53                 Width -> 0,
54                 Mass -> Automatic,
55                 LaTeX -> "\\eta^+",
56                 OutputName -> "etp" }},
57
58      {VB,   { Description -> "B-Boson"}},
59      {VG,   { Description -> "Gluon"}},
60      {VWB,  { Description -> "W-Bosons"}},
61      {gB,   { Description -> "B-Boson Ghost"}},
62      {gG,   { Description -> "Gluon Ghost" }},
63      {gWB,  { Description -> "W-Boson Ghost"}}
64
65      };
66
67
68
69  ParticleDefinitions[EWSB] = {
70
71      {hh,  {  Description -> "Higgs",
72               PDG -> {25,35},
73               PDG.IX -> {101000001,101000002},
74               Mass -> Automatic  }},
75      {Ah,  {  Description -> "Pseudo-Scalar Higgs",
76               PDG -> {0},
77               PDG.IX ->{0},
78               Mass -> {0},
79               Width -> {0} }},
80      {Hpm, {  Description -> "Charged Higgs",
81               PDG -> {0,2001},
82               PDG.IX -> {0,101000004}  }},
83
84      {etR,   {  Description -> "CP-even eta scalar",
85                 PDG -> {1001},
86                 Mass -> Automatic,
87                 ElectricCharge -> 0,
88                 LaTeX -> "\\eta_R",
89                 OutputName -> "etR" }},
90      {etI,   {  Description -> "CP-odd eta scalar",
91                 PDG -> {1002},
92                 Mass -> Automatic,
93                 ElectricCharge -> 0,
94                 LaTeX -> "\\eta_I",
95                 OutputName -> "etI" }},
96      {etp,   {  Description -> "Charged eta scalar",
97                 PDG -> {1003},
98                 Mass -> Automatic,
99                 ElectricCharge -> 1,
100                LaTeX -> "\\eta^+",
101                OutputName -> "etp" }},
102
103     {VP,   { Description -> "Photon"}},
104     {VZ,   { Description -> "Z-Boson", Goldstone -> Ah }},
```

```
      {VWp,  { Description -> "W+ - Boson", Goldstone -> Hpm[{1}]}},
      {VG,   { Description -> "Gluon" }},

      {gP,   { Description -> "Photon Ghost"}},
      {gWp,  { Description -> "Positive W+ - Boson Ghost"}},
      {gWpC, { Description -> "Negative W+ - Boson Ghost" }},
      {gZ,   { Description -> "Z-Boson Ghost" }},
      {gG,   { Description -> "Gluon Ghost" }},

      {Fd,   { Description -> "Down-Quarks"}},
      {Fu,   { Description -> "Up-Quarks"}},
      {Fe,   { Description -> "Leptons" }},
      {Fv,   { Description -> "Neutrinos" }},
      {Chi,  { Description -> "Singlet Fermions",
               PDG -> {1012,1014},
               PDG.IX ->{-110000004,-110000005},
               FeynArtsNr -> 11,
               ElectricCharge -> 0,
               LaTeX -> "\\chi^0",
               OutputName -> "Chi" }},
      {Cha,  { Description -> "Charged Fermions",
               PDG -> {-1013},
               PDG.IX ->{-110000006},
               Mass -> Automatic,
               FeynArtsNr -> 12,
               ElectricCharge -> -1,
               LaTeX -> "\\chi^-",
               OutputName -> "Cha" }},
       {TsI,  { Description -> "Pseudo-Scalar Ts",
                PDG -> {0},
                PDG.IX ->{0},
                Mass -> {0},
                Width -> {0},
                OutputName -> "TsI" }}

};

WeylFermionAndIndermediate =
{
   {H,      {LaTeX -> "H"}},
   {Ts,     {LaTeX -> "\\Omega"}},
   {Tf,     {LaTeX -> "\\Sigma"}},
   {Et,     {LaTeX -> "\\eta"}},
   {dR,     {LaTeX -> "d_R" }},
   {eR,     {LaTeX -> "e_R" }},
   {lep,    {LaTeX -> "l" }},
   {uR,     {LaTeX -> "u_R" }},
   {q,      {LaTeX -> "q" }},
   {eL,     {LaTeX -> "e_L" }},
   {dL,     {LaTeX -> "d_L" }},
   {uL,     {LaTeX -> "u_L" }},
   {vL,     {LaTeX -> "\\nu_L" }},
   {DR,     {LaTeX -> "D_R" }},
   {ER,     {LaTeX -> "E_R" }},
   {UR,     {LaTeX -> "U_R" }},
   {EL,     {LaTeX -> "E_L" }},
   {DL,     {LaTeX -> "D_L" }},
   {UL,     {LaTeX -> "U_L" }},
   {X0,     {LaTeX -> "X^0"}},
   {Xm,     {LaTeX -> "X^-"}},
   {Xp,     {LaTeX -> "X^+"}},
   {VL,     {LaTeX -> "V_L" }},
   {phiH,   {LaTeX -> "\\phi_H" }},
   {Tsp,  {   LaTeX -> "\\Omega^+",
              OutputName -> "Tsp" }},
   {Tsm,  {   LaTeX -> "\\Omega^-",
              OutputName -> "Tsm" }},
   {TsR,    {LaTeX -> "\\phi_\\Omega" }},
   {TsI,    {LaTeX -> "\\sigma_\\Omega" }},
   {etR,    {LaTeX -> "\\phi_\\eta" }},
   {etI,    {LaTeX -> "\\sigma_\\eta" }},
   {n,      {LaTeX -> "N" }},
   {nR,     {LaTeX -> "\\nu_R" }}
};
```

parameters.m

```
(* ::Package:: *)

ParameterDefinitions = {

{g1,        { Description -> "Hypercharge-Coupling"}},
{g2,        { Description -> "Left-Coupling"}},
{g3,        { Description -> "Strong-Coupling"}},
{AlphaS,    {Description -> "Alpha Strong"}},
{e,         { Description -> "electric charge"}},

{Gf,        { Description -> "Fermi's constant"}},
```

```
{aEWinv,    { Description -> "inverse weak coupling constant at mZ"}},

{Yu,        { Description -> "Up-Yukawa-Coupling",
              DependenceNum ->  Sqrt[2]/v* { {Mass[Fu,1],0,0},
                                            {0,Mass[Fu,2],0},
                                            {0,0,Mass[Fu,3]}}
            }
},
{Yd,        { Description -> "Down-Yukawa-Coupling",
              DependenceNum ->  Sqrt[2]/v* {{Mass[Fd,1],0,0},
                                           {0, Mass[Fd,2],0},
                                           {0, 0, Mass[Fd,3]}}}},

{Ye,        { Description -> "Lepton-Yukawa-Coupling",
                      DependenceNum ->  Sqrt[2]/v* {{Mass[Fe,1],0,0},
                                                   {0, Mass[Fe,2],0},
                                                   {0, 0, Mass[Fe,3]}}}},


{ThetaW,    { Description -> "Weinberg-Angle",
              DependenceNum -> ArcSin[Sqrt[1 - Mass[VWp]^2/Mass[VZ]^2]]}},

{ZZ, {Description -> "Photon-Z Mixing Matrix"}},
{ZW, {Description -> "W Mixing Matrix", Dependence -> 1/Sqrt[2] {{1, 1},{I,-I}} } },

{Vu,        {Description ->"Left-Up-Mixing-Matrix"}},
{Vd,        {Description ->"Left-Down-Mixing-Matrix"}},
{Uu,        {Description ->"Right-Up-Mixing-Matrix"}},
{Ud,        {Description ->"Right-Down-Mixing-Matrix"}},
{Ve,        {Description ->"Left-Lepton-Mixing-Matrix"}},
{Ue,        {Description ->"Right-Lepton-Mixing-Matrix"}},

(* Scalar sector *)

{v,  { Description -> "EW-VEV",
       DependenceNum -> Sqrt[4*Mass[VWp]^2/(g2^2)],
       DependenceSPheno -> None  }},

{\[Beta],   { Description -> "Pseudo Scalar mixing angle"  }},
{\[Alpha],  { Description -> "Scalar mixing angle" }},

{mH2, { Description -> "SM Higgs Mass Parameter",
        LaTeX -> "m_\\phi^2" }},

{v3,   {LaTeX -> "v_3",
        LesHouches -> {HDM,1},
        OutputName-> v3 }},

{mEt2, {LaTeX -> "m_\\eta^2",
        LesHouches -> {HDM,2},
        OutputName-> mEt2 }},

{mT2,  {LaTeX -> "m_\\Omega^2",
        LesHouches -> {HDM,3},
        OutputName-> mT2 }},

{mu1,  {LaTeX -> "\\mu_1",
        LesHouches -> {HDM,4},
        OutputName-> mu1 }},

{mu2,  {LaTeX -> "\\mu_2",
        LesHouches -> {HDM,5},
        OutputName-> mu2 }},

{lambda1,   {LaTeX -> "\\lambda_1",
             LesHouches -> {HDM,6},
             OutputName-> lam1 }},

{lambda2,   {LaTeX -> "\\lambda_2",
             LesHouches -> {HDM,7},
             OutputName-> lam2 }},

{lambda3,   {LaTeX -> "\\lambda_3",
             LesHouches -> {HDM,8},
             OutputName-> lam3 }},

{lambda4,   {LaTeX -> "\\lambda_4",
             LesHouches -> {HDM,9},
             OutputName-> lam4 }},

{lambda5,   {Real -> True,
             LaTeX -> "\\lambda_5",
             LesHouches -> {HDM,10},
             OutputName-> lam5 }},

{lambdaT1,  {LaTeX -> "\\lambda^\\Omega_1",
             LesHouches -> {HDM,11},
             OutputName-> lT1 }},

{lambdaT2,  {LaTeX -> "\\lambda^\\Omega_2",
```

```
             LesHouches -> {HDM,12},
             OutputName-> lT2 }},

{lambdaTet, {LaTeX -> "\\lambda^\\eta",
             LesHouches -> {HDM,13},
             OutputName-> lTet }},

{ZH,        { Description->"Scalar-Mixing-Matrix"}},
{ZP,        { Description->"Charged-Mixing-Matrix"}},

(* Yukawa sector *)

{Yn,   {LaTeX -> "Y_N",
        LesHouches -> YN,
        OutputName->Yn }},

{Yt,   {LaTeX -> "Y_\\Sigma",
        LesHouches -> YT,
        OutputName->Yt }},

{Ymix, {LaTeX -> "Y_\\Omega",
        LesHouches -> {HDM,14},
        OutputName->Ymix }},

{Mn,   {LaTeX -> "M_N",
        LesHouches -> {HDM,15},
        OutputName->Mn }},

{Mv,   {LaTeX -> "M_\\Sigma",
        LesHouches -> {HDM,16},
        OutputName->Mv }},

{ZX, {Description -> "Singlet fermion Mixing Matrix",
      LaTeX -> "Z^{\\chi^0}",
      LesHouches -> ZXMIX,
      OutputName -> ZX }},

{Vv, {Description ->"Neutrino-Mixing-Matrix"}}

};
```

SPheno.m

```
OnlyLowEnergySPheno = True;

MINPAR={
  {1,lambda1Input},
  {2,lambda2Input},
  {3,lambda3Input},
  {4,lambda4Input},
  {5,lambda5Input},
  {6,lambdaT1Input},
  {7,lambdaT2Input},
  {8,lambdaTetInput},
  {9,mEt2Input},
  {10,mu1Input},
  {11,mu2Input},
  {12,v3Input},
  {13,YmixInput},
  {14,MnInput},
  {15,MvInput}
};

ParametersToSolveTadpoles = {mH2,mT2};
(* Tad1Loop[a_]=0; *)

BoundaryLowScaleInput={
  {v, vSM},
  {Ye, YeSM},
  {Yd, YdSM},
  {Yu, YuSM},
  {g1, g1SM},
  {g2, g2SM},
  {g3, g3SM},
  {lambda1,lambda1Input},
  {lambda2,lambda2Input},
  {lambda3,lambda3Input},
  {lambda4,lambda4Input},
  {lambda5,lambda5Input},
  {lambdaT1,lambdaT1Input},
  {lambdaT2,lambdaT2Input},
  {lambdaTet,lambdaTetInput},
  {mEt2,mEt2Input},
  {mu1,mu1Input},
  {mu2,mu2Input},
  {v3,v3Input},
  {Ymix, YmixInput},
  {Mn, MnInput},
```

```
  {Mv, MvInput},
  {Yn, LHInput[Yn]},
  {Yt, LHInput[Yt]}
};


ListDecayParticles = {Fu,Fe,Fd,Fv,VZ,VWp,hh,Hpm,etR,etI,etp,Chi,Cha};
ListDecayParticles3B = {{Fu,"Fu.f90"},{Fe,"Fe.f90"},{Fd,"Fd.f90"}};
```

D.2 DarkBSNu

DarkBSNu.m

```
Off[General::spell]

Model`Name = "DarkBSNu";
Model`NameLaTeX ="DarkBS model with neutrino masses";
Model`Authors = "D. Sierra, F. Staub, A. Vicente, P. Rocha-Moran";
Model`Date = "2016-06-12";


(* Extension with neutrino masses = Paulina 2016-06-12 *)
(* Added 2nd F generation and renamed Yukawa couplings = Avelino 2016-16-12 *)


(*-------------------------------------------*)
(*   Particle Content*)
(*-------------------------------------------*)

(* Global Symmetries *)
Global[[1]] = {Z[2], Z2};

(* Gauge Groups *)

Gauge[[1]]={B,   U[1], hypercharge, g1,False,1};
Gauge[[2]]={WB, SU[2], left,        g2,True,1};
Gauge[[3]]={G,  SU[3], color,       g3,False,1};
Gauge[[4]]={Bp,  U[1], Uchi,        gX,False,1};


(* Matter Fields *)

FermionFields[[1]] = {q, 3, {uL, dL},     1/6, 2,  3, 0, 1};
FermionFields[[2]] = {l, 3, {vL, eL},    -1/2, 2,  1, 0, 1};
FermionFields[[3]] = {d, 3, conj[dR],     1/3, 1, -3, 0, 1};
FermionFields[[4]] = {u, 3, conj[uR],    -2/3, 1, -3, 0, 1};
FermionFields[[5]] = {e, 3, conj[eR],       1, 1,  1, 0, 1};

FermionFields[[6]] = {lL, 2, {v4, e4},    -1/2, 2,  1,  2, 1};
FermionFields[[7]] = {lR, 2, {e5, v5},     1/2, 2,  1, -2, 1};
FermionFields[[8]] = {qL, 1, {u4, d4},     1/6, 2,  3,  2, 1};
FermionFields[[9]] = {qR, 1, {d5, u5},    -1/6, 2, -3, -2, 1};

FermionFields[[10]] = {FeL, 2, feL,  0, 1, 1, 2, 1};
FermionFields[[11]] = {FeR, 2, conj[feR],  0, 1, 1, -2, 1};


ScalarFields[[1]] =  {H, 1, {Hp, H0},   1/2, 2,  1,  0,  1};
ScalarFields[[2]] =  {Phi, 1, phi,        0, 1,  1,  2,  1};
ScalarFields[[3]] =  {Chi, 1, chi,        0, 1,  1, -1, -1};

ScalarFields[[4]] =  {S,  1, s,     0, 1, 1, -4, 1};


(*-----------------------------------------------*)
(*   DEFINITION                                  *)
(*-----------------------------------------------*)

NameOfStates={GaugeES, EWSB};

(* ----- Before EWSB ----- *)

DEFINITION[GaugeES][LagrangianInput]= {
        {LagHC, {AddHC->True}},
        {LagNoHC,{AddHC->False}},
        {LagNmass, {AddHC->True}},
        {LagFmass, {AddHC->True}},
        {SPotNoHC, {AddHC->False}},
        {SPotHC, {AddHC->True}}
};

LagNoHC = -mH2 conj[H].H - mPhi2 Phi.conj[Phi] - mChi2 Chi.conj[Chi] - 1/2 \[Lambda] conj[H].H.conj[H].H \
-1/2 LamP Phi.conj[Phi].Phi.conj[Phi] -1/2 LamC Chi.conj[Chi].Chi.conj[Chi] \
```

```
- LamCP conj[Phi].Phi.conj[Chi].Chi - LamHP conj[H].H.conj[Phi].Phi - LamHC conj[H].H.conj[Chi].Chi;
LagHC =  -(Yd conj[H].d.q + Ye conj[H].e.l + Yu H.u.q + mQ qL.qR + mL lL.lR + lamQ Phi.qR.q + Mu Phi.Chi.Chi);

(* Terms contributing to neutrino mass *)
LagNmass = -(lamL Phi.lR.l + YL H.lL.FeR + YLt conj[H].lR.FeL + hYuk S.FeL.FeL + hYukt conj[S].FeR.FeR ) ;
LagFmass = -(mF FeL.FeR);

(* S potential *)
SPotNoHC = - mS2 conj[S].S - 1/2 LamS conj[S].S.conj[S].S - LamHS conj[H].H.conj[S].S \
- LamPS conj[Phi].Phi.conj[S].S - LamCS conj[Chi].Chi.conj[S].S;
SPotHC = - Mup Phi.Phi.S;

(* Gauge Sector *)

DEFINITION[EWSB][GaugeSector] =
{
  {{VB,VWB[3],VBp},{VP,VZ,VZp},ZZ},
  {{VWB[1],VWB[2]},{VWp,conj[VWp]},ZW}
};


(* ----- VEVs ---- *)

DEFINITION[EWSB][VEVs]=
{    {H0, {v, 1/Sqrt[2]}, {sigmaH, \[ImaginaryI]/Sqrt[2]},{phiH, 1/Sqrt[2]}},
     {phi, {vP, 1/Sqrt[2]}, {sigmaP, \[ImaginaryI]/Sqrt[2]},{phiP, 1/Sqrt[2]}},
     {chi, {0,0}, {sigmaC, \[ImaginaryI]/Sqrt[2]},{phiC, 1/Sqrt[2]}},
     {s, {vS, 1/Sqrt[2]}, {sigmaS, \[ImaginaryI]/Sqrt[2]},{phiS, 1/Sqrt[2]}}
};


DEFINITION[EWSB][MatterSector]=   {
    {{phiH,phiP,phiS},{hh,ZH}},
    {{sigmaH,sigmaP,sigmaS},{Ah,ZA}},
    {{{dL,d4}, {conj[dR],d5}}, {{DL,Vd}, {DR,Ud}}},
    {{{uL,u4}, {conj[uR],u5}}, {{UL,Vu}, {UR,Uu}}},
    {{{eL,e4}, {conj[eR],e5}}, {{EL,Ve}, {ER,Ue}}},
    {{vL,v5,v4,conj[feR],feL}, {VL,UV}}
};


(*-------------------------------------------------------*)
(* Dirac-Spinors *)
(*-------------------------------------------------------*)

DEFINITION[EWSB][DiracSpinors]={
 Fd ->{  DL, conj[DR]},
 Fe ->{  EL, conj[ER]},
 Fu ->{  UL, conj[UR]},
 Fv ->{  VL, conj[VL]}};

DEFINITION[EWSB][GaugeES]={
 Fd1 ->{  FdL, 0},
 Fd2 ->{  0, FdR},
 Fu1 ->{  Fu1, 0},
 Fu2 ->{  0, Fu2},
 Fe1 ->{  Fe1, 0},
 Fe2 ->{  0, Fe2}};
```

particles.m

```
ParticleDefinitions[GaugeES] = {
      {H0,  {    PDG -> {0},
                 Width -> 0,
                 Mass -> Automatic,
                 FeynArtsNr -> 1,
                 LaTeX -> "H^0",
                 OutputName -> "H0" }},


      {Hp,  {    PDG -> {0},
                 Width -> 0,
                 Mass -> Automatic,
                 FeynArtsNr -> 2,
                 LaTeX -> "H^+",
                 OutputName -> "Hp" }},

      {s,  {    PDG -> {0},
                 Width -> 0,
                 Mass -> Automatic,
                 FeynArtsNr -> 3,
                 LaTeX -> "s^0",
                 OutputName -> "s" }},


      {VB,   { Description -> "B-Boson"}},
      {VG,   { Description -> "Gluon"}},
      {VWB,  { Description -> "W-Bosons"}},
```

```
      {gB,   { Description -> "B-Boson Ghost"}},
      {gG,   { Description -> "Gluon Ghost" }},
      {gWB,  { Description -> "W-Boson Ghost"}}

      };

ParticleDefinitions[EWSB] = {


    {hh   ,  {  Description -> "Higgs",
                PDG -> {25,35,45},
                PDG.IX -> {101000001,101000002,101000003} }},

    {Ah   ,  {  Description -> "Pseudo-Scalar Higgs",
                PDG -> {0,0,36},
                PDG.IX ->{0,0,101000004},
                Width ->{0,0,External}
                Mass ->{0,0,LesHouches} }},


     {Hp,     { Description -> "Charged Higgs",
                PDG -> {0},
                PDG.IX ->{0},
                Width -> {0},
                Mass -> {0},
                LaTeX -> {"H^+","H^-"},
                OutputName -> {"Hp","Hm"} }},

      {VP,   { Description -> "Photon"}},
      {VZ,   { Description -> "Z-Boson",
               Goldstone -> Ah[{1}] }},
      {VZp,   { Description -> "Z'-Boson",
               Goldstone -> Ah[{2}] }},
      {VG,   { Description -> "Gluon" }},
      {VWp,  { Description -> "W+ - Boson",
               Goldstone -> Hp }},
      {gP,   { Description -> "Photon Ghost"}},
      {gWp,  { Description -> "Positive W+ - Boson Ghost"}},
      {gWpC, { Description -> "Negative W+ - Boson Ghost" }},
      {gZ,   { Description -> "Z-Boson Ghost" }},
      {gZp,  { Description -> "Z'-Ghost" }},
      {gG,   { Description -> "Gluon Ghost" }},

      {phiC,   {  Description -> "CP-even Chi scalar",
                  PDG -> {1001},
                  Mass -> LesHouches,
                  ElectricCharge -> 0,
                  LaTeX -> "\\chi_R",
                  OutputName -> "chiR" }},
      {sigmaC,   {  Description -> "CP-odd Chi scalar",
                  PDG -> {1002},
                  Mass -> LesHouches,
                  ElectricCharge -> 0,
                  LaTeX -> "\\chi_I",
                  OutputName -> "chiI" }},

      {Fd,   { Description -> "Down-Quarks",
               PDG -> {1,3,5,7},
               PDG.IX->{-110890201,-110890202,-110890203,-110890204} }},
      {Fu,   { Description -> "Up-Quarks",
               PDG -> {2,4,6,8},
               PDG.IX->{110100401,110100402,110100403,110100404} }},
      {Fe,   { Description -> "Leptons",
               PDG -> {11,13,15,17,19},
               PDG.IX -> {-110000601,-110000602,-110000603,-110000604,-110000605} }},
      {Fv,   { Description -> "Neutrinos",
               PDG -> {12,14,16,1018,1020,2018,2020,3018,3020,4018,4020},
               PDG.IX ->{-110000001,-110000002,-110000003,-110000004,-110000005,-110000006,-110000007,
               -110000008,-110000009,-110000010,-110000011} }}

};


WeylFermionAndIndermediate = {

    {H,      {   PDG -> {0},
                 Width -> 0,
                 Mass -> Automatic,
                 LaTeX -> "H",
                 OutputName -> "" }},

   {dR,     {LaTeX -> "d_R" }},
   {eR,     {LaTeX -> "e_R" }},
   {lep,    {LaTeX -> "l" }},
   {uR,     {LaTeX -> "u_R" }},
   {q,      {LaTeX -> "q" }},
   {eL,     {LaTeX -> "e_L" }},
   {dL,     {LaTeX -> "d_L" }},
   {uL,     {LaTeX -> "u_L" }},
   {vL,     {LaTeX -> "\\nu_L" }},
```

```
118
119    {DR,     {LaTeX -> "D_R" }},
120    {ER,     {LaTeX -> "E_R" }},
121    {UR,     {LaTeX -> "U_R" }},
122    {EL,     {LaTeX -> "E_L" }},
123    {DL,     {LaTeX -> "D_L" }},
124    {UL,     {LaTeX -> "U_L" }}
125 };
```

parameters.m

```
1  ParameterDefinitions = {
2
3  {g1,        { Description -> "Hypercharge-Coupling"}},
4  {g2,        { Description -> "Left-Coupling"}},
5  {g3,        { Description -> "Strong-Coupling"}},
6
7
8  {gX,       {LaTeX -> "g_X",
9              LesHouches -> {GAUGE,4},
10             OutputName -> gX}},
11
12 {g1X,       {LaTeX -> "\\tilde{g}",
13             LesHouches -> {GAUGE,10},
14             OutputName -> g1X}},
15 {gX1,       {LaTeX -> "\\bar{g}",
16             LesHouches -> {GAUGE,11},
17             OutputName -> gX1}},
18
19
20 {AlphaS,    {Description -> "Alpha Strong"}},
21 {e,         { Description -> "electric charge"}},
22
23 {Gf,        { Description -> "Fermi's constant"}},
24 {aEWinv,    { Description -> "inverse weak coupling constant at mZ"}},
25
26 {Yu,        { Description -> "Up-Yukawa-Coupling",
27               DependenceNum ->  Sqrt[2]/v* {{Mass[Fu,1],0,0},
28                                            {0, Mass[Fu,2],0},
29                                            {0, 0, Mass[Fu,3]}}}},
30
31 {Yd,        { Description -> "Down-Yukawa-Coupling",
32               DependenceNum ->  Sqrt[2]/v* {{Mass[Fd,1],0,0},
33                                            {0, Mass[Fd,2],0},
34                                            {0, 0, Mass[Fd,3]}}}},
35
36 {Ye,        { Description -> "Lepton-Yukawa-Coupling",
37               DependenceNum ->  Sqrt[2]/v* {{Mass[Fe,1],0,0},
38                                            {0, Mass[Fe,2],0},
39                                            {0, 0, Mass[Fe,3]}}}},
40
41
42 {\[Lambda],  { Description -> "SM Higgs Selfcouplings",
43               DependenceNum -> Mass[hh]^2/(2 v^2)}},
44 {v,          { Description -> "EW-VEV",
45               DependenceNum -> Sqrt[4*Mass[VWp]^2/(g2^2)],
46               DependenceSPheno -> None  }},
47
48 {vP,   {LaTeX ->"v_\\phi",
49          OutputName -> vP,
50          LesHouches -> {DBS,20}}},
51
52 {mPhi2, {LaTeX -> "m_{\\phi}^2",
53        OutputName->mPhi2,
54        LesHouches ->  {DBS,1}}},
55
56 {mChi2, {LaTeX -> "m_{\\chi}^2",
57        OutputName->mX2,
58        LesHouches ->  {DBS,2}}},
59
60 {mQ, {LaTeX -> "m_Q",
61        OutputName->mQ,
62        LesHouches ->  {DBS,3}}},
63
64 {mL, {LaTeX -> "m_L",
65        OutputName->mL,
66        LesHouches -> ML }},
67
68 {LamP, {LaTeX -> "\\lambda_{\\phi}",
69        OutputName->LamP,
70        LesHouches ->  {DBS,10}}},
71
72 {LamC, {LaTeX -> "\\lambda_{\\chi}",
73        OutputName->LamC,
74        LesHouches ->  {DBS,11}}},
75
76 {LamCP, {LaTeX -> "\\lambda_{\\phi\\chi}",
77        OutputName->LamCP,
```

```
78        LesHouches ->  {DBS,12}}},
79
80  {LamHP, {LaTeX -> "\\lambda_{H\\phi}",
81        OutputName->LamHP,
82        LesHouches ->  {DBS,13}}},
83
84  {LamHC, {LaTeX -> "\\lambda_{H\\chi}",
85        OutputName->LamHC,
86        LesHouches ->  {DBS,14}}},
87
88  {lamQ, {LaTeX -> "\\lambda_Q",
89        OutputName->lamQ,
90        LesHouches ->  LAMQ}},
91
92  {lamL, {LaTeX -> "\\lambda_L",
93        OutputName->lamL,
94        LesHouches ->  LAML}},
95
96  {Mu, {LaTeX -> "\\mu",
97       Real -> True,
98       OutputName->Mu,
99       LesHouches ->  {DBS,7}}},
100
101
102 {mH2,         { Description -> "SM Higgs Mass Parameter"}},
103
104 {ThetaW,    { Description -> "Weinberg-Angle",
105               DependenceNum -> ArcSin[Sqrt[1 - Mass[VWp]^2/Mass[VZ]^2]]  }},
106
107 {ThetaWp,  { LaTeX -> "{\\Theta'}_W",
108              Real ->True,
109              DependenceSPheno -> ArcCos[Abs[ZZ[3,3]]],
110              OutputName-> TWp,
111              LesHouches -> {ANGLES,10}      }},
112
113 {ZH, { Description->"Scalar-Mixing-Matrix",
114        LaTeX -> "Z^H",
115        DependenceOptional -> None,
116        Real -> True,
117        Value -> None,
118        LesHouches -> SCALARMIX,
119        OutputName-> ZH     }},
120
121 {ZA, { Description->"Pseudo-Scalar-Mixing-Matrix",
122        LaTeX -> "Z^A",
123        DependenceOptional -> None,
124        Real -> True,
125        Value -> None,
126        LesHouches -> PSEUDOSCALARMIX,
127        OutputName-> ZA      }},
128
129 {UV, { Description -> "Neutrino-Mixing-Matrix",
130        LaTeX -> "U^V",
131        Dependence ->  None,
132        DependenceOptional -> None,
133        Value -> None,
134        LesHouches -> UVMIX,
135        OutputName-> UV      }},
136
137 {ZZ, {Description -> "Photon-Z Mixing Matrix",
138       Dependence->  {{Cos[ThetaW],-Sin[ThetaW] Cos[ThetaWp], Sin[ThetaW] Sin[ThetaWp] },
139                      {Sin[ThetaW],Cos[ThetaW] Cos[ThetaWp],-Cos[ThetaW] Sin[ThetaWp]},
140                      {0, Sin[ThetaWp], Cos[ThetaWp]}} }},
141
142 {ZW, {Description -> "W Mixing Matrix",
143        Dependence ->   1/Sqrt[2] {{1, 1},
144                  {\[ImaginaryI],-\[ImaginaryI]}} }},
145
146
147 {Vu,        {Description ->"Left-Up-Mixing-Matrix"}},
148 {Vd,        {Description ->"Left-Down-Mixing-Matrix"}},
149 {Uu,        {Description ->"Right-Up-Mixing-Matrix"}},
150 {Ud,        {Description ->"Right-Down-Mixing-Matrix"}},
151 {Ve,        {Description ->"Left-Lepton-Mixing-Matrix"}},
152 {Ue,        {Description ->"Right-Lepton-Mixing-Matrix"}},
153
154 (* New parameters in the neutrino extended model *)
155
156 {YL, {LaTeX -> "Y_L",
157       OutputName->YL,
158       LesHouches -> YL }},
159
160 {YLt, {LaTeX -> "\\widetilde Y_L",
161        OutputName->YLt,
162        LesHouches -> YLT }},
163
164 {hYuk, {LaTeX -> "h",
165         OutputName->hYuk,
166         LesHouches -> HYUK }},
167
```

```
{hYukt, {LaTeX -> "\\widetilde h",
         OutputName->hYukt,
         LesHouches -> HYUKT }},

{mF, {LaTeX -> "m_F",
      OutputName->mF,
      LesHouches -> MF }},

{mS2, {LaTeX -> "m_S^2",
       OutputName->mS2,
       LesHouches -> {DBS,30} }},

{LamS, {LaTeX -> "\\lambda_S",
        OutputName->LamS,
        LesHouches -> {DBS,31} }},

{LamHS, {LaTeX -> "\\lambda_{HS}",
         OutputName->LamHS,
         LesHouches -> {DBS,32} }},

{LamPS, {LaTeX -> "\\lambda_{\\phi S}",
         OutputName->LamPS,
         LesHouches -> {DBS,33} }},

{LamCS, {LaTeX -> "\\lambda_{\\chi S}",
         OutputName->LamCS,
         LesHouches -> {DBS,34} }},

{Mup, {LaTeX -> "\\mu^\\prime",
       Real -> True,
       OutputName->Mup,
       LesHouches ->  {DBS,35}}},

{vS,   {LaTeX ->"v_S",
        OutputName -> vS,
        LesHouches -> {DBS,36}}}

 };
```

SPheno.m

```
OnlyLowEnergySPheno = True;

MINPAR={
  {1, LambdaInput},
  {2, LPInput},
  {3, LCInput},
  {4, LCPInput},
  {5, LHPInput},
  {6, LHCInput},
  {7, MuInput},
  {10, mChi2Input},
  {11, mQInput},
  {20, gXInput},
  {21, MZpMass},
  {30, LSInput},
  {31, LHSInput},
  {32, LPSInput},
  {33, LCSInput},
  {34, MupInput},
  {35, vSInput}
};

ParametersToSolveTadpoles = {mH2, mPhi2, mS2};

QuadruplePrecision = {Fv};

DEFINITION[MatchingConditions]=Default[OHDM];

BoundaryLowScaleInput={
  {lamQ,      LHInput[lamQ]},
  {lamL,      LHInput[lamL]},
  {\[Lambda], LambdaInput},
  {LamP,   LPInput},
  {LamC,   LCInput},
  {LamCP,  LCPInput},
  {LamHP,  LHPInput},
  {LamHC,  LHCInput},
  {Mu,     MuInput},
  {mChi2,  mChi2Input},
  {mQ,     mQInput},
  {mL,     LHInput[mL]},
  {gX,     gXInput},
  {g1X, 0},
  {gX1, 0},
  {vP, Sqrt[MZpMass^2 - 16*gXInput^2*vSInput^2]/(2*gX)},
  {LamS,   LSInput},
  {LamHS,  LHSInput},
```

```
  {LamPS,  LPSInput},
  {LamCS,  LCSInput},
  {Mup,    MupInput},
  {vS,     vSInput},
  {YL,    LHInput[YL]},
  {YLt,   LHInput[YLt]},
  {hYuk,  LHInput[hYuk]},
  {hYukt, LHInput[hYukt]},
  {mF,    LHInput[mF]}
};


ListDecayParticles = {Fu, Fe, Fd, Fv, hh, Ah, VZp};
ListDecayParticles3B = {{Fu,"Fu.f90"},{Fe,"Fe.f90"},{Fd,"Fd.f90"},{Fv,"Fv.f90"}};
```

Bibliography

[1] M. Baak, M. Goebel, J. Haller, A. Hoecker, D. Kennedy, R. Kogler, K. Moenig, M. Schott and J. Stelzer, *The Electroweak Fit of the Standard Model after the Discovery of a New Boson at the LHC*, *Eur. Phys. J.* **C72** (2012) 2205, [1209.2716].

[2] R. Parker, C. Yu, W. Zhong, B. Estey and H. Müller, *Measurement of the fine-structure constant as a test of the Standard Model*, *Science* **360** (2018) 191–195.

[3] S. L.Glashow, *The renormalizability of vector meson interactions*, *Nucl. Phys.* **10** (1959) 107–117.

[4] A. Salam and J. C. Ward, *Weak and electromagnetic interactions*, *Il Nuovo Cimento* **11** (1959) 568–577.

[5] S. Weinberg, *A Model of Leptons*, *Phys. Rev. Lett.* **19** (1967) 1264–1266.

[6] G. Danby, J-M. Gaillard, K. Goulianos, L. M.Lederman, N. Mistry, M. Schwartz and J. Steinberger. *Observation of High-Energy Neutrino Reactions and the Existence of Two Kinds of Neutrinos*, *Phys. Rev. Lett.* **9** (1962) 36–44.

[7] Super-Kamiokande collaboration, Y. Fukada et al., *Evidence for oscillation of atmospheric neutrinos*, *Phys. Rev. Lett.* **81** (1998) 1562-1567, [9807003].

[8] SNO collaboration, Q. R.Ahmad et al., *Measurement of the rate of* $\nu_e + d \rightarrow p + p + e^-$ *interactions produced by* ^8B *solar neutrinos at the Sudbury Neutrino Observatory*, *Phys. Rev. Lett.* **87** (2001) 071301, [0106015].

[9] SNO collaboration, Q. R.Ahmad et al., *Direct evidence for neutrino flavor transformation from neutral current interactions in the Sudbury Neutrino Observatory*, *Phys. Rev. Lett.* **89** (2002) 011301, [nucl-ex/0204008].

[10] KamLAND collaboration, K. Eguchi et al., *First results from KamLAND: Evidence for reactor anti-neutrino disappearance*, *Phys.Rev.Lett.* **90** (2003) 021802.

[11] Daya Bay collaboration, F. P. An et al., *Observation of electron-antineutrino disappearance at Daya Bay*, *Phys.Rev.Lett.* **108** (2012) 171803, [1203.1669].

[12] T2K collaboration, K. Abe et al., *Indication of Electron Neutrino Appearance from an Accelerator-produced Off-axis Muon Neutrino Beam*, *Phys.Rev.Lett.* **107** (2011) 041801, [1106.2822].

[13] Planck collaboration, P. A.R.Ade et al., *Planck 2015 results. XIII. Cosmological parameters*, *Astron. Astrophys.* **594** (2016) A13, [1502.01589].

[14] A. D.Sakharov, *Violation of CP Invariance, C asymmetry, and baryon asymmetry of the universe*, *Pisma Zh. Eksp. Teor. Fiz.* **5** (1967) 32-35.

[15] W. Rodejohann, *Neutrino-less Double Beta Decay and Particle Physics*, *Int. J. Mod. Phys.* **E20** (2011) 1833-1930, [1106.1334].

[16] S. Dell'Oro, S. Marcocci, M. Viel and F. Vissani, *Neutrinoless double beta decay: 2015 review*, *Adv.High Energy Phys.* **2016** (2016) 2162659, [1601.07512].

[17] L. Calibbi and G. Signorelli, *Charged Lepton Flavour Violation: An Experimental and Theoretical Introduction*, *Riv. Nuovo Cim* **41** (2018) 71–174, [1709.00294].

[18] MEG II collaboration, A. M. Baldini et al., *The design of the MEG II experiment*, *Eur. Phys. J* **C78** (2018) 380, [1801.04688].

[19] A. Blondel et al., *Research Proposal for an Experiment to Search for the Decay $\mu \to eee$, (2013)*, [1301.6113].

[20] Mu2e collaboration, R. M. Carey et al., *Proposal to search for $\mu^- N \to e^- N$ with a single event sensitivity below* 10^{-16}, (2008).

[21] Mu2e collaboration, D. Glenzinski, *The Mu2e Experiment at Fermilab*, *AIP Conf. Proc.* **1222** (2010) 383.

[22] Mu2e collaboration, R. J. Abrams et al., *Mu2e Conceptual Design Report, (2012)*, [1211.7019].

[23] Mu2e collaboration, L. Bartoszek et al., *Mu2e Technical Design Report*, [1501.05241].

[24] Mu2e collaboration, R. H. Bernstein et al., *The Mu2e Experiment*, *Front.in Phys* **7** (2019) 1, [1901.11099].

[25] DeeMe collaboration, M. Aoki, *A new idea for an experimental search for $\mu - e$ conversion*, *PoS* **ICHEP2010** (2010) 279.

[26] DeeMe collaboration, H. Natori, *DeeMe experiment - An experimental search for a mu-e conversion reaction at J-PARC MLF*, *Nucl. Phys. Proc. Suppl.* **248-250** (2014) 52.

[27] COMET collaboration, Y. G. Cui et al., *Conceptual design report for experimental search for lepton flavor violating $\mu^- \to e^-$ conversion at sensitivity of* 10^{-16} *with a slow-extracted bunched proton beam (COMET), (2009)*.

[28] COMET collaboration, Y. Kuno, *A search for muon-to-electron conversion at J-PARC: The COMET experiment*, *PTEP* **2013** (2013) 022C01.

[29] COMET collaboration, J. C. Angélique et al., *COMET - A submission to the 2020 update of the European Strategy for Particle Physics on behalf of the COMET collaboration*, [1812.07824].

[30] R. J. Barlow, *The PRISM/PRIME project*, *Nucl. Phys. Proc. Suppl.* **218** (2011) 44.

[31] S. L. Glashow, D. Guadagnoli and K. Lane, *Lepton Flavor Violation in B Decays?*, *Phys. Rev. Lett.* **114** (2015) 091801, [1411.0565].

[32] A. Celis, J. Fuentes-Martin, M. Jung and H. Serodio, *Family nonuniversal Z' models with protected flavor-changing interactions*, *Phys. Rev.* **D92** (2015) 015007, [1505.03079].

[33] R. Alonso, B. Grinstein and J. Martin Camalich, *Lepton universality violation and lepton flavor conservation in B-meson decays*, *JHEP* **10** (2015) 184, [1505.05164].

[34] S. M. Boucenna, J. W. F. Valle and A. Vicente, *Are the B decay anomalies related to neutrino oscillations?*, *Phys. Lett.* **B750** (2015) 367–371, [1503.07099].

[35] M. Hirsch, R. A. Lineros, S. Morisi, J. Palacio, N. Rojas and J. W. F. Valle, *WIMP dark matter as radiative neutrino mass messenger*, *JHEP* **10** (2013) 149 [1307.8134].

[36] D. Aristizabal Sierra, F. Staub and A. Vicente, *Shedding light on the $b \to s$ anomalies with a dark sector*, *Phys. Rev.* **D92** (2015) 015001, [1503.06077].

[37] P. Rocha-Moran, A. Vicente, *Lepton Flavor Violation in the singlet-triplet scotogenic model*, *JHEP* **07** (2016) 078, [1605.01915].

[38] P. Rocha-Moran, A. Vicente, *Lepton Flavor Violation in a Z' model for the $b \to s$ anomalies*, *Phys. Rev.* **D99** (2019) 035016, [1810.02135]

[39] P. W.Higgs, *Broken Symmetries and the Masses of Gauge Bosons*, *Phys. Rev. Lett.* **13** (1964) 508–509.

[40] ATLAS collaboration, G. Adad et al., *Observation of a new particle in the search for the Standard Model Higgs boson with the ATLAS detector at the LHC*, *Phys. Lett.* **B716** (2012) 1-29, [1207.7214].

[41] CMS collaboration, S. Chatrchyan et al., *Observation of a new boson at a mass of 125 GeV with the CMS experiment at the LHC*, *Phys. Lett.* **B716** (2012) 30-61, [1207.7235].

[42] ALEPH collaboration, D. Decamp et al., *Determination of the Number of Light Neutrino Species*, *Phys. Lett.* **B231** (1989) 519–529.

[43] Particle Data Group collaboration, M. Tanabashi et al., *Review of Particle Physics*, *Phys. Rev.* **D98** (2018) 030001.

[44] G. 't Hooft and M.J.G. Veltman, *Regularization and Renormalization of Gauge Fields*, *Nucl. Phys.* **B44** (1972) 189-213.

[45] N. Cabibbo, *Unitary Symmetry and Leptonic Decays*, *Phys. Rev. Lett.* **10** (1963) 531–533

[46] M. Kobayashi and T. Maskawa, *CP Violation in the Renormalizable Theory of Weak Interaction*, *Prog. Theor. Phys.* **49** (1973) 652–657.

[47] L.L. Chau and W.Y. Keung, *Comments on the Parametrization of the Kobayashi-Maskawa Matrix*, *Phys. Rev. Lett.* **53** (1984) 1802.

[48] G. C.Branco, L. Lavoura and J. P.Silva, *CP Violation*, *Int. Ser. Monogr. Phys.* **103** (1999) 1–536.

[49] T. Gershon and V. V.Gligorov, *CPviolation in theBsystem*, *Reports on Progress in Physics* **80** (2017) 046201.

[50] J. H.Christenson, J. W.Cronin, V. L.Fitch and R. Turlay, *Evidence for the 2π Decay of the K_2^0 Meson*, *Phys. Rev. Lett.* **13** (1964) 138–140.

[51] Belle collaboration, K. Abe et al., *Observation of large CP violation in the neutral B meson system*, *Phys. Rev. Lett.* **87** (2001) 091802, [hep-ex/0107061].

[52] LHCb collaboration, *Observation of CP violation in charm decays*, (2019), [https://cds.cern.ch/record/2668357].

[53] T. D.Lee and C-N. Yang, *Question of Parity Conservation in Weak Interactions*, *Phys. Rev.* **104** (1956) 254-258.

[54] GALLEX collaboration, P. Anselmann et al., *Solar neutrinos observed by GALLEX at Gran Sasso*, *Phys. Lett.* **B285** (1992) 376-389.

[55] Kamiokande collaboration, F. Fukuda et al., *Solar neutrino data covering solar cycle 22*, *Phys. Rev. Lett.* **77** (1996) 1683-1686.

[56] B. T. Cleveland, T. Daily, R. Davis Jr., J. R. Distel, K. Lande, C. K. Lee, P. S. Wildenhain and J. Ullman, *Measurement of the solar electron neutrino flux with the Homestake chlorine detector*, *Astrophys. J.* **496** (1998) 505–526.

[57] M. Lattanzi and M. Gerbino, *Status of neutrino properties and future prospects - Cosmological and astrophysical constraints*, *Front.in Phys.* **5** (2018) 70, [1712.07109].

[58] S. Weinberg, *Baryon and Lepton Nonconserving Processes*, *Phys. Rev. Lett.* **43** (1979) 1566-1570.

[59] H. Georgi, H. R.Quinn and S. Weinberg, *Hierarchy of Interactions in Unified Gauge Theories*, *Phys. Rev. Lett.* **33** (1974) 451-454.

[60] H. Fritzsch and P. Minkowski, *Unified Interactions of Leptons and Hadrons*, *Annals Phys.* **93** (1975) 193-266.

[61] R. N.Mohapatra and R. E.Marshak, *Local B-L Symmetry of Electroweak Interactions, Majorana Neutrinos and Neutron Oscillations*, *Phys. Rev. Lett.* **44** (1980) 1316-1319.

[62] W. H.Furry, *On Transition Probabilities in Double Beta-Disintegration*, *Phys. Rev.* **56** (1939) 1184–1193.

[63] J. Schechter and J. W.F.Valle, *Neutrinoless Double beta Decay in SU(2) x U(1) Theories*, *Phys. Rev.* **D25** (1982) 2951.

[64] B. Pontecorvo, *Mesonium and anti-mesonium*, *Sov. Phys. JETP* **6** (1957) 429.

[65] M. Gell-Mann and A. Pais, *Behavior of Neutral Particles under Charge Conjugation*, *Phys.Rev.* **97** (1955) 1387–1389.

[66] R. Davis Jr and D.S. Harmer, *Attempt to observe the $Cl^{37}(\bar{\nu}e^{-})Ar^{37}$ reaction induced by reactor antineutrinos*, *Bull. Am. Phys. Soc.***4** (1959) 217.

[67] B. Pontecorvo, *Inverse beta processes and nonconservation of lepton charge*, *Sov. Phys. JETP* **7** (1958) 172-173.

[68] B. Pontecorvo, *Electron and Muon Neutrinos*, *Sov. Phys. JETP* **10** (1960) 1236-1240.

[69] G. Danby, J. M.Gaillard, A. Konstantin, L. M.Lederman, N. B.Mistry, M. Schwartz and J. Steinberger, *Observation of High-Energy Neutrino Reactions and the Existence of Two Kinds of Neutrinos*, *Phys. Rev. Lett.* **9** (1962) 36-44.

[70] Z. Maki, M. Nakagawa and S. Sakata, *Remarks on the unified model of elementary particles*, *Prog. Theor. Phys.* **28** (1962) 870-880.

[71] B. Pontecorvo, *Neutrino Experiments and the Problem of Conservation of Leptonic Charge*, *Sov. Phys. JETP* **26** (1968) 984-988.

[72] L. Wolfenstein, *Neutrino Oscillations in Matter*, *Phys. Rev.* **D17** (1978) 2369-2374.

[73] S. P.Mikheyev, A. Yu.Smirnov, *Resonance Amplification of Oscillations in Matter and Spectroscopy of Solar Neutrinos*, *Sov. J. Nucl. Phys.* **42** (1985) 913-917.

[74] E. K. Akhmedov, R. Johansson, M. Lindner, T. Ohlsson and T. Schwetz , *Series expansions for three flavor neutrino oscillation probabilities in matter*, *Phys. Lett.* **B714** (2012) 224–230, [hep-ph/0402175].

[75] S. M.Bilenky, J. Hosek and S. T.Petcov, *On Oscillations of Neutrinos with Dirac and Majorana Masses*, *Phys. Lett.* **94B** (1980) 495-498.

[76] J. Schechter and J. W.F.Valle, *Neutrino Masses in SU(2) x U(1) Theories*, *Phys. Rev.* **D22** (1980) 2227.

[77] P. F. de Salas, D. V. Forero, C. A. Ternes, M. Tortola and J. W. F. Valle, *Status of neutrino oscillations 2018: 3σ hint for normal mass ordering and improved CP sensitivity*, *Phys. Lett.* **B782** (2018) 633–640, [1708.01186].

[78] SAGE collaboration, J. N. Abdurashitov et al., *Measurement of the solar neutrino capture rate with gallium metal. III: Results for the 2002–2007 data-taking period*, *Phys. Rev.* **C80** (2009) 015807, [0901.2200].

[79] Super-Kamiokande collaboration, J. Hosaka et al., *Solar neutrino measurements in super-Kamiokande-I*, *Phys.Rev.D* **73** (2006) 112001, [hep-ex/0508053].

[80] Super-Kamiokande collaboration, J. Cravens et al., *Solar neutrino measurements in Super-Kamiokande-II*, *Phys.Rev.D* **78** (2008) 032002, [0803.4312].

[81] Super-Kamiokande collaboration, K. Abe et al., *Solar neutrino results in Super-Kamiokande-III*, *Phys.Rev.D* **83** (2011) 052010, [1010.0118].

[82] Y. Nakano, "PhD Thesis, University of Tokyo." http://www-sk.icrr.u-tokyo.ac.jp/sk/_pdf/articles/2016/doc_thesis_naknao.pdf, 2016.

[83] SNO collaboration, B. Aharmim et al., *Independent Measurement of the Total Active B-8 Solar Neutrino Flux Using an Array of He-3 Proportional Counters at the Sudbury Neutrino Observatory*, *Phys.Rev.Lett.* **101** (2008) 111301, [0806.0989].

[84] SNO collaboration, B. Aharmim et al., *Low Energy Threshold Analysis of the Phase I and Phase II Data Sets of the Sudbury Neutrino Observatory*, *Phys. Rev.* **C81** (2010) 055504, [0910.2984].

[85] F. Kaether, W. Hampel, G. Heusser, J. Kiko and T. Kirsten, *Reanalysis of the GALLEX solar neutrino flux and source experiments*, *Phys. Lett.* **B685** (2010) 47–54, [1001.2731].

[86] Borexino collaboration, G. Bellini et al., *Final results of Borexino Phase-I on low energy solar neutrino spectroscopy*, *Phys. Rev.* **D89** (2014) 112007, [1308.0443].

[87] KamLAND collaboration, A. Gando et al., *Constraints on θ_{13} from A Three-Flavor Oscillation Analysis of Reactor Antineutrinos at KamLAND*, *Phys. Rev.* **D83** (2011) 052002, [1009.4771].

[88] Super-Kamiokande collaboration, K. Abe et al., *Atmospheric neutrino oscillation analysis with external constraints in Super-Kamiokande I-IV*, *Phys. Rev.* **D97** (2018) 7, [1710.09126].

[89] ANTARES collaboration, S. Adrian-Martinez et al., *Measurement of Atmospheric Neutrino Oscillations with the ANTARES Neutrino Telescope*, *Phys. Lett.* **B714** (2012) 224–230, [1206.0645].

[90] IceCube collaboration, M. G. Aartsen et al., *Determining neutrino oscillation parameters from atmospheric muon neutrino disappearance with three years of IceCube DeepCore data*, *Phys. Rev.* **D91** (2015) 7, [1410.7227].

[91] K2K collaboration, M. H. Ahn et al., *Measurement of Neutrino Oscillation by the K2K Experiment*, *Phys. Rev.* **D74** (2006) 072003, [hep-ex/0606032].

[92] MINOS collaboration, P. Adamson et al., *Combined analysis of ν_μ disappearance and $\nu_\mu \to \nu_e$ appearance in MINOS using accelerator and atmospheric neutrinos*, *Phys. Rev. Lett.* **112** (2014) 191801, [1403.0867].

[93] OPERA collaboration, N. Agafonova et al., *Observation of a first ν_τ candidate in the OPERA experiment in the CNGS beam*, *Phys. Lett.* **B691** (2010) 138-145, [1006.1623].

[94] NOvA collaboration, A. Radovic, "JETP January 2018, NOvA Oscillation Results." http://nova-docdb.fnal.gov/cgi-bin/ShowDocument?docid=25938, January, 2018.

[95] Daya Bay collaboration, F. P. An et al., *Measurement of electron antineutrino oscillation based on 1230 days of operation of the Daya Bay experiment*, *Phys. Rev.* **D95** (2017) 7, [1610.04802].

[96] Double Chooz collaboration, Y. Abe et al., *Improved measurements of the neutrino mixing angle θ_{13} with the Double Chooz detector*, *JHEP* **10** (2014) 086, [1406.7763].

[97] RENO collaboration, M. Y. Pac, *Recent Results from RENO*, *PoS* **NuFact2017** (2018) 038, [1801.04049].

[98] T2K collaboration, M. Hartz, "T2K NEUTRINO OSCILLATION RESULTS WITH DATA UP TO 2017 SUMMER." http://www.t2k.org/docs/talk/282, August, 2017.

[99] NOvA collaboration, A. Himmel, "First Oscillation Results with Neutrino and Antineutrino Beams in NOvA." http://nova-docdb.fnal.gov/cgi-bin/ShowDocument?docid=30273, June, 2018.

[100] H. V.Klapdor-Kleingrothaus et al., *Latest results from the Heidelberg-Moscow double beta decay experiment*, *Eur. Phys. J.* **A12** (2001) 147-154, [hep-ph/0103062].

[101] GERDA collaboration, M. Agostini et al., *Improved Limit on Neutrinoless Double-β Decay of ^{76}Ge from GERDA Phase II*, *Phys.Rev.Lett.* **120** (2018) 132503, [1803.11100].

[102] CUORE collaboration, C. Alduino et al., *First Results from CUORE: A Search for Lepton Number Violation via $0\nu\beta\beta$ Decay of ^{130}Te*, *Phys.Rev.Lett.* **120** (2018) 132501, [1710.07988].

[103] KamLAND-Zen collaboration, J. Shirai, *Results and future plans for the KamLAND-Zen experiment*, *J. Phys. Conf. Ser.* **888** (2017) 012031.

[104] EXO collaboration, J.B. Albert et al., *Search for Neutrinoless Double-Beta Decay with the Upgraded EXO-200 Detector*, *Phys.Rev.Lett.* **120** (2018) 072701, [1707.08707].

[105] MAJORANA collaboration, C. Aalseth et al., *Search for Neutrinoless Double-β Decay in ^{76}Ge with the Majorana Demonstrator*, *Phys.Rev.Lett.* **120** (2018) 132502, [1710.11608].

[106] Ch. Kraus et al., *Final results from phase II of the Mainz neutrino mass search in tritium beta decay*, *Eur. Phys. J.* **C40** (2005) 447-468, [hep-ex/0412056].

[107] V. N.Aseev et al., *An upper limit on electron antineutrino mass from Troitsk experiment*, *Phys. Rev.* **D84** (2011) 112003, [1108.5034].

[108] KATRIN collaboration, A. Osipowicz et al., *KATRIN: A Next generation tritium beta decay experiment with sub-eV sensitivity for the electron neutrino mass. Letter of intent*, [hep-ex/0109033].

[109] KATRIN collaboration, D. Parno, *KATRIN: Toward a High-Precision Neutrino-Mass Determination with Tritium*, *Talk at XXVIII International Conference on Neutrino Physics and Astrophysics, 4–9 June 2018, Heidelberg, Germany*.

[110] LSND collaboration, C. Athanassopoulos et al., *Candidate events in a search for anti-muon-neutrino —> $\bar{\nu}$ anti-electron-neutrino oscillations*, *Phys.Rev.Lett.* **75** (1995) 2650-2653, [nucl-ex/9504002].

[111] MINIBOONE collaboration, A. A.Aguilar-Arevalo et al., *A Combined $\nu_\mu \to \nu_e$ and $\bar{\nu}_\mu \to \bar{\nu}_e$ Oscillation Analysis of the MiniBooNE Excesses*, (2012), [1207.4809].

[112] J. N. Bachall, M. H. Pinsonneault and S. Basu, *Solar models: Current epoch and time dependences, neutrinos, and helioseismological properties*, *Astrophys. J.* **555** (2001) 990-1012, [-ph/0010346].

[113] J. Engel and J. Menendez, *Status and Future of Nuclear Matrix Elements for Neutrinoless Double-Beta Decay: A Review*, *Rept. Prog. Phys.* **80** (2017) 046301, [1610.06548].

[114] P. F. de Salas, S. Gariazzo, O. Mena, C. A. Ternes and M. Tortola, *Neutrino Mass Ordering from Oscillations and Beyond: 2018 Status and Future Prospects*, *Front. Astron. Space Sci.***5** (2018) 36, [1806.11051].

[115] G. Mangano, G. Miele, S. Pastor, T. Pinto, O. Pisanti and P. D. Serpico, *Relic neutrino decoupling including flavor oscillations*, *Nucl.Phys.* **B729** (2005) 221–234, [hep-ph/0506164].

[116] S. Vagnozzi, S. Dhawan, M. Gerbino, K. Freese, A. Goobar and O. Mena, *Constraints on the sum of the neutrino masses in dynamical dark energy models with $w(z) \geq -1$ are tighter than those obtained in ΛCDM*, [1801.08553].

[117] S. Vagnozzi, E. Giusarma, O. Mena, K. Freese, M. Gerbino, S. Ho et al., *Unveiling ν secrets with cosmological data: neutrino masses and mass hierarchy*, *Phys.Rev.D* **96** (2017) 123503, [1701.08172].

[118] E. Giusarma, M. Gerbino, O. Mena, S. Vagnozzi, S. Ho and K. Freese, *Improvement of cosmological neutrino mass bounds*, *Phys.Rev.D* **94** (2016) 083522, [1605.04320].

[119] A. J. Cuesta, V. Niro and L. Verde, *Neutrino mass limits: robust information from the power spectrum of galaxy surveys*, *Phys.Dark Univ.* **13** (2016) 77–86, [1511.05983].

[120] N. Palanque-Delabrouille et al., *Neutrino masses and cosmology with Lyman-alpha forest power spectrum*, *JCAP* **11** (2015) 011, [1506.05976].

[121] E. Di Valentino, E. Giusarma, O. Mena, A. Melchiorri and J. Silk, *Cosmological limits on neutrino unknowns versus low redshift priors*, *Phys.Rev.D* **93** (2016) 083527, [1511.00975].

[122] P. Minkowski, $\mu \to e\gamma$ *at a Rate of One Out of* 10^9 *MuonDecays?*, *Phys. Lett.* **67B** (1977) 421-428.

[123] T. Yanagida, *Horizontal gauge symmetry and masses of neutrinos*, *Conf. Proc.* **C7902131** (1979) 95-99.

[124] R. N.Mohapatra and G. Senjanovic, *Neutrino Mass and Spontaneous Parity Nonconservation*, *Phys. Rev. Lett.* **44** (1980) 912

[125] M. Gell-Mann, P. Ramond and R. Slansky, *Complex Spinors and Unified Theories*, *Conf. Proc.* **C790927** (1979) 315-321, [1306.4669].

[126] M. Magg and C. Wetterich, *Neutrino Mass Problem and Gauge Hierarchy*, *Phys. Lett.* **94B** (1980) 61-64.

[127] S. Kanemura and K. Yagyu, *Radiative corrections to electroweak parameters in the Higgs triplet model and implication with the recent Higgs boson searches*, *Phys. Rev.* **D85** (2012) 115009, [1201.6287].

[128] R. Foot, H. Lew, X. He, and C. G.Joshi, *Seesaw Neutrino Masses Induced by a Triplet of Leptons*, *Z. Phys.* **C44** (1989) 441.

[129] R. N. Mohapatra and J. W. F. Valle, *Neutrino Mass and Baryon Number Nonconservation in Superstring Models*, *Phys. Rev.* **D34** (1986) 1642.

[130] M. C. Gonzalez-Garcia and J. W. F. Valle, *Fast Decaying Neutrinos and Observable Flavor Violation in a New Class of Majoron Models*, *Phys. Lett.* **B216** (1989) 360-366.

[131] F. . Deppisch and J. W. F. Valle, *Enhanced lepton flavor violation in the supersymmetric inverse seesaw model*, *Phys. Rev.* **D72** (2005) 036001, [hep-ph/0406040].

[132] G. 't Hooft, *Naturalness, chiral symmetry, and spontaneous chiral symmetry breaking*, *NATO Sci. Ser. B* **59** (1980) 135.

[133] A. Zee, *A Theory of Lepton Number Violation, Neutrino Majorana Mass, and Oscillation*, , *Phys. Lett.* **93B** (1980) 389.

[134] J. A. Casas and A. Ibarra, *Oscillating neutrinos and* $\mu \to e, \gamma$, *Nucl. Phys.* **B618** (2001) 171, [hep-ph/0103065].

[135] A. Ibarra and G. G. Ross, *Neutrino phenomenology: The Case of two right-handed neutrinos*, *Phys. Lett.* **B591** (2004) 285, [hep-ph/0312138].

[136] I. Cordero-Carrión, M. Hirsch and A. Vicente, *Master Majorana neutrino mass parametrization*, *(*2018), [1812.03896].

[137] W. J. Marciano and A. I. Sanda, *Exotic Decays of the Muon and Heavy Leptons in Gauge Theories*, *Phys. Lett* **67B** (1977) 303-305.

[138] S. T. Petcov, *The Processes $\mu \to e\gamma$, $\mu \to ee\bar{e}$, $\nu' \to \nu\gamma$ in the Weinberg-Salam Model with Neutrino Mixing*, *Sov. J. Nucl. Phys* **25** (1977) 340.

[139] S. M. Bilenky, S. T. Petcov and B. Pontecorvo, *Lepton Mixing, $\mu \to e + \gamma$ Decay and Neutrino Oscillations*, *Phys. Lett* **67B** (1977) 309.

[140] T. P. Cheng and L. F. Li, *Muon-number-nonconservation effects in a gauge theory with $V + A$ currents and heavy neutral leptons*, *Phys. Rev. D* **16** (1977) 1425–1443.

[141] B. W. Lee, S. Pakvasa, R. E. Shrock and H. Sugawara, *Muon and Electron Number Nonconservation in a V-A Gauge Model*, *Phys. Rev. Lett* **38** (1977) 937.

[142] B. W. Lee and R. E. Shrock, *Natural Suppression of Symmetry Violation in Gauge Theories: Muon - Lepton and Electron Lepton Number Nonconservation*, *Phys. Rev* **D16** (1977) 1444.

[143] G. Feinberg, *Decays of the mu Meson in the Intermediate-Meson Theory*, *Phys. Rev* **110** (1958) 1482-1483.

[144] Anonymous, *Minutes of the 1954 Thanksgiving Meeting Held at Chicago, Illinois, November 26-27, 1954*, *Phys. Rev.* **98** (1955) 220–221.

[145] D. Berley, J. Lee and M. Bardon, *Upper Limit for the Decay Mode $\mu \to e + \gamma$*, *Phys. Rev. Lett.* **2** (1959) 357–359.

[146] S. Oneda and J. C. Pati, *$V - A$ Four-Fermion Interaction and the Intermediate Charged Vector Meson*,

[147] MEG collaboration, A. M. Baldini et al., *Search for the lepton flavour violating decay $\mu^+ \to e^+\gamma$ with the full dataset of the MEG experiment*, *Eur. Phys. J* **C76** (2016) 434, [1605.05081].

[148] SINDRUM collaboration, U. Bellgardt, et al., *Search for the Decay $\mu^+ \to e^+e^+e^-$*, *Nucl. Phys.* **B299** (1988) 1.

[149] SINDRUM II collaboration, W. H. Bertl, et al., *A Search for muon to electron conversion in muonic gold*, *Eur. Phys. J.* **C47** (2006) 337.

[150] R. H. Bernstein and P. S. Cooper, *Charged Lepton Flavor Violation: An Experimenter's Guide*, *Phys. Rept.* **532** (2013) 27, [1307.5787].

[151] S. Mihara, J. P. Miller, P. Paradisi and G. Piredda, *Charged Lepton Flavor-Violation Experiments*, *Ann. Rev. Nucl. Part. Sci.* **63** (2013) 531.

[152] G. Signorelli, *Charged Lepton Flavor Violation Experiments*, Proceedings, *11th Conference on Flavor Physics and CP Violation (FPCP 2013): Armacao dos Buzios, Rio de Janeiro, Brazil, May 20-24* (2013), [1307.8346].

[153] A. Papa, *Charged lepton flavour violation searches at the Paul Scherrer Institut: Status of the MEGII and Mu3e experiments*, *EPJ Web Conf* **179** (2018) 01018.

[154] A. Baldini et al., *A submission to the 2020 update of the European Strategy for Particle Physics on behalf of the COMET, MEG, Mu2e and Mu3e collaborations*, [1812.06540].

[155] T. Aushev, et al., *Physics at Super B Factory, (2010)*, [1002.5012].

[156] Belle, Babar collaboration, A. J. Bevan, et al., *The Physics of the B Factories*, *Eur. Phys. J.* **C74** (2014) 3026, [1406.6311].

[157] HFLAV collaboration, Y. Amhis et al., *Averages of b-hadron, c-hadron, and τ-lepton properties as of summer 2016*, *Eur. Phys. J* **C77** (2017) 895, [1612.07233].

[158] A. Lusiani, *HFLAV τ branching fractions fit and measurements of $|V_{us}|$ with τ lepton data*, [1811.06470].

[159] Particle Data Group collaboration, C. Patrignani et al., *Review of Particle Physics*, *Chin. Phys* **C40** (2016) 100001.

[160] BaBar collaboration, B. Aubert, et al., *Searches for Lepton Flavor Violation in the Decays $\tau^{\pm} \to e^{\pm}\gamma$ and $\tau^{\pm} \to \mu^{\pm}\gamma$*, *Phys. Rev. Lett.* **104** (2010) 021802, [0908.2381].

[161] K. Hayasaka, et al., *Search for Lepton Flavor Violating τ Decays into Three Leptons with 719 Million Produced $\tau^{+}\tau^{-}$ Pairs*, *Phys. Lett.* **B687** (2010) 139, [1001.3221].

[162] SINDRUM II collaboration, C. Dohmen, et al., *Test of lepton flavor conservation in $\mu \to e$ conversion on titanium*, *Phys. Lett.* **B317** (1993) 631-636.

[163] *Search for the $\mu \to e$ conversion process at an ultimate sensitivity of the order of 10^{-18} with PRISM*, LOI to J-PARC 50-GeV PS, LOI-25, http://www-ps.kek.jp/jhf-np/LOIlist/pdf/L25.pdf.

[164] W. Buchmuller and D. Wyler, *Effective Lagrangian Analysis of New Interactions and Flavor Conservation*, *Nucl. Phys.* **B268** (1986) 621-653.

[165] Y. Kuno and Y. Okada, *Muon decay and physics beyond the standard model*, *Rev. Mod. Phys.* **73** (2001) 151, [hep-ph/9909265].

[166] T. Appelquist, J. Carazzone, *Infrared Singularities and Massive Fields*, , *Phys. Rev.* **D11** (1975) 2856.

[167] H. Georgi, *Effective field theory*, *Ann. Rev. Nucl. Part. Sci* **43** (1993) 209–252.

[168] B. Grzadkowski, M. Iskrzynski, M. Misiak and J. Rosiek *Dimension-six terms in the Standard Model Lagrangian*, *JHEP* **10** (2010) 85, [1008.4884].

[169] A. Crivellin, S. Najjari and J. Rosiek *Lepton Flavor Violation in the Standard Model with general Dimension-Six Operators*, *JHEP* **04** (2014) 167, [1312.0634].

[170] G. M. Pruna and A. Signer *The $\mu \to e\gamma$ decay in a systematic effective field theory approach with dimension 6 operators*, *JHEP* **10** (2014) 014, [1408.3565].

[171] G.M. Pruna and A. Singer, *Lepton-flavour violating decays in theories with dimension 6 operators*, *EPJ Web Conf.* **118** (2016) 01031, [1511.04421].

[172] F. Staub, *Sarah*, [0806.0538].

[173] F. Staub, *From Superpotential to Model Files for FeynArts and CalcHep/CompHep*, *Comput. Phys. Commun.* **181** (2010) 1077, [0909.2863].

[174] F. Staub, *Automatic Calculation of supersymmetric Renormalization Group Equations and Self Energies*, *Comput. Phys. Commun.* **182** (2011) 808, [1002.0840].

[175] F. Staub, *SARAH 3.2: Dirac Gauginos, UFO output, and more*, *Comput. Phys. Commun.* **184** (2013) 1792, [1207.0906].

[176] F. Staub, *SARAH 4 : A tool for (not only SUSY) model builders*, *Comput. Phys. Commun.* **185** (2014) 1773, [1309.7223].

[177] F. Staub, *Exploring new models in all detail with SARAH*, *Adv. High Energy Phys.* **2015** (2015) 840780, [1503.04200].

[178] A. Vicente, *Computer tools in particle physics*, *2015* , [1507.06349].

[179] W. Porod, *SPheno, a program for calculating supersymmetric spectra, SUSY particle decays and SUSY particle production at e^+e^- colliders*, *Comput. Phys. Commun.* **153** (2003) 275, [hep-ph/0301101].

[180] W. Porod and F. Staub, *SPheno 3.1: Extensions including flavour, CP-phases and models beyond the MSSM*, *Comput. Phys. Commun.* **183** (2012) 2458, [1104.1573].

[181] G. Belanger, F. Boudjema, A. Pukhov and A. Semenov, *MicrOMEGAs: A Program for calculating the relic density in the MSSM*, *Comput. Phys. Commun.* **149** (2002) 103-120, [hep-ph/0112278].

[182] G. Belanger, F. Boudjema, A. Pukhov and A. Semenov, *MicrOMEGAs 2.0: A Program to calculate the relic density of dark matter in a generic model*, *Comput. Phys. Commun.* **176** (2007) 367-382, [hep-ph/0607059].

[183] D. Barducci, G. Belanger, J. Bernon, F. Boudjema, J. Da Silva, S. Kraml, U. Laa and A. Pukhov, *Collider limits on new physics within micrOMEGAs$_4$.3*, *Comput. Phys. Commun.* **222** (2018) 327-338, [1606.03834].

[184] J. Alwall, R. Frederix, S. Frixione, V. Hirschi, F. Maltoni, O. Mattelaer, H. -S.Shao, T. Stelzer, P. Torrielli and M. Zaro, *The automated computation of tree-level and next-to-leading order differential cross sections, and their matching to parton shower simulations*, *JHEP* **07** (2014) 079, [1405.0301].

[185] W. Porod, F. Staub and A. Vicente, *A Flavor Kit for BSM models*, *Eur. Phys. J.* **C74** (2014) 2992, [1405.1434].

[186] T. Hahn and M. Perez-Victoria, *Automatized one loop calculations in four-dimensions and D-dimensions*, *Comput. Phys. Commun.* **118** (1999) 153-165, [hep-ph/9807565].

[187] T. Hahn, *Generating Feynman diagrams and amplitudes with FeynArts 3*, *Comput. Phys. Commun.* **140** (2001) 418-431, [hep-ph/0012260].

[188] T. Hahn, *Automatic loop calculations with FeynArts, FormCalc, and LoopTools*, *Nucl. Phys. Proc. Suppl.* **89** (2000) 231-236, [hep-ph/0005029].

[189] T. Hahn, *New features in FormCalc 4*, *Nucl. Phys. Proc. Suppl.* **135** (2004) 333-337, [hep-ph/0406288].

[190] T. Hahn, *New developments in FormCalc 4.1*, *eConf* **C050318** (2005) 0604, [hep-ph/0506201].

[191] B.C. Nejad, T. Hahn, J. N.Lang and E. Mirabella, *FormCalc 8: Better Algebra and Vectorization*, *J. Phys. Conf. Ser.* **523** (2014) 012050, [1310.0274].

[192] E. Ma, *Verifiable radiative seesaw mechanism of neutrino mass and dark matter*, *Phys. Rev.* **D73** (2006) 077301, [hep-ph/0601225].

[193] E. Ma, *Common origin of neutrino mass, dark matter, and baryogenesis*, *Phys. Rev.* **A21** (2006) 1777, [hep-ph/0605180].

[194] J. Kubo, E. Ma and D. Suematsu, *Cold Dark Matter, Radiative Neutrino Mass, $\mu \to e\gamma$, and Neutrinoless Double Beta Decay*, *Phys. Lett.* **B642** (2006) 0604114, [hep-ph/0604114].

[195] T. Hambye, K. Kannike, E. Ma and M. Raidal, *Emanations of Dark Matter: Muon Anomalous Magnetic Moment, Radiative Neutrino Mass, and Novel Leptogenesis at the TeV Scale*, *Phys. Rev.* **D75** (2007) 095003, [hep-ph/0609228].

[196] D. Aristizabal Sierra, J. Kubo, D. Restrepo, D. Suematsu and O. Zapata, *Radiative seesaw: Warm dark matter, collider and lepton flavour violating signals*, *Phys. Rev.* **D79** (2009) 013011, [0808.3340].

[197] D. Suematsu, T. Toma, and T. Yoshida, *Reconciliation of CDM abundance and mu $\to$ e gamma in a radiative seesaw model*, *Phys. Rev.* **D79** (2009) 093004, [0903.0287].

[198] G. B.Gelmini, E. Osoba and S. Palomares-Ruiz, *Inert-Sterile Neutrino: Cold or Warm Dark Matter Candidate*, *Phys. Rev.* **D81** (2010) 063529, [0912.2478].

[199] A. Adulpravitchai, M. Lindner and A. Merle, *Confronting Flavour Symmetries and extended Scalar Sectors with Lepton Flavour Violation Bounds*, *Phys. Rev.* **D80** (2009) 055031, [0907.2147].

[200] M. Aoki and S. Kanemura, *Probing the Majorana nature of TeV-scale radiative seesaw models at collider experiments*, *Phys. Lett.* **B689** (2010) 28, [1001.0092].

[201] Y. H.Ahn and H. Okada, *Non-zero θ_{13} linking to Dark Matter from Non-Abelian Discrete Flavor Model in Radiative Seesaw*, *Phys. Rev.* **D85** (2012) 073010, [1201.4436].

[202] D. Schmidt, T. Schwetz, and T. Toma, *Direct Detection of Leptophilic Dark Matter in a Model with Radiative Neutrino Masses*, *Phys. Rev.* **D85** (2012) 073009, [1201.0906].

[203] E Ma, *Radiative Scaling Neutrino Mass and Warm Dark Matter*, *Phys. Lett.* **B717** (2012) 235, [1206.1812].

[204] S. Kashiwase and D. Suematsu, *Baryon number asymmetry and dark matter in the neutrino mass model with an inert doublet*, *Phys. Rev.* **D86** (2012) 053001, [1207.2594].

[205] S. Kashiwase and D. Suematsu, *Leptogenesis and dark matter detection in a TeV scale neutrino mass model with inverted mass hierarchy*, *Eur. Phys. J.* **C73** (2013) 2484, [1301.2087].

[206] T. Toma and A. Vicente, *Lepton Flavor Violation in the Scotogenic Model*, *JHEP* **01** (2014) 160, [1312.2840].

[207] J. Racker, *Mass bounds for baryogenesis from particle decays and the inert doublet model*, *JCAP* **1403** (2014) 025, [1308.1840].

[208] M. Klasen, C. E.Yaguna, J. D.Ruiz-Alvarez, D. Restrepo and O. Zapata, *Scalar dark matter and fermion coannihilations in the radiative seesaw model*, *JCAP* **1304** (2013) 044 [1302.5298].

[209] S.-Y.Ho and J. Tandean, *Probing Scotogenic Effects in Higgs Boson Decays*, *Phys. Rev.* **D87** (2013) 095015, [1303.5700].

[210] S.-Y. Ho and J. Tandean, *Probing Scotogenic Effects in e^+e^- Colliders*, *Phys. Rev.* **D89** (2014) 114025, [1312.0931].

[211] A. Vicente and C. E. Yaguna, *Probing the scotogenic model with lepton flavor violating processes*, *JHEP* **02** (2015) 144, [1412.2545].

[212] G. Faisel S.-Y. Ho and J. Tandean, *Exploring X-Ray Lines as Scotogenic Signals*, *Phys. Lett.* **B738** (2014) 380, [1408.5887].

[213] E. Molinaro C. E. Yaguna and O. Zapata, *FIMP realization of the scotogenic model*, *JCAP* **1407** (2014) 015, [1405.1259].

[214] T. A. Chowdhury and S. Nasri, *Lepton Flavor Violation in the Inert Scalar Model with Higher Representations*, *JHEP* **12** (2015) 040, [1506.00261].

[215] R. Bouchand and A. Merle, *Running of Radiative Neutrino Masses: The Scotogenic Model*, *JHEP* **07** (2012) 084, [1205.0008].

[216] A. Merle and M. Platscher, *Parity Problem of the Scotogenic Neutrino Model*, *Phys. Rev.* **D92** (2015) 095002, [1502.03098].

[217] A. Merle and M. Platscher, *Running of radiative neutrino masses: the scotogenic model — revisited*, *JHEP* **11** (2015) 148, [1507.06314].

[218] E. Ma, *Dark Scalar Doublets and Neutrino Tribimaximal Mixing from A(4) Symmetry*, *Phys. Lett.* **B671** (2009) 366, [0808.1729].

[219] A. Adulpravitchai, M. Lindner, A. Merle and R. N. Mohapatra, *Radiative Transmission of Lepton Flavor Hierarchies*, *Phys. Lett.* **B680** (2009) 476, [0908.0470].

[220] E. Ma, I. Picek and B. Radovčić, *New Scotogenic Model of Neutrino Mass with $U(1)D$ Gauge Interaction*, *Phys. Lett.* **B726** (2013) 744, [1308.5313].

[221] E. Ma and A. Natale, *Scotogenic Z_2 or $U(1)D$ Model of Neutrino Mass with $\Delta(27)$ Symmetry*, *Phys. Lett.* **B734** (2014) 403, [1403.6772].

[222] J.-H. Yu, *Hidden Gauged $U(1)$ Model: Unifying Scotogenic Neutrino and Flavor Dark Matter* , *Phys. Rev.* **D93** (2016) 113007, [1601.02609].

[223] A. Ahriche, K. L. McDonald, and S. Nasri, *The Scale-Invariant Scotogenic Model*, *JHEP* **06** (2016) 182, [1604.05569].

[224] D. Restrepo, O. Zapata and C. E. Yaguna, *Models with radiative neutrino masses and viable dark matter candidates*, *JHEP* **11** (2013) 011 [1308.3655].

[225] E. Ma and D. Suematsu, *Fermion Triplet Dark Matter and Radiative Neutrino Mass*, *Mod. Phys. Lett.* **A24** (2009) 583, [0809.0942].

[226] W. Chao *Dark matter, LFV and neutrino magnetic moment in the radiative seesaw model with fermion triplet*, *Int.J. Mod. Phys.* **A30** (2015) 1550007 [1202.6394].

[227] G. D.Nilendra and E. Ma, *Pattern of Symmetry Breaking with Two Higgs Doublets*, *Phys. Rev.* **D18** (1978) 2574.

[228] M. A. Díaz, B. Koch and S. Urrutia-Quiroga, *Constraints to Dark Matter from Inert Higgs Doublet Model*, (2015), [1511.04429].

[229] F. S. Queiroz and C. E. Yaguna, *The CTA aims at the Inert Doublet Model*, *JCAP* **1602** (2016) 038 [1511.05967].

[230] C. Garcia-Cely, M. Gustafsson, and A. Ibarra, *Probing the Inert Doublet Dark Matter Model with Cherenkov Telescopes*, *JCAP* **1602** (2016) 043 [1512.02801].

[231] D. V. Forero, M. Tortola and J. W. F. Valle, *Neutrino oscillations refitted*, *Phys. Rev.* **D90** (2014) 093006, [1405.7540].

[232] A. Merle, M. Platscher, N. Rojas, J. W. F. Valle and A. Vicente *Consistency of WIMP Dark Matter as radiative neutrino mass messenger*, (2016), [1603.05685].

[233] MEG collaboration, J. Adam, et al., *New constraint on the existence of the $\mu^+ \to e^+\gamma$ decay*, *Phys. Rev. Lett.* **110** (2013) 201801, [1303.0754].

[234] F. von der Pahlen, G. Palacio, D. Restrepo and O. Zapata, *Radiative Type III Seesaw Model and its collider phenomenology*, (2016), [1605.01129].

[235] LHCb collaboration, R. Aaij et al., *Differential branching fraction and angular analysis of the decay $B_s^0 \to \phi\mu^+\mu^-$*, *JHEP* **07** (2013) 084, [1305.2168].

[236] LHCb collaboration, R. Aaij et al., *Measurement of Form-Factor-Independent Observables in the Decay $B^0 \to K^{*0}\mu^+\mu^-$*, *Phys. Rev. Lett.* **111** (2013) 191801, [1308.1707].

[237] LHCb collaboration, R. Aaij et al., *Angular analysis of the $B^0 \to K^{*0}\mu^+\mu^-$ decay using 3 fb^{-1} of integrated luminosity*, *JHEP* **02** (2016) 104, [1512.04442].

[238] LHCb collaboration, R. Aaij et al., *Test of lepton universality using $B^+ \to K^+\ell^+\ell^-$ decays*, *Phys. Rev. Lett.* **113** (2014) 151601, [1406.6482].

[239] M. Bordone, G. Isidori and A. Pattori, *On the Standard Model predictions for R_K and R_{K^*}*, *Eur. Phys. J.* **C76** (2016) 440, [1605.07633].

[240] Belle collaboration, A. Abdesselam et al., *Angular analysis of $B^0 \to K^*(892)^0\ell^+\ell^-$*, in *Proceedings, LHCSki 2016 - A First Discussion of 13 TeV Results: Obergurgl, Austria, April 10-15, 2016*, [1604.04042].

[241] Belle collaboration, S. Wehle et al., *Lepton-Flavor-Dependent Angular Analysis of $B \to K^*\ell^+\ell^-$*, *Phys. Rev. Lett.* **118** (2017) 111801, [1612.05014].

[242] LHCb collaboration, R. Aaij et al., *Search for lepton-universality violation in $B^+ \to K^+\ell^+\ell^-$ decays*, *(2019)*, [1903.09252].

[243] LHCb collaboration, R. Aaij et al., *Test of lepton universality with $B^0 \to K^{*0}\ell^+\ell^-$ decays*, *JHEP* **08** (2017) 055, [1705.05802].

[244] BaBar collaboration, J. P. Lees et al., *Measurement of an Excess of $\bar{B} \to D^{(*)}\tau^-\bar{\nu}_\tau$ Decays and Implications for Charged Higgs Bosons*, *Phys. Rev.* **D88** (2013) 072012, [1303.0571].

[245] S. Descotes-Genon, L. Hofer, J. Matias and J. Virto, *Global analysis of $b \to s\ell\ell$ anomalies*, *JHEP* **06** (2016) 092, [1510.04239].

[246] B. Capdevila, A. Crivellin, S. Descotes-Genon, J. Matias and J. Virto, *Patterns of New Physics in $b \to s\ell^+\ell^-$ transitions in the light of recent data*, *JHEP* **01** (2018) 093, [1704.05340].

[247] W. Altmannshofer, P. Stangl and D. M. Straub, *Interpreting Hints for Lepton Flavor Universality Violation*, *Phys. Rev.* **D96** (2017) 055008, [1704.05435].

[248] G. D'Amico, M. Nardecchia, P. Panci, F. Sannino, A. Strumia, R. Torre et al., *Flavour anomalies after the R_{K^*} measurement*, *JHEP* **09** (2017) 010, [1704.05438].

[249] G. Hiller and I. Nisandzic, *R_K and R_{K^*} beyond the standard model*, *Phys. Rev.* **D96** (2017) 035003, [1704.05444].

[250] L.-S. Geng, B. Grinstein, S. Jäger, J. Martin Camalich, X.-L. Ren and R.-X. Shi, *Towards the discovery of new physics with lepton-universality ratios of $b \to s\ell\ell$ decays*, *Phys. Rev.* **D96** (2017) 093006, [1704.05446].

[251] M. Ciuchini, A. M. Coutinho, M. Fedele, E. Franco, A. Paul, L. Silvestrini et al., *On Flavourful Easter eggs for New Physics hunger and Lepton Flavour Universality violation*, *Eur. Phys. J.* **C77** (2017) 688, [1704.05447].

[252] A. K. Alok, B. Bhattacharya, A. Datta, D. Kumar, J. Kumar and D. London, *New Physics in $b \to s\mu^+\mu^-$ after the Measurement of R_{K^*}*, *Phys. Rev.* **D96** (2017) 095009, [1704.07397].

[253] T. Hurth, F. Mahmoudi, D. Martinez Santos and S. Neshatpour, *Lepton nonuniversality in exclusive $b \to s\ell\ell$ decays*, *Phys. Rev.* **D96** (2017) 095034, [1705.06274].

[254] A. J. Buras, F. De Fazio and J. Girrbach, *The Anatomy of Z' and Z with Flavour Changing Neutral Currents in the Flavour Precision Era*, *JHEP* **02** (2013) 116, [1211.1896].

[255] W. Altmannshofer and D. M. Straub, *New physics in $b \to s$ transitions after LHC run 1*, *Eur. Phys. J.* **C75** (2015) 382, [1411.3161].

[256] G. Bélanger, C. Delaunay and S. Westhoff, *A Dark Matter Relic From Muon Anomalies*, *Phys. Rev.* **D92** (2015) 055021, [1507.06660].

[257] B. Allanach, F. S.Queiroz, A. Strumia, and S. Sun, *Z' models for the LHCb and $g-2$ muon anomalies*, *Phys.Rev.* **D93** (2016) 055045, [1511.07447].

[258] M. Bauer and M. Neubert, *Flavor anomalies, the 750 GeV diphoton excess, and a dark matter candidate*, *Phys. Rev.) **D93** (2016) 115030*, [1512.06828].

[259] A. Celis, W.-Z. Feng, and M. Vollmann, *Dirac dark matter and $b \to s\ell^+\ell^-$ with* U(1) *gauge symmetry*, *Phys. Rev.* **D95** (2017) 035018, [1608.03894].

[260] W. Altmannshofer, S. Gori, S. Profumo, and F. S.Queiroz, *Explaining dark matter and B decay anomalies with an $L_\mu - L_\tau$ model*, *JHEP* **12** (2016) 106, [1609.04026].

[261] P. Ko, T. Nomura, and H. Okada, *A flavor dependent gauge symmetry, Predictive radiative seesaw and LHCb anomalies*, *Phys. Lett.* **B772** (2017) 547–552, [1701.05788].

[262] P. Ko, T. Nomura, and H. Okada, *Explaining $B \to K^{(*)}\ell^+\ell^-$ anomaly by radiatively induced coupling in $U(1)_{\mu-\tau}$ gauge symmetry*, *Phys. Rev.* **D95** (2017) 111701, [1702.02699].

[263] J. M.Cline, J. M.Cornell, D. London, and R. Watanabe, *Hidden sector explanation of B-decay and cosmic ray anomalies*, *Phys. Rev.* **D95** (2017) 095015, [1702.00395].

[264] F. Sala and D. M Straub, *A New Light Particle in B Decays?*, *Phys. Lett.* **B774** (2017) 205–209, [1704.06188].

[265] J. Ellis, M. Fairbairn, and P. Tunney, *Anomaly-Free Models for Flavour Anomalies*, *Eur. Phys. J.* **C78** (2018) 238, [1705.03447].

[266] J. Kawamura, S. Okawa, and Y. Omura, *Interplay between the $b \to s\ell\ell$ anomalies and dark matter physics*, *Phys. Rev.* **D96** (2017) 075041, [1706.04344].

[267] S. Baek, *Dark matter contribution to $b \to s\mu^+\mu^-$ anomaly in local $U(1)_{L_\mu - L_\tau}$ model*, *Phys. Lett.* **B781** (2018) 376-382, [1707.04573].

[268] J. M.Cline, *B decay anomalies and dark matter from vectorlike confinement*, *Phys. Rev.* **D97** (2018) 015013, [1710.02140].

[269] J. M.Cline and J. M Cornell, *$R(K^{(*)})$ from dark matter exchange*, *Phys. Lett.* **B782** (2018) 232-237, [1711.10770].

[270] L. Dhargyal, *A simple model to explain the observed muon sector anomalies, small neutrino masses, baryon-genesis and dark-matter*, (2017), [1711.09772].

[271] C.-W. Chiang and H. Okada, *A simple model for explaining muon-related anomalies and dark matter*, (2017), [1711.07365].

[272] A. Falkowski, S. F.King, E. Perdomo, and M. Pierre, *Flavourful Z' portal for vector-like neutrino Dark Matter and $R_{K^{(*)}}$*, *JHEP* **08** (2018) 061, [1803.04430].

[273] G. Arcadi, T. Hugle, and F. S.Queiroz, *The Dark $L_\mu - L_\tau$ Rises via Kinetic Mixing*, *Phys. Lett.* **B784** (2018) 151-158, [1803.05723].

[274] S. Baek, C. Yu, *Dark matter for $b \to s\mu^+\mu^-$ anomaly in a gauged $U(1)_X$ model*, *JHEP* **11** (2018) 054, [1806.05967].

[275] S. Baek, *Scalar dark matter behind $b \to s\mu\mu$ anomaly*, (2019), [1901.04761].

[276] L. M. Krauss and F. Wilczek, *Discrete Gauge Symmetry in Continuum Theories*, *Phys. Rev. Lett.* **62** (1989) 1221.

[277] B. Petersen, M. Ratz and R. Schieren, *Patterns of remnant discrete symmetries*, *JHEP* **08** (2009) 111, [0907.4049].

[278] D. Aristizabal Sierra, M. Dhen, C. S. Fong and A. Vicente, *Dynamical flavor origin of $\mathbb{Z}_N$ symmetries*, *Phys. Rev.* **D91** (2015) 096004, [1412.5600].

[279] A. Vicente, *Anomalies in $b \to s$ transitions and dark matter*, *Adv. High Energy Phys.* **2018** (2018) 3905848, [1803.04703].

[280] G. 't Hooft, *Naturalness, chiral symmetry, and spontaneous chiral symmetry breaking*, *NATO Sci. Ser. B* **59** (1980) 135–157.

[281] A. Abada and M. Lucente, *Looking for the minimal inverse seesaw realisation*, *Nucl. Phys.* **B885** (2014) 651–678, [1401.1507].

[282] L. Basso, A. Belyaev, D. Chowdhury, M. Hirsch, S. Khalil, S. Moretti et al., *Proposal for generalised Supersymmetry Les Houches Accord for see-saw models and PDG numbering scheme*, *Comput. Phys. Commun.* **184** (2013) 698–719, [1206.4563].

[283] A. Abada, D. Das, A. M. Teixeira, A. Vicente and C. Weiland, *Tree-level lepton universality violation in the presence of sterile neutrinos: impact for R_K and R_π*, *JHEP* **02** (2013) 048, [1211.3052].

[284] A. Abada, M. E. Krauss, W. Porod, F. Staub, A. Vicente and C. Weiland, *Lepton flavor violation in low-scale seesaw models: SUSY and non-SUSY contributions*, *JHEP* **11** (2014) 048, [1408.0138].

[285] A. Crivellin, L. Hofer, J. Matias, U. Nierste, S. Pokorski and J. Rosiek, *Lepton-flavour violating B decays in generic Z' models*, *Phys. Rev.* **D92** (2015) 054013, [1504.07928].

[286] ATLAS collaboration, M. Aaboud et al., *Search for new high-mass phenomena in the dilepton final state using 36 fb^1 of proton-proton collision data at $\sqrt{s}$ = 13 TeV with the ATLAS detector*, *JHEP* **1710** (2017) 182, [1707.02424].

[287] CMS collaboration, A. M. Sirunyan et al., *Search for high-mass resonances in dilepton final states in proton-proton collisions at $\sqrt{s}$ = 13 TeV*, *JHEP* **1806** (2018) 120, [1803.06292].

[288] F.-Z. Xu, W. Zhang, J. Li and T. Li, *Search for the vectorlike leptons in the $U(1)_X$ model inspired by the B-meson decay anomalies*, *Phys. Rev.* **D98** (2018) 115033, [1809.01472].

[289] D. A. Faroughy, A. Greljo and J. F. Kamenik, *Confronting lepton flavor universality violation in B decays with high-p_T tau lepton searches at LHC*, *Phys. Lett.* **B764** (2017) 126–134, [1609.07138].

[290] G. Cacciapaglia, A. Deandrea, N. Gaur, D. Harada, Y. Okada and L. Panizzi, *The LHC potential of Vector-like quark doublets*, *JHEP* **1811** (2018) 055, [1806.01024].

[291] D. Guadagnoli, M. Reboud and O. Sumensari, *A gauged horizontal $SU(2)$ symmetry and $R_{K^{(*)}}$*, *JHEP* **11** (2018) 163, [1807.03285].

[292] D. Bečirević, O. Sumensari and R. Zukanovich Funchal, *Lepton flavor violation in exclusive $b \to s$ decays*, *Eur. Phys. J.* **C76** (2016) 134, [1602.00881].

[293] L. Di Luzio, M. Kirk and A. Lenz, *Updated B_s-mixing constraints on new physics models for $b \to s\ell^+\ell^-$ anomalies*, *Phys. Rev.* **D97** (2018) 095035, [1712.06572].

[294] Heavy Flavor Averaging Group (HFAG) collaboration, Y. Amhis et al., *Averages of b-hadron, c-hadron, and τ-lepton properties as of summer 2014*, [1412.7515].

[295] J. Albrecht, F. Bernlochner, M. Kenzie, S. Reichert, D. Straub and A. Tully, *Future prospects for exploring present day anomalies in flavour physics measurements with Belle II and LHCb*, [1709.10308].

[296] J. Hisano, T. Moroi, K. Tobe and M. Yamaguchi, *Lepton flavor violation via right-handed neutrino Yukawa couplings in supersymmetric standard model*, *Phys. Rev.* **D53** (1996) 2442, [hep-ph/9510309].

[297] T. S. Kosmas, S. Kovalenko, and I. Schmidt, *Nuclear μ^--e^- conversion in strange quark sea*, *Phys. Lett.* **B511** (2001) 203, [hep-ph/0102101].

[298] A. Crivellin M. Hoferichter and M. Procura, *Improved predictions for $\mu \to e$ conversion in nuclei and Higgs-induced lepton flavor violation*, *Phys. Rev.* **D89** (2014) 093024, [1404.7134].

[299] H. C. Chiang, E. Oset, T. S. Kosmas, A. Faessler and J. D. Vergados, *Coherent and incoherent (μ^-, e^-) conversion in nuclei*, *Nucl. Phys.* **A559** (1993) 526.

List of Figures

List of Tables